MULTIDISCIPLINARY CENTER FOR EARTHQUAKE ENGINEERING RESEARCH

A National Center of Excellence in Advanced Technology Applications

ISSN 1520-295X

Assessment of Performance of Bolu Viaduct in the 1999 Duzce Earthquake in Turkey

by

P.C. Roussis, M.C. Constantinou, M. Erdik,
E. Durukal and M. Dicleli
University at Buffalo, State University of New York
Department of Civil, Structural and Environmental Engineering
Ketter Hall
Buffalo, NY 14260

Technical Report MCEER-02-0001

May 8, 2002

This research was conducted at the University at Buffalo, State University of New York and was -supported by the Federal Highway Administration under contract number DTFH61-98-C-00094.

MCEER
MULTIDISCIPLINARY CENTER FOR EARTHQUAKE ENGINEERING RESEARCH
A National Center of Excellence in Advanced Technology Applications

Assessment of Performance of Bolu Viaduct in the 1999 Duzce Earthquake in Turkey

by

P.C. Roussis[1], M.C. Constantinou[2], M. Erdik[3], E. Durukal[4] and M. Dicleli[5]

Publication Date: May 8, 2002
Submittal Date: December 3, 2001

Technical Report MCEER-02-0001

Task Number 094-F-4.1

FHWA Contract Number DTFH61-98-C-00094

1 Graduate Research Assistant, Department of Civil, Structural and Environmental Engineering, University at Buffalo, State University of New York
2 Professor and Chairman, Department of Civil, Structural and Environmental Engineering, University at Buffalo, State University of New York
3 Professor and Chairman, Department of Earthquake Engineering, Kandilli Observatory and Earthquake Research Institute, Bogazici University, Istanbul, Turkey
4 Assistant Professor, Department of Earthquake Engineering, Kandilli Observatory and Earthquake Research Institute, Bogazici University, Istanbul, Turkey
5 Assistant Professor, Department of Civil Engineering and Construction, Bradley University, Peoria, Illinois

MULTIDISCIPLINARY CENTER FOR EARTHQUAKE ENGINEERING RESEARCH
University at Buffalo, State University of New York
Red Jacket Quadrangle, Buffalo, NY 14261

Preface

The Multidisciplinary Center for Earthquake Engineering Research (MCEER) is a national center of excellence in advanced technology applications that is dedicated to the reduction of earthquake losses nationwide. Headquartered at the University at Buffalo, State University of New York, the Center was originally established by the National Science Foundation in 1986, as the National Center for Earthquake Engineering Research (NCEER).

Comprising a consortium of researchers from numerous disciplines and institutions throughout the United States, the Center's mission is to reduce earthquake losses through research and the application of advanced technologies that improve engineering, pre-earthquake planning and post-earthquake recovery strategies. Toward this end, the Center coordinates a nationwide program of multidisciplinary team research, education and outreach activities.

MCEER's research is conducted under the sponsorship of two major federal agencies, the National Science Foundation (NSF) and the Federal Highway Administration (FHWA), and the State of New York. Significant support is also derived from the Federal Emergency Management Agency (FEMA), other state governments, academic institutions, foreign governments and private industry.

The Center's Highway Project develops improved seismic design, evaluation, and retrofit methodologies and strategies for new and existing bridges and other highway structures, and for assessing the seismic performance of highway systems. The FHWA has sponsored three major contracts with MCEER under the Highway Project, two of which were initiated in 1992 and the third in 1998.

Of the two 1992 studies, one performed a series of tasks intended to improve seismic design practices for new highway bridges, tunnels, and retaining structures (MCEER Project 112). The other study focused on methodologies and approaches for assessing and improving the seismic performance of existing "typical" highway bridges and other highway system components including tunnels, retaining structures, slopes, culverts, and pavements (MCEER Project 106). These studies were conducted to:

- assess the seismic vulnerability of highway systems, structures, and components;
- develop concepts for retrofitting vulnerable highway structures and components;
- develop improved design and analysis methodologies for bridges, tunnels, and retaining structures, which include consideration of soil-structure interaction mechanisms and their influence on structural response; and
- develop, update, and recommend improved seismic design and performance criteria for new highway systems and structures.

The 1998 study, "Seismic Vulnerability of the Highway System" (FHWA Contract DTFH61-98-C-00094; known as MCEER Project 094), was initiated with the objective of performing studies to improve the seismic performance of bridge types not covered under Projects 106 or 112, and to provide extensions to system performance assessments for highway systems. Specific subjects covered under Project 094 include:

- development of formal loss estimation technologies and methodologies for highway systems;
- analysis, design, detailing, and retrofitting technologies for special bridges, including those with flexible superstructures (e.g., trusses), those supported by steel tower substructures, and cable-supported bridges (e.g., suspension and cable-stayed bridges);
- seismic response modification device technologies (e.g., hysteretic dampers, isolation bearings); and
- soil behavior, foundation behavior, and ground motion studies for large bridges.

In addition, Project 094 includes a series of special studies, addressing topics that range from non-destructive assessment of retrofitted bridge components to supporting studies intended to assist in educating the bridge engineering profession on the implementation of new seismic design and retrofitting strategies.

The research discussed in this report was performed within Project 094, Task F-4.1, "Earthquake Reconnaissance." The report describes the impact of the destructive 1999 Duzce (Turkey) earthquake on the Bolu Viaduct, a 2.3-km long seismically isolated structure which was essentially complete when the earthquake occurred. The viaduct suffered a complete failure of its seismic isolation system and narrowly avoided total collapse due to excessive differential ground, substructure, and superstructure movement.

The report presents an evaluation of the design of the seismic isolation system of this structure and an assessment of its performance in the Duzce earthquake. The evaluation of design and assessment of performance are important in developing experience in the design of seismically isolated structures and in validating analysis and design specifications.

ABSTRACT

The Bolu Viaduct is a 2.3-km long seismically isolated structure which was nearly complete when it was hit by the powerful November 12, 1999 Duzce earthquake in Turkey. The viaduct suffered complete failure of the seismic isolation system and narrowly avoided total collapse due to excessive superstructure movement.

This report presents an evaluation of the design of the seismic isolation system of this structure and an assessment of the performance of the structure in the Duzce earthquake. The evaluation of design and assessment of performance are important in developing experience in the design of seismically isolated structures and in validating analysis and design specifications.

ACKNOWLEDGEMENTS

Financial support for this project was provided by the Multidisciplinary Center of Earthquake Engineering Research (MCEER), Highway Project, Task D3-1. MCEER is, in turn, supported by the Federal Highway Administration.

TABLE OF CONTENTS

TABLE OF CONTENTS (continued)

LIST OF FIGURES

LIST OF FIGURES (continued)

FIGURE **TITLE** **PAGE**

LIST OF FIGURES (continued)

FIGURE **TITLE** **PAGE**

LIST OF TABLES

SECTION 1

INTRODUCTION

Before overcoming the devastating impact of August 17, 1999 Kocaeli earthquake, Turkey was hit by another new and almost as powerful earthquake on November 12, 1999. Called the Duzce earthquake, it caused loss of life and considerable damage. Also, it caused damage to a seismically isolated viaduct, part of the Trans European Motorway, which was under construction at the time of the earthquake.

The viaduct featured a seismic isolation system with elastoplastic characteristics which, on the basis of the current AASHTO Guide Specifications for Seismic Isolation Design (American Association of State Highway and Transportation Officials, 1999), is classified as one with insufficient restoring force capability and its use is disallowed. Moreover, the 1991 predecessor of the AASHTO Guide Specifications for Seismic Isolation Design (American Association of State Highway and Transportation Officials, 1991) would have allowed the use of the system but would have required that the isolation bearings were designed to have large displacement capacity.

The Bolu Viaduct design was not strictly based on either of the aforementioned AASHTO documents and resulted in an isolation system displacement capacity that was substantially less than what AASHTO prescribes.

Accordingly, the performance of this seismically isolated structure becomes important in validating the AASHTO specifications and, generally, in developing experience in the behavior of this type of structure. Therefore, the objectives of this study are: (a) to assess the performance of the structure in the Duzce earthquake, and (b) to investigate whether the structure would have experienced damage in the Duzce earthquake had it been designed in accordance to AASHTO Specifications.

SECTION 2

DESCRIPTION OF THE STRUCTURE

2.1 Description of the Viaduct

Viaduct 1 is part of the Bolu Mountain Project, located in north-central Turkey. This 1.5 billion dollar project, consisting of two viaducts and a tunnel, aims at improving transportation in the mountainous terrain to the west of Bolu between Istanbul and Ankara. The Bolu Mountain Project is, in turn, part of the Trans-European-Motorway (TEM) running from Ankara to Europe parallel to the North Anatolian Fault Zone.

Viaduct 1 (Figure 2.1), with its dual 59 spans and 2.3-km structure was approximately 95% complete at the time of the November 12, 1999 Duzce earthquake. It consists of seven lines of simply supported prestressed concrete box girders seated on sliding pot bearings with stainless steel-PTFE sliding interfaces. The viaduct also incorporates an energy dissipation system in the form of yielding steel devices, installed on each pier cap (Marioni, 1997; Marioni, 2000; Ghasemi et al., 2000).

Figure 2-1 General View of Bolu Viaduct 1

The superstructure is made continuous over 10-span sections by means of span-connecting slabs. An elevation is shown in Figure 2.2. It comprises 11 piers and 10 deck spans with a total length of 392.2 m. The piers are single, octagonal, hollow-core reinforced-concrete columns, 4.5 by 8.0 m in plan dimension, with heights varying from 37 m (P10) to 47 m (P20). The piers rest on massive 3m-thick reinforced concrete pile

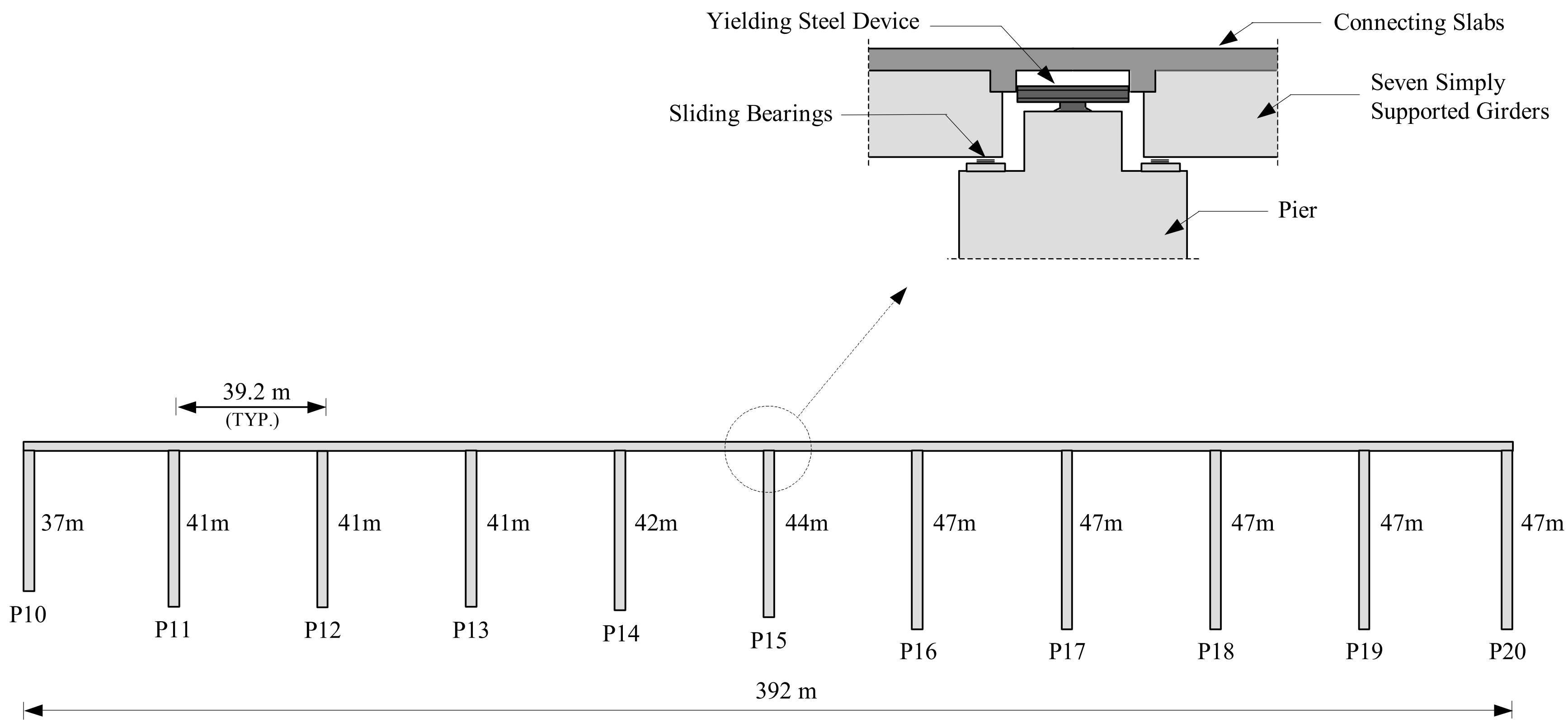

Figure 2-2 Elevation of Viaduct Between Expansion Joints (Segment of Viaduct Analyzed in this Study)

caps, which are supported on twelve 1.8m-diameter bored cast-in-situ reinforced concrete piles in alluvium. The pile length is up to 37.5 m (Calvi et al., 2001; Barr et al., 2001).

2.2 Description of the Isolation System

The isolation system consists of lubricated multi-directional sliding bearings and yielding steel devices. Figure 2.3 shows the elevation of Pier 15 along with the sliding bearings that support the superstructure. Restraint against horizontal movements is achieved by means of yielding steel (energy dissipating) devices placed between the piers and the superstructure. There is one such device on top of every pier.

Each one of these devices consists of 16 C-shaped crescent moon elements in a radially symmetric configuration and is connected to the superstructure and substructure as shown in Figure 2.4. Moreover, shock transmission (or lock-up) devices are incorporated into the units in the longitudinal viaduct direction between the crescent moon shaped elements and the substructure. This system allows free longitudinal movement of the superstructure relative to the substructure due to creep, shrinkage, and temperature, and locks up under high-speed movement to engage the yielding steel devices (Ciampi and Marioni, 1991; Tsopelas and Constantinou, 1997). Under seismic conditions, the behavior of the system is nearly elastoplastic as shown in Figure 2.5. This figure presents the lateral force-displacement loop of a yielding steel device used at the viaduct at displacement amplitude of 320 mm and very low velocity of movement (Universita de Pavia, 1993). Samples of test results for these devices may be also found in Priestley et al. (1996), Marioni (1997), Marioni (2000) and Ghasemi et al. (2000).

The sliding bearings were designed to have a capacity of 210 mm. Testing of the energy dissipating devices was conducted up to a displacement of 480 mm, a value referred to as the ultimate displacement (Marioni, 1997; Marioni, 2000). There is an apparent inconsistency in the design with the yielding steel devices capable of deforming to 480 mm and the sliding bearings having a displacement capacity of 210 mm.

Furthermore, cable restrainers were utilized at the expansion joints in order to prevent the end girders from falling off their supports when displacements exceed the capacity of the isolation system. These restrainers may have been instrumental in preventing collapse of the end girders in the Duzce earthquake.

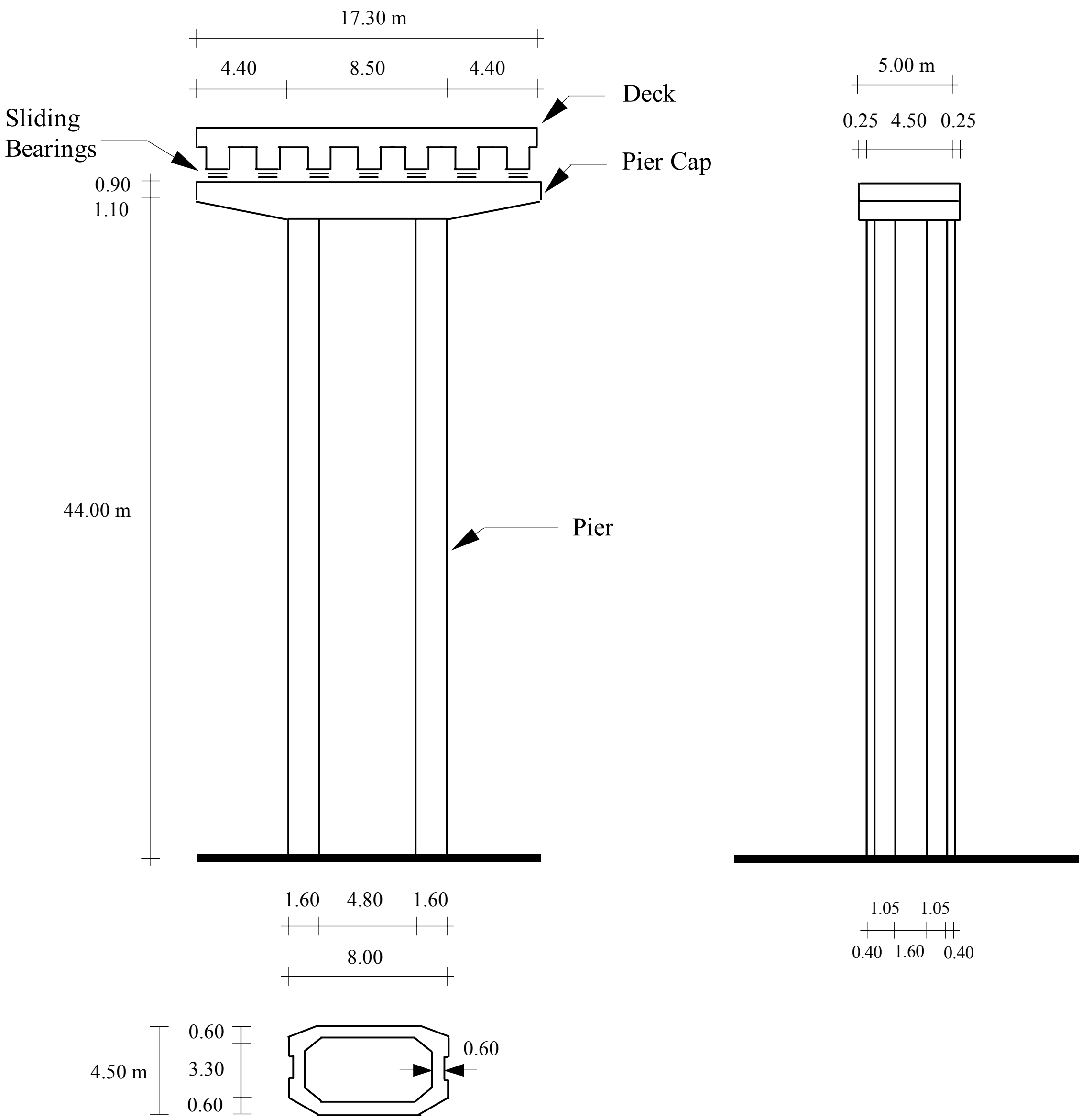

Figure 2-3 Elevation of Pier P15

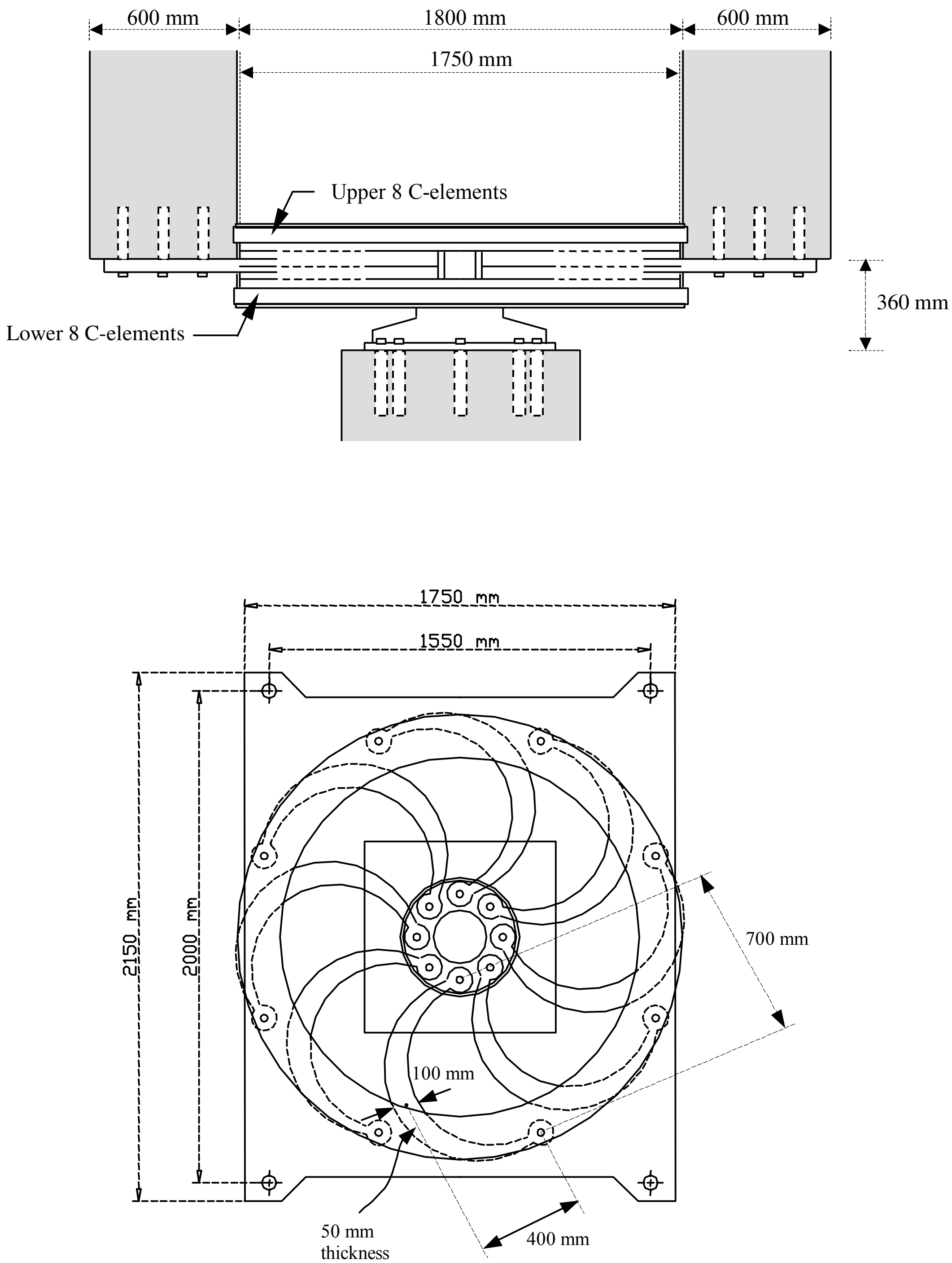

Figure 2-4 Schematic of Yielding Steel Device

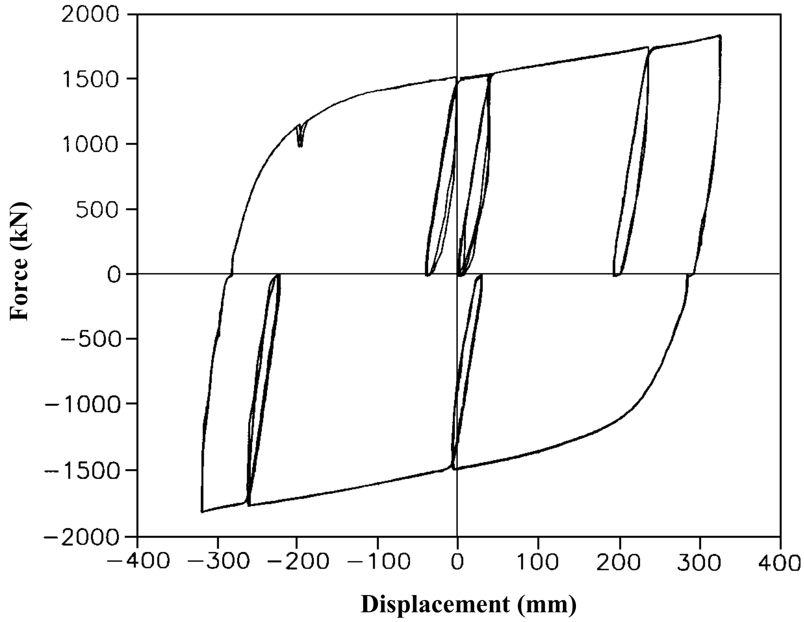

Figure 2-5 Lateral Force-Displacement Loop of Yielding Steel Device at Amplitude of 320mm (from Universita de Pavia, 1993)

2.3 Design of Structure

Turkey is an affiliate AASHTO State. However, the design concept for the viaduct involved the application of mixed criteria, using the then applicable AASHTO Standard Specifications (American Association of State Highway and Transportation Officials, 1992) and seismic isolation guidelines developed by the designer. The 1991 AASHTO Guide Specifications for Seismic Isolation Design (American Association of State Highway and Transportation Officials, 1991) were not available at the time of the development of specifications for the Bolu Viaduct. The design of the viaduct was based on seismic forces and displacements that were determined by means of nonlinear time-history analysis performed with artificial accelerograms matching the A=0.4, soil type II, AASHTO spectrum (American Association of State Highway and Transportation Officials, 1992), that is shown in Figure 2.6.

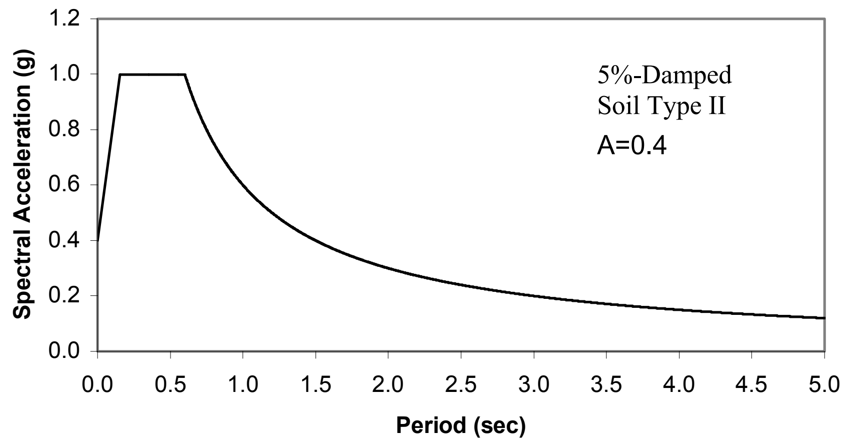

Figure 2-6 5%-Damped AASHTO Design Spectrum for A=0.4, Soil Type II

The structure was analyzed using a finite element model, considering the substructure to be uncracked. The foundation was modeled through elastic springs (both for rotation and translation) with stiffness in accordance with field test results. The yielding steel devices between each pier top and the deck were modeled using "truss" elements with nonlinear material properties matching the full-scale test results (e.g., Figure 2.5). The original analysis was carried out using seven uni-directional artificial ground acceleration histories and the design values for forces and displacements were taken as the mean values of the maxima obtained from the seven analyses (Marioni, 1997; Marioni, 2000).

The assumed bilinear hysteretic behavior of the seismic isolation system per pier location utilized in the design is shown schematically in Figure 2.7 (Astaldi S.p.A., 2000). This behavior is the combination of the inelastic behavior of the energy dissipating devices and of the sliding bearings, which support a tributary weight W=14200 kN per pier location. The yield force F_y=1520 kN consists primarily of the yield strength of the energy dissipating crescent-moon devices (approximately 1400 kN) with the remaining being the friction force in the lubricated sliding bearings (coefficient of sliding friction less than 0.01). The yield force and yield displacement (38 mm) of the system are consistent with theory (Ciampi and Marioni, 1991). The post-yielding stiffness K_p appears in the experimental results of Figure 2.5 to be equal to 1080 kN/m. This value of the post-yielding stiffness K_p (equal to 0.027 times the elastic stiffness K_e) is very low so that the isolation system does not meet the criteria for lateral restoring force of either the 1991 or the 1999 AASHTO Guide Specifications for Seismic Isolation Design (Section 12.2, American Association of State Highway and Transportation Officials, 1991 and 1999). Whereas the 1991 AASHTO Guide Specifications would have allowed the use of this system, the 1999 AASHTO Guide Specifications would have prohibited its use.

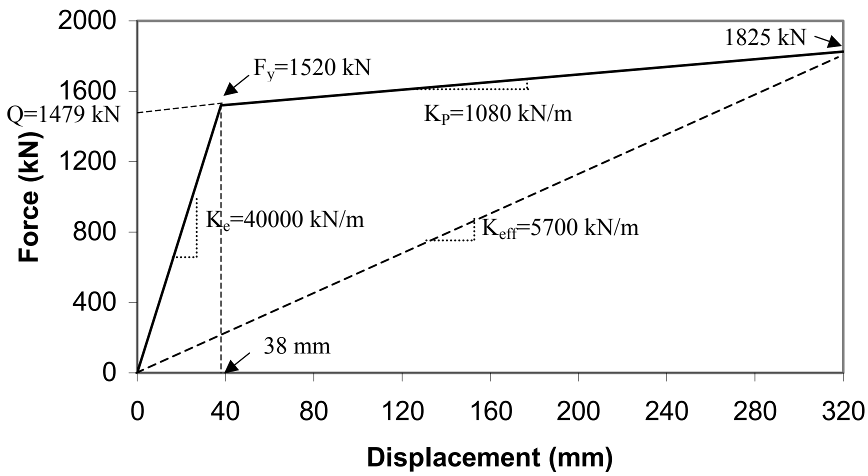

Figure 2-7 Assumed Bilinear Hysteretic Behavior of Seismic Isolation System at each Pier Location (from Astaldi S.p.A., 2000)

Marioni (2000) reported the design displacement (displacement in the design earthquake) to be 320 mm, for which the effective stiffness is K_{eff}=5700 kN/m. However, it is not known why the design displacement was calculated to be 320 mm, but that isolation bearings had a displacement capacity of only 210 mm. The design is inconsistent with the AASHTO Guide Specifications for Seismic Isolation Design (American Association of State Highway and Transportation Officials, 1991) in the following:

(a) The system had insufficient lateral restoring force capability. Specifically, the lateral restoring force at the design displacement of 320 mm is 1825 kN and the lateral force at 50-percent of the design displacement is 1652 kN. The two figures differ by 1825-1652=173 kN or 173/14200=0.012W, where W is the tributary weight. The 1991 AASHTO Guide Specifications require the difference to exceed 0.025W. The isolation system should have been capable of accommodating displacements equal to the greater of three times the design displacement (as calculated by the single mode analysis method of the 1991 AASHTO) or $36AS_i$ inches where A=0.4 and S_i= 1.5 (site coefficient for soil profile II). Analysis utilizing the characteristics of Figure 2.7 results in a design displacement of 263 mm. $36AS_i$ is 550 mm. Therefore, the isolation system should have been designed to have a minimum displacement capacity of three times 263 mm or 790 mm. This figure is greater than either the capacity of the installed system (210 mm) or the calculated response of 320 mm (Marioni, 2000).

(b) Since the system has insufficient restoring force capability, three-dimensional nonlinear dynamic analysis should have been used. Such an analysis requires at least three pairs of horizontal ground motion histories selected from recorded events and scaled to represent the applicable response spectrum. The maximum response parameters computed in the three dynamic analyses should be used in design. However, the displacement capacity of the isolation system could not be less than the 790 mm determined by the simplified method of analysis.

2.4 Observed Damage in the 1999 Duzce Earthquake

In 1999 two devastating earthquakes on the North Anatolian Fault in Turkey impacted the Bolu Mountain Project (Erdik, 2000). The first earthquake, the Kocaeli earthquake, occurred on August 17, 1999 and had its epicenter at about 120 km from the viaduct. The performance of the viaduct during this event was satisfactory. Motions at the sliding bearings of the deck relative to the pier cap have been estimated to be 80 mm in the longitudinal direction and 60 mm in the transverse direction (Purdue Univ., 2000; Barr et al., 2001). The crescent-shaped yielding steel devices experienced limited inelastic action and some residual permanent displacement occurred.

The second major earthquake struck on November 12, 1999 and it was centered near the town of Duzce in the province of Bolu. Figure 2.8 presents a general map of the region and illustrates the location of Viaduct 1, the epicenter of the earthquake, the extent of the fault rupture and the location of strong ground motion stations that produced significant records. The map of Figure 2.8 shows the fault extending to and crossing the viaduct, which must have been subjected to significant directivity and fling effects and the associated large velocity pulses and permanent tectonic deformations. The viaduct suffered complete failure of the bearings and energy dissipation devices. The significant superstructure movement relative to the substructure resulted in excessive translation of the girders and collapse was just narrowly avoided.

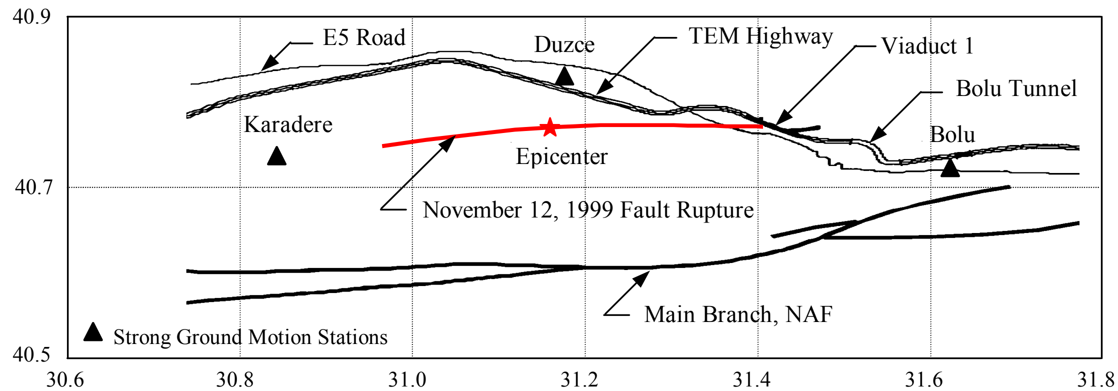

Figure 2-8 General Map of Region Showing Location of Viaduct 1 and Surface Rupture During the Duzce Earthquake

The viaduct superstructure experienced a westward permanent displacement relative to the piers, leaving all the ends of the girders off-set from their supports (Figures 2.9 and 2.10). Significant permanent displacements developed as shown in Figure 2.11 with permanent offsets of the order of 1000 mm longitudinally and 500 mm transversely. At nearly all locations, the sliding bearings suffered complete failure with their parts dislocated and ejected from the bearing pedestals (Figures 2.12 and 2.13). Observation of the scratch signs on the surface of stainless steel plates (resembling the number six) indicates that the bearings slid off probably in a very early stage before any significant cyclic movement (Figure 2.14). This supports the scenario that the bridge was subjected to a near-fault pulse-type motion (Ghasemi et al., 2000). Figure 2.15 shows a view of failed connections of the energy dissipation devices at an expansion joint.

The fault surface intersected the viaduct axis at Pier 45 at an angle of about 25 degrees (Erdik, 2000; Purdue Univ., 2000). Pier 45 rotated about its vertical axis by as much as 12 degrees due to the horizontal differential motion across the fault surface rupture (Figure 2.16). Other than this, damage to the piers of the viaduct was minimal.

Figure 2-9   Girders Off-Set from their Supports

Figure 2-10   Close-up View of Girders on Pier Tops Showing Significant Permanent Offset of Girders

Figure 2-11 Permanent Displacements as Seen at Expansion Joints

Figure 2-12 Damage and Permanent Displacement at Sliding Bearings

Figure 2-13 Close-up View of Failed Sliding Bearings (Note that Stainless Steel Plate was Ejected from Bearing)

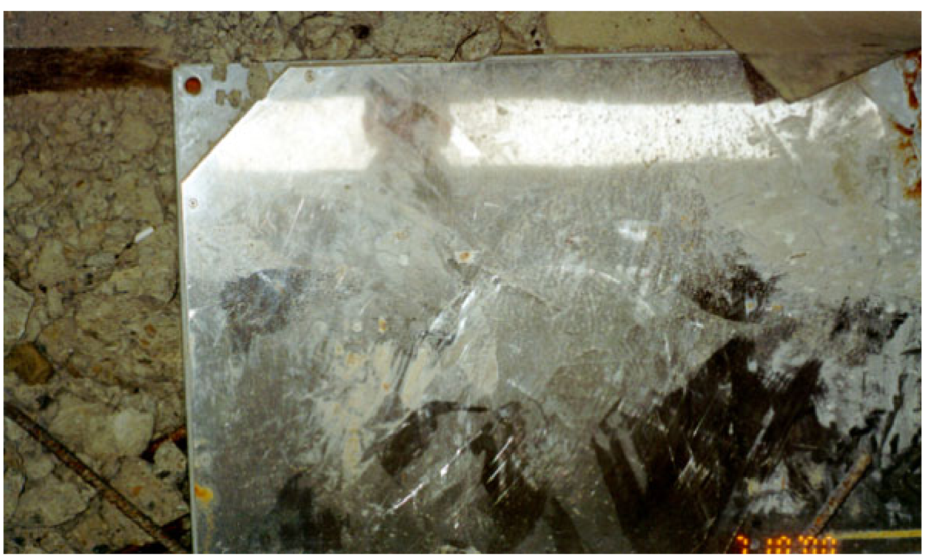

Figure 2-14 Typical Trace on Displaced/Ejected Bearing Plates

Figure 2-15 View of Energy Dissipating Devices at Expansion Joint Showing Failure of Connections of the Energy Dissipating Device to Deck

Figure 2-16 Rotation of Pier 45 about Vertical Axis

SECTION 3

DEVELOPMENT OF MODEL FOR ANALYSIS OF STRUCTURE

3.1 Finite Element Model for Dynamic Analysis

A typical section of ten spans (from P10 to P20) was analyzed using the finite element program ANSYS (Swanson Analysis Systems IP, Inc. 1996). The analysis was based on a three-dimensional model, the main characteristics of which are described below. In the finite element model, the piers and deck are modeled using three-dimensional beam elements (BEAM4). Each pier has been subdivided in three beam elements and each deck span in four beam elements. Rigid elements were introduced at each pier top, in order to model the height difference between the deck's centroid and the top of each bearing (Figure 3.1).

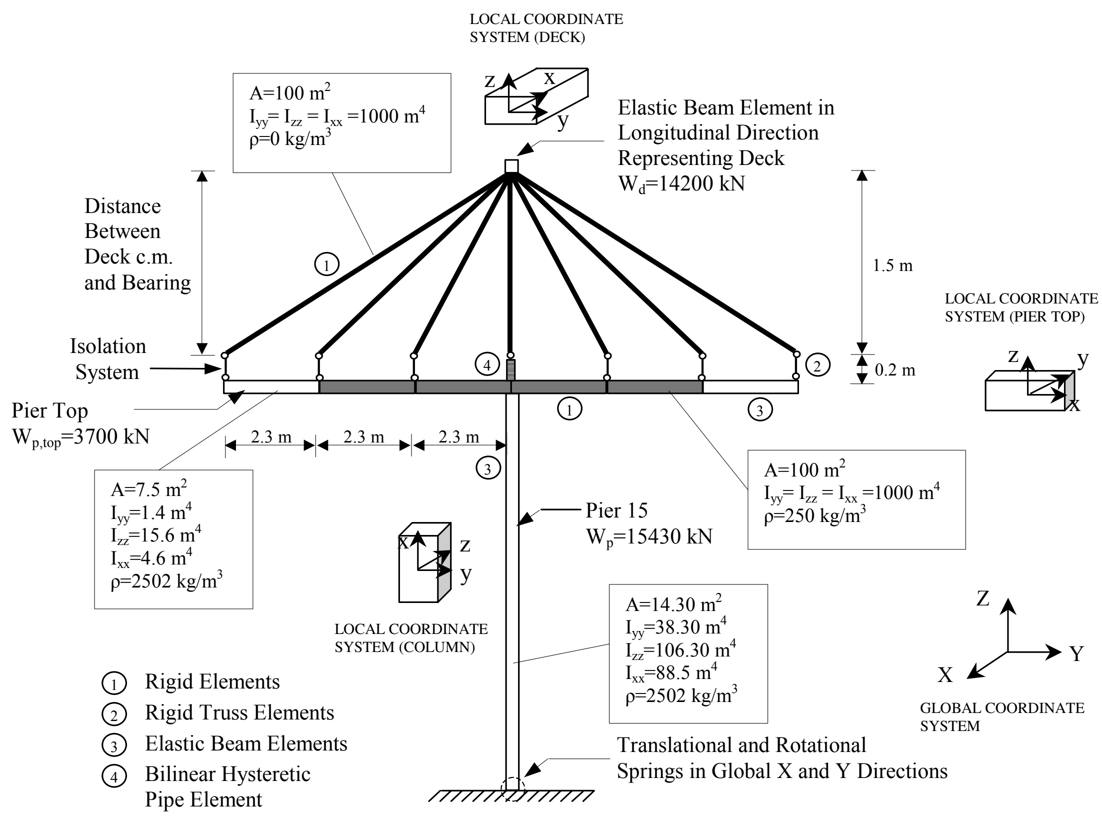

Figure 3-1 Schematic of Pier Top in Finite Element Model

Parameters in the finite element model were based on the recommendations of the contractor (Astaldi S.p.A., 2000). Specifically, distributed masses have been applied at pier and deck elements. Moreover, to properly model bridge continuity, pier stiffnesses, ground spring stiffnesses, masses, and isolator properties at the end piers P10 and P20 (Figure 2.2) have been modeled with half of their full values. The data used in the model are presented in Table 3.1. Note that the local x-, y-, and z-axes of the various elements in the model are shown in Figure 3.1.

Table 3-1 Material and Geometric Properties of Pier and Deck Elements

Properties	Piers	Pier Top		Deck	Pier-to-Deck Rigid Elements
		Flexible Portion	Rigid Portion		
Cross sectional area (m^2)	14.30	7.5	100	12.88	100
Moment of inertia about local axis y, I_{yy} (m^4)	38.30	1.4	1000	0.581	1000
Moment of inertia about local axis z, I_{zz} (m^4)	106.30	15.6	1000	328.0	1000
Torsional geometric parameter, I_{xx} (m^4)	88.5	4.6	1000	2.33	1000
Young's modulus (N/m^2)	2.36×10^{10}	2.36×10^{10}	2.36×10^{10}	3.12×10^{10}	2.36×10^{10}
Poisson's ratio	0.17	0.17	0.17	0.17	0.17
Density (Kg/m^3)	2502	2502	250	2867	0

At the ground level, elastic translational and rotational springs (element COMBIN14 of ANSYS) were used at each pier base to model the foundation stiffness. The characteristics of these springs are presented in Table 3.2 (Astaldi S.p.A., 2000). Note that these stiffnesses were assigned in the global X, Y, and Z directions.

Table 3-2 Pier Foundation Spring Stiffnesses

Pier	Height (m)	Rotational Stiffness (Nm)	Translational Stiffness (N/m)
P10	37	$3.4x10^{11}$	$2.8\ x10^{9}$
P11	41	$3.4\ x10^{11}$	$2.8\ x10^{9}$
P12	41	$3.4\ x10^{11}$	$2.8\ x10^{9}$
P13	41	$3.8\ x10^{11}$	$3.9\ x10^{9}$
P14	42	$3.8\ x10^{11}$	$3.9\ x10^{9}$
P15	44	$3.8\ x10^{11}$	$3.9\ x10^{9}$
P16	47	$3.8\ x10^{11}$	$3.9\ x10^{9}$
P17	47	$3.5\ x10^{11}$	$3.5\ x10^{9}$
P18	47	$3.2\ x10^{11}$	$3.1\ x10^{9}$
P19	47	$2.9\ x10^{11}$	$2.6\ x10^{9}$
P20	47	$2.6\ x10^{11}$	$2.2\ x10^{9}$

The sliding bearings were modeled as very stiff vertical truss elements using element LINK8 (Figure 3.1). The elements were defined by their length (0.2 m), their cross-sectional area (0.0742 m^2), and Young's modulus $E=2.36x10^{10}\ N/m^2$. The small friction force in these bearings was lumped and included in the hysteretic behavior of the energy dissipating devices.

The energy dissipating units have been modeled through fixed-pinned thin-walled pipe elements (PIPE20), which are capable of describing bilinear hysteretic behavior of the type shown in Figure 2.7. The pipe element is convenient in the description of bilinear hysteretic behavior of the yielding steel devices, because by adjusting the thickness of the element one can control the transition from elastic to inelastic behavior. For describing the inelastic behavior, the bilinear kinematic hardening (BKIN) model was activated in the ANSYS program. The length, L, of the pipe element was specified to be 200 mm, and the outer diameter, D_{out}, and thickness, t, to be 10 mm and 1 mm, respectively (Figure 3.2). Based on the assumed element geometry and the force-displacement relationship depicted in Figure 2.7, one can construct the stress-strain relationship required in ANSYS.

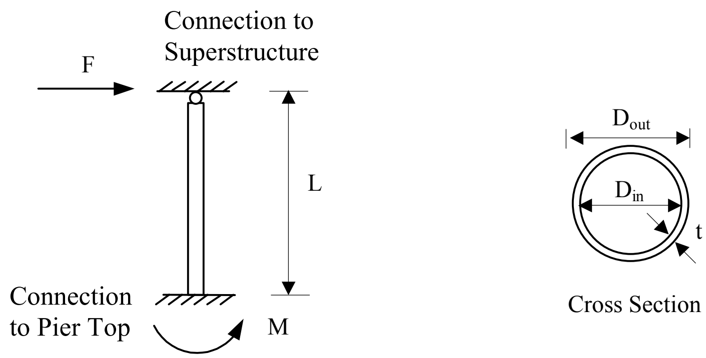

Figure 3-2   Geometry of Pipe Element in Finite Element Model

The elastic modulus is calculated using the equation

$$K = \frac{3EI}{L^3} \quad , \qquad E = \frac{KL^3}{3I} = 368000 \text{ GPa}$$

where

$$I = \frac{\pi(D_{out}{}^4 - D_{in}{}^4)}{64} = 2.9 \times 10^{-10} \text{ m}^4$$

$K = 40000$ kN/m, is the elastic stiffness (see Figure 2.7)

The post-elastic modulus, E_t, is, then, computed such that the ratio of $\frac{E_t}{E} = \frac{K_p}{K} = 0.027$, resulting in E_t=9920 GPa. The yield stress, σ_y, is calculated from the following equation:

$$M = F_y L = \sigma_y Z \text{, so that } \sigma_y = \frac{F_y L}{Z} = 3740 \text{ GPa}$$

where

$F_y = 1520$ kN; is the force at yield displacement (see Figure 2.7), and

$Z = \frac{D_{out}{}^3}{6} - \frac{D_{in}{}^3}{6} = 8.13 \times 10^{-8}$ m^3; is the plastic section modulus for pipe.

Note that the pipe element was selected to have a diameter of 10mm and thickness of 1 mm. One may say that this element is extremely small, but is irrelevant because the analysis performed in this case did not include any geometric nonlinearities. The resulting stress-strain relation is shown in Figure 3.3.

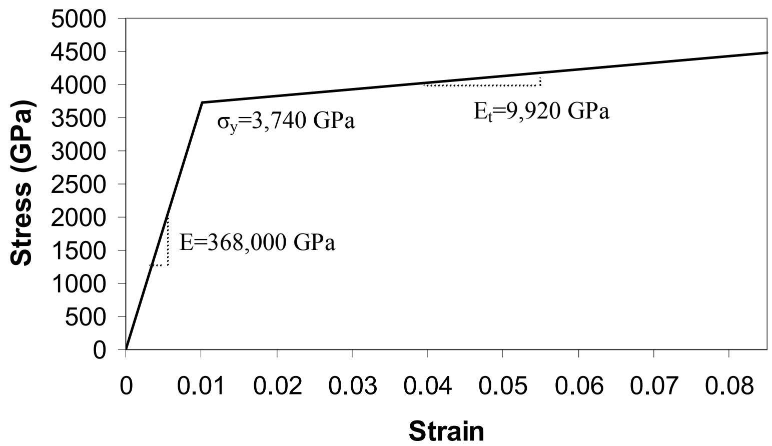

Figure 3-3 Stress-Strain Relation Used for Element Representing Isolation System Behavior in ANSYS

Appendix A presents a detailed description of the ANSYS model.

3.1.1 Modal Analysis

To understand the dynamic behavior of the structural system, a modal analysis was first performed. The calculated natural frequencies and mode shapes can provide insight into how the structure responds when those modes are excited. Furthermore, results from modal analysis are important because they provide means for validating the nonlinear model in ANSYS, and for establishing parameters to define the damping matrix needed in the time-history analysis.

The linear character of the modal analysis dictates the use of linear elements and material properties. In particular, the bilinear behavior of the seismic isolation devices was approximated by considering the effective stiffness at the reported design displacement (Marioni, 1997; Marioni, 2000) of 320 mm, namely, $K_{eff} = 5700$ kN/m (Figure 2.7). The first twenty natural frequencies and the associated modal participation mass fractions calculated in ANSYS are presented in Table 3.3. Appendix B contains graphs of the mode shapes.

Table 3-3 Calculated Natural Frequencies and Modal Participation Mass Fractions of Linearized System

Mode	Frequency (Hz)	Modal Participation Mass Fraction					
		Long. (X)	Trans. (Y)	Ver. (Z)	RotX	RotY	RotZ
1	0.284	0.706	0.000	0.000	0.000	0.000	0.000
2	0.298	0.000	0.842	0.000	0.725	0.000	0.988
3	0.305	0.000	0.158	0.000	0.272	0.000	0.011
4	0.495	0.000	0.000	0.000	0.000	0.072	0.000
5	0.717	0.000	0.000	0.000	0.000	0.140	0.000
6	0.738	0.000	0.000	0.250	0.000	0.150	0.000
7	0.795	0.000	0.000	0.000	0.000	0.166	0.000
8	0.882	0.000	0.000	0.294	0.000	0.000	0.000
9	0.949	0.011	0.000	0.000	0.000	0.000	0.000
10	0.959	0.022	0.000	0.002	0.000	0.017	0.000
11	0.966	0.019	0.000	0.000	0.000	0.000	0.000
12	0.974	0.042	0.000	0.001	0.000	0.000	0.000
13	0.980	0.055	0.000	0.001	0.000	0.193	0.000
14	0.995	0.002	0.000	0.000	0.000	0.000	0.000
15	1.075	0.036	0.000	0.000	0.000	0.000	0.000
16	1.100	0.000	0.000	0.000	0.003	0.252	0.000
17	1.117	0.000	0.000	0.439	0.000	0.000	0.000
18	1.150	0.034	0.000	0.009	0.000	0.001	0.000
19	1.176	0.001	0.000	0.000	0.000	0.001	0.000
20	1.177	0.072	0.000	0.003	0.000	0.007	0.000

Having calculated the natural frequencies of the system, the form of damping in the dynamic analysis may be explicitly defined. In particular, by assuming Rayleigh damping, the damping matrix is given as

$$[C] = a[M] + b[K] \tag{3-1}$$

where $[M]$ and $[K]$ are the system mass and stiffness matrix, respectively.

Coefficients a and b may be determined by selecting the damping ratios at two frequencies, say m and n:

$$\xi_m = \frac{a}{2\omega_m} + \frac{b\omega_m}{2}; \qquad \xi_n = \frac{a}{2\omega_n} + \frac{b\omega_n}{2} \tag{3-2}$$

which result in

$$a = \frac{2\xi_m \omega_m \omega_n^{\;2} - 2\xi_n \omega_n \omega_m^{\;2}}{\omega_n^{\;2} - \omega_m^{\;2}}; \qquad b = \frac{2\xi_n \omega_n - 2\xi_m \omega_m}{\omega_n^{\;2} - \omega_m^{\;2}} \tag{3-3}$$

Parameters a and b were assigned values: $a = 49.267 \times 10^{-3}$ and $b = 6.588 \times 10^{-3}$, so that the damping ratio in the first 20 modes is in the range of 0.02 to 0.03. Figure 3.4 presents the distribution of values of damping ratio for the first 20 modes of the model based on the utilized values of parameters a and b.

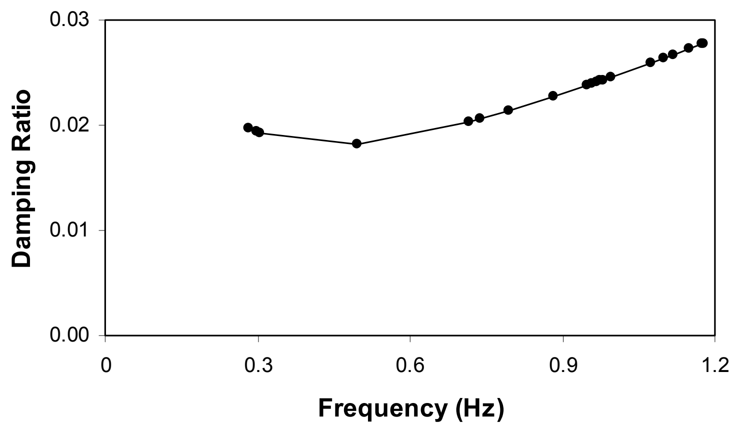

Figure 3-4 Damping Ratio Distribution for First Twenty Modes in ANSYS Model

3.1.2 Nonlinear Response History Analysis

Nonlinear response history analysis was carried out in ANSYS (Swanson Analysis Systems IP, Inc., 1996) using the Newmark integration scheme with a time step of 0.002 sec. Furthermore, a Newton-Raphson iteration procedure was used in each time step for the equilibrium iteration process. Viscous damping in the system was specified to be of the Rayleigh type with coefficients a =0.04927 and b =0.00658.

3.2 Selection of Motions for Dynamic Analysis

3.2.1 Motions for Assessing Performance in the 1999 Duzce Earthquake

The strong ground motion stations operated by the General Directory of Disaster Affairs in Turkey recorded 20 records of the 1999 Duzce earthquake. Of these, the Bolu and Duzce station records (see Figure 2.8) are significant for the assessment of the performance of the viaduct. Moreover, two temporary stations installed at Karadere (see Figure 2.8) by the University of Paris and Columbia University for aftershock investigation of the August 17 earthquake yielded additional relevant records.

Table 3.4 presents the peak ground acceleration (PGA), velocity (PGV) and displacement (PGD) of the Bolu, Duzce and the two Karadere records. These values were obtained following correction of the recorded ground accelerations.

Table 3-4 Peak Ground Motion Values of Records at Stations Near the Bolu Viaduct

Station	Component	PGA (g)	PGV (cm/sec)	PGD (cm)
Bolu [1]	NS	0.728	56.4	23.1
	EW	0.822	62.1	13.6
Duzce [1]	NS	0.348	60.0	42.1
	EW	0.535	83.5	51.6
Karadere 496 [2]	NS	0.750	39	17
	EW	0.750	38	11
Karadere 375 [2]	NS	1.097	47	8
	EW	0.641	21	4

[1] Based on Data at PEER Strong Motion Database (http://peer.berkeley.edu/smcat/)

[2] Based on Analysis Performed at Kandilli Observatory and Earthquake Research Institute, Bogazici University, Istanbul, Turkey

Figure 3.5 presents the 5-percent damped response spectra of the horizontal components of the Bolu, Duzce and Karadere records and compares them to the AASHTO design spectrum. It is evident that the spectral values of the eight recorded components far exceed the design spectral values in the short period range (period less than about 0.6 sec) and that, with the exception of the Duzce records, they are below the design spectral values in the long period range (period larger than about 1.5 sec). Particularly, the four

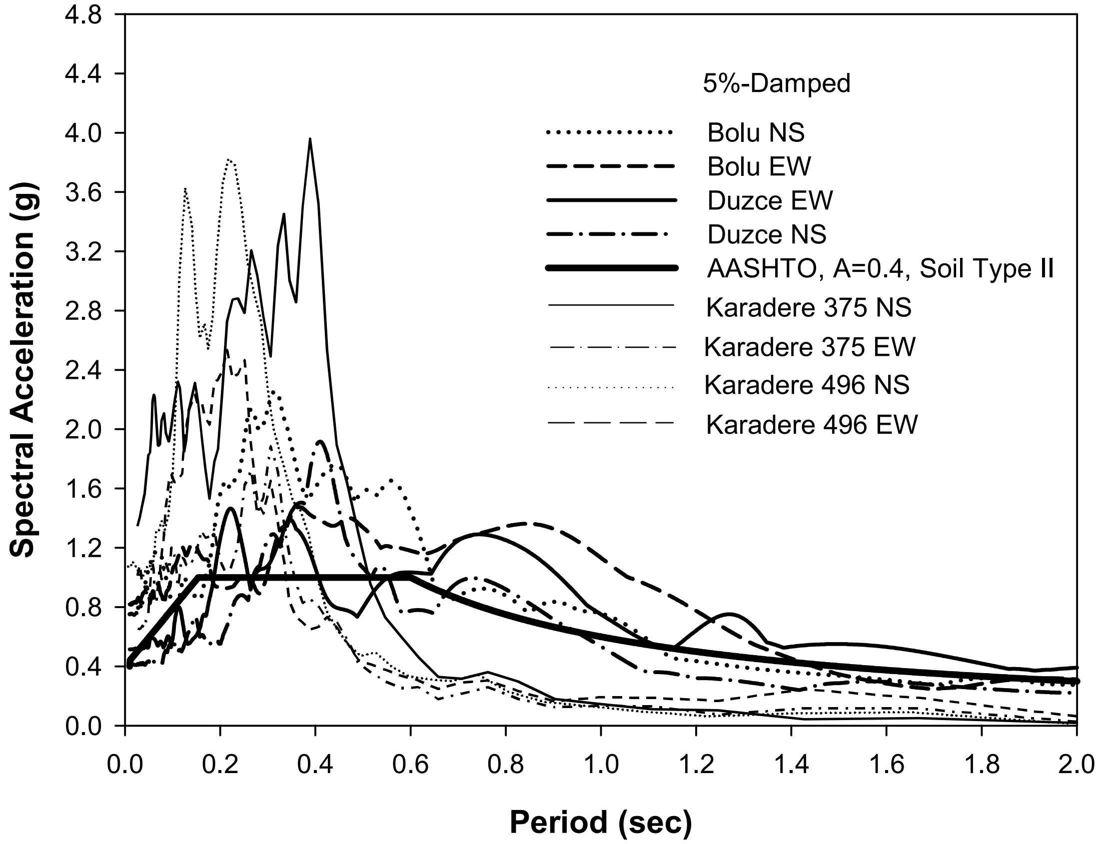

Figure 3-5 Response Spectra of Horizontal Components of Records at Bolu, Duzce and Karadere Stations in 1999 Duzce Earthquake

recorded components at Karadere exhibit very low spectral acceleration values at long periods. Since these records cannot be critical in the analysis of the seismically isolated viaduct, no further analysis with Karadere records was performed.

Figures 3.6 to 3.9 present time histories of the ground motions and the response spectra of each of the horizontal components of the Bolu and Duzce records. The Duzce records contain long duration and long period energy content, which is indicative of basin response and softening of soil media. The Duzce station is located in a one-story building which was undamaged in the earthquake. The building is located in a basin with alluvium up to a depth of about 100 m. The Bolu records are high-intensity ground motions with characteristics indicating effects of directivity and sudden stopping phase of rupture. The

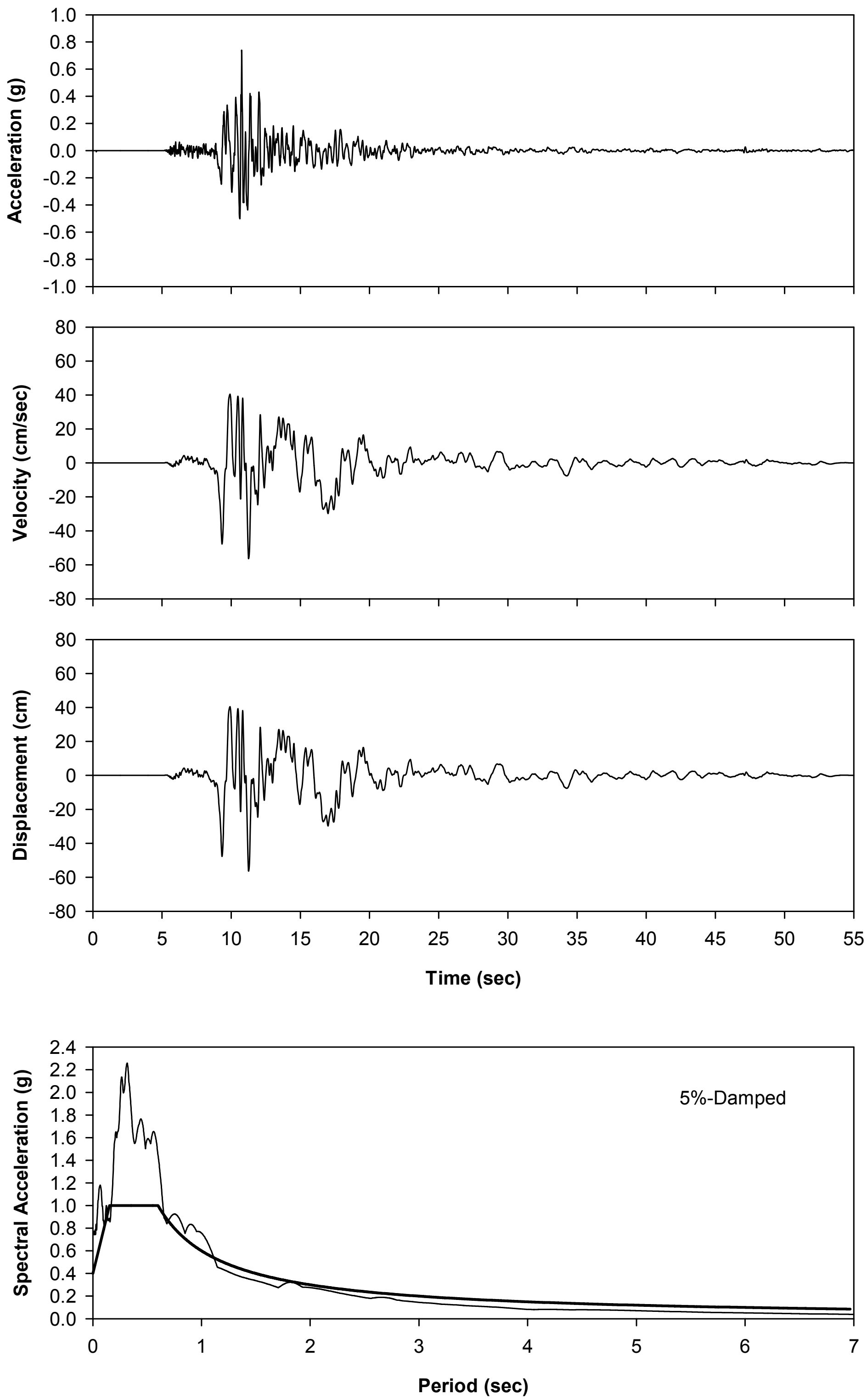

Figure 3-6 Histories of Ground Acceleration, Velocity and Displacement and Response Spectrum of NS Component of Record at Bolu

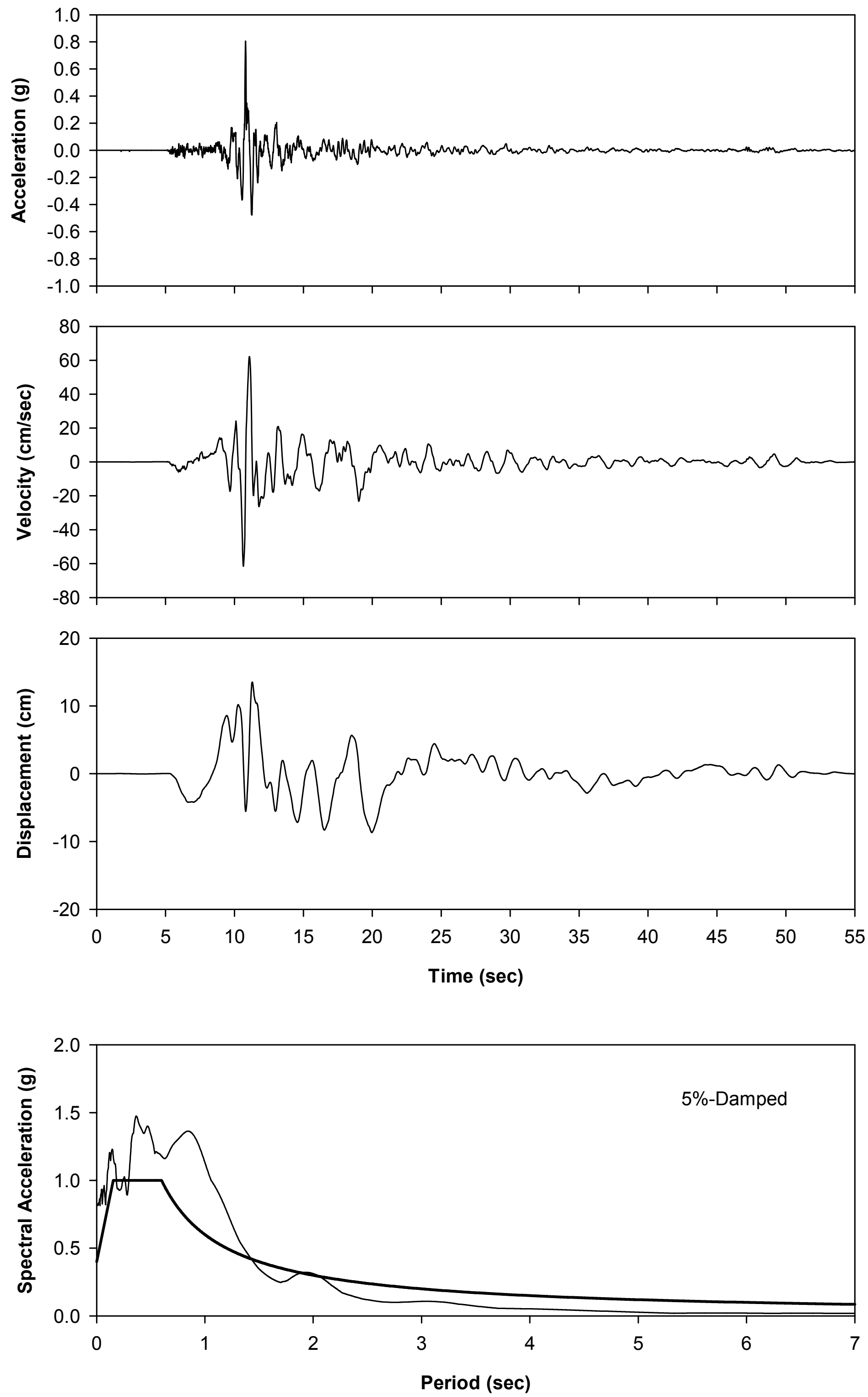

Figure 3-7 Histories of Ground Acceleration, Velocity and Displacement and Response Spectrum of EW Component of Record at Bolu

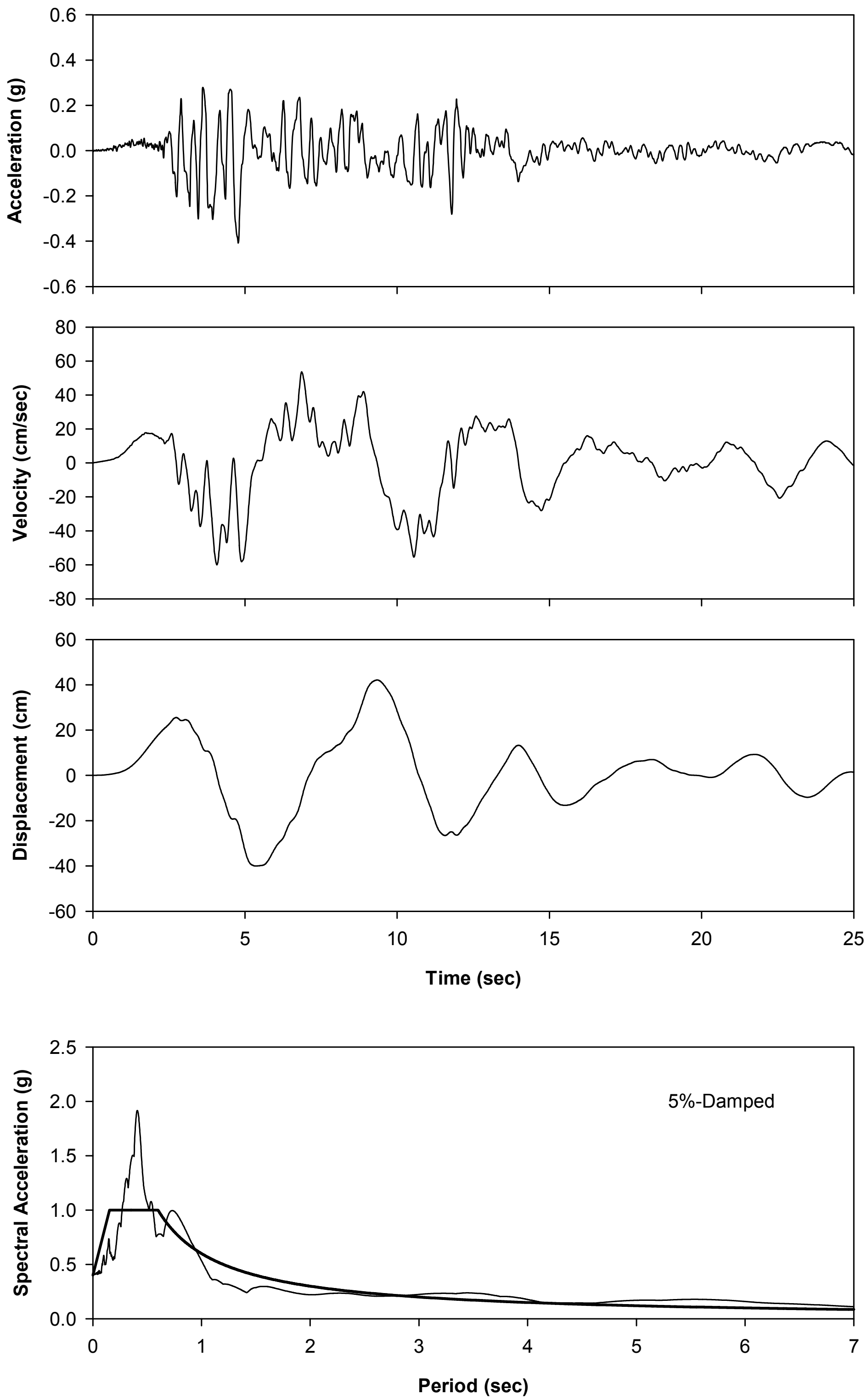

Figure 3-8 Histories of Ground Acceleration, Velocity and Displacement and Response Spectrum of NS Component of Record at Duzce

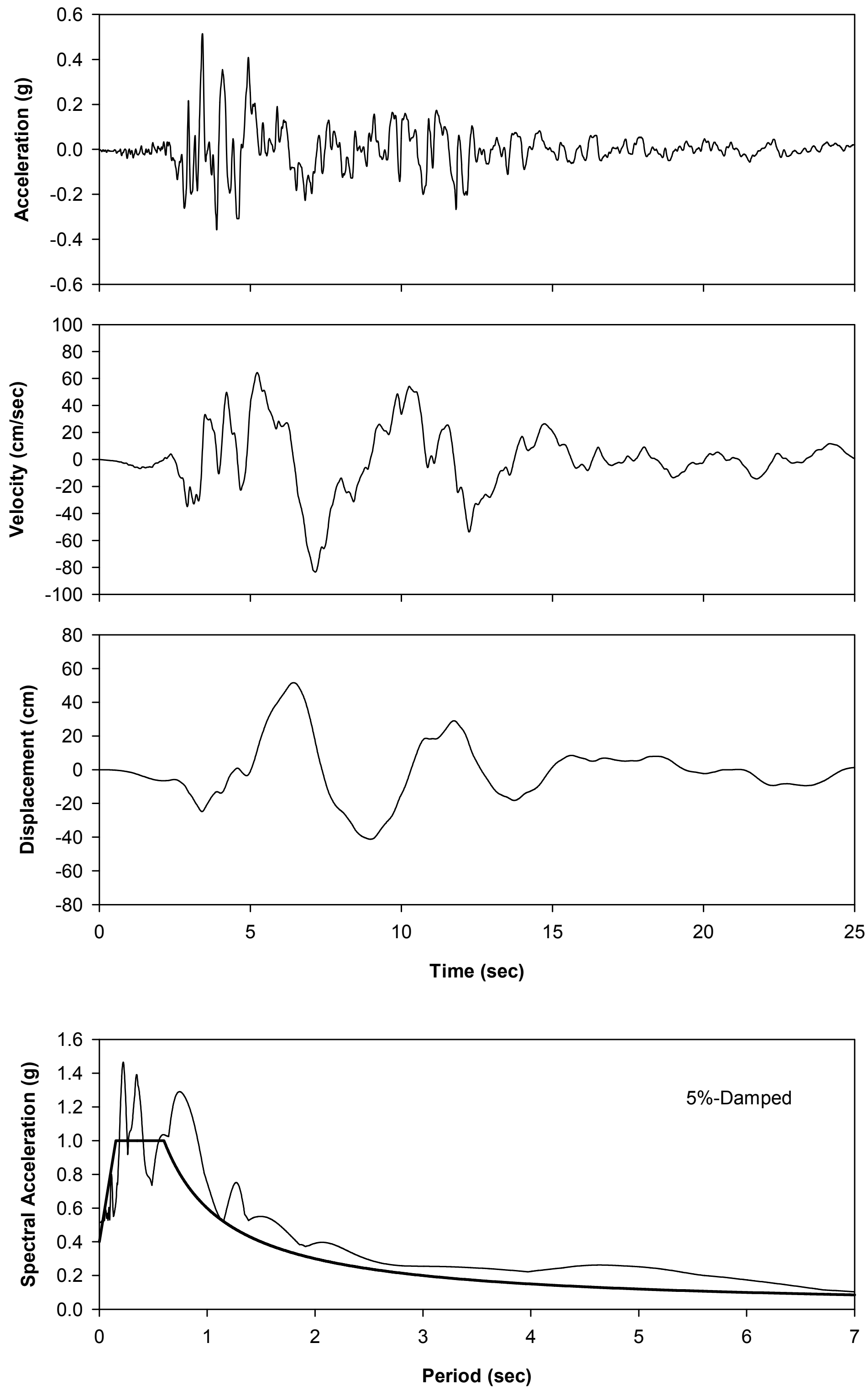

Figure 3-9 Histories of Ground Acceleration, Velocity and Displacement and Response Spectrum of EW Component of Record at Duzce

Bolu station is located in a building founded on soft, deep sediment. The building was severely damaged in the earthquake.

The two records at Bolu and Duzce were used to assess the performance of the Bolu Viaduct during the Duzce earthquake. However, it is recognized that neither of the two records truly represents the conditions experienced by the viaduct in the vicinity of the fault. Accordingly, the ground motion at the Bolu Viaduct site has been simulated on the basis of stipulated earthquake source parameters and this simulated motion was also used for the assessment of the performance of the viaduct. The simulated motion is described in the next section.

3.2.2 Simulated Near-Fault Ground Motion in the Vicinity of the Bolu Viaduct

The simulation of the ground motion in the vicinity of the Bolu Viaduct followed the so-called hybrid methodology. In this methodology, a deterministic approach is utilized to simulate the ground motion in the low frequency range (generally between zero and 1 Hz) and a stochastic process is utilized to simulate the high frequency components of the motion.

The approach described by Anderson and Luco (1983) and Luco and Anderson (1983) was utilized for simulating the low-frequency components of the ground motion. The following parameters were utilized in the simulation: (a) moving ramp-type dislocation function with maximum displacement of 560 cm and rise time of 1 sec (based on inversion for the Duzce earthquake), (b) P-wave velocity of 5 km/sec, (c) S-wave velocity of 2.9 km/sec, (d) rupture velocity of 2.6 km/sec, (e) vertical fault plane and (f) 18 km wide fault plane. Simulations were performed for a point at distance of 500 m from the fault trace.

The simulation of the high frequency content of the motion was based on the methodology of Boore (1983) and Silva and Green (1989) utilizing the following parameters: M_w=7.2, fault distance of 1 km and good soil conditions.

Figures 3.10 and 3.11 present histories of the simulated ground acceleration, velocity and displacement in parallel and in normal to the fault directions. The figures also present the response spectra of the two simulated components and compare these spectra to the

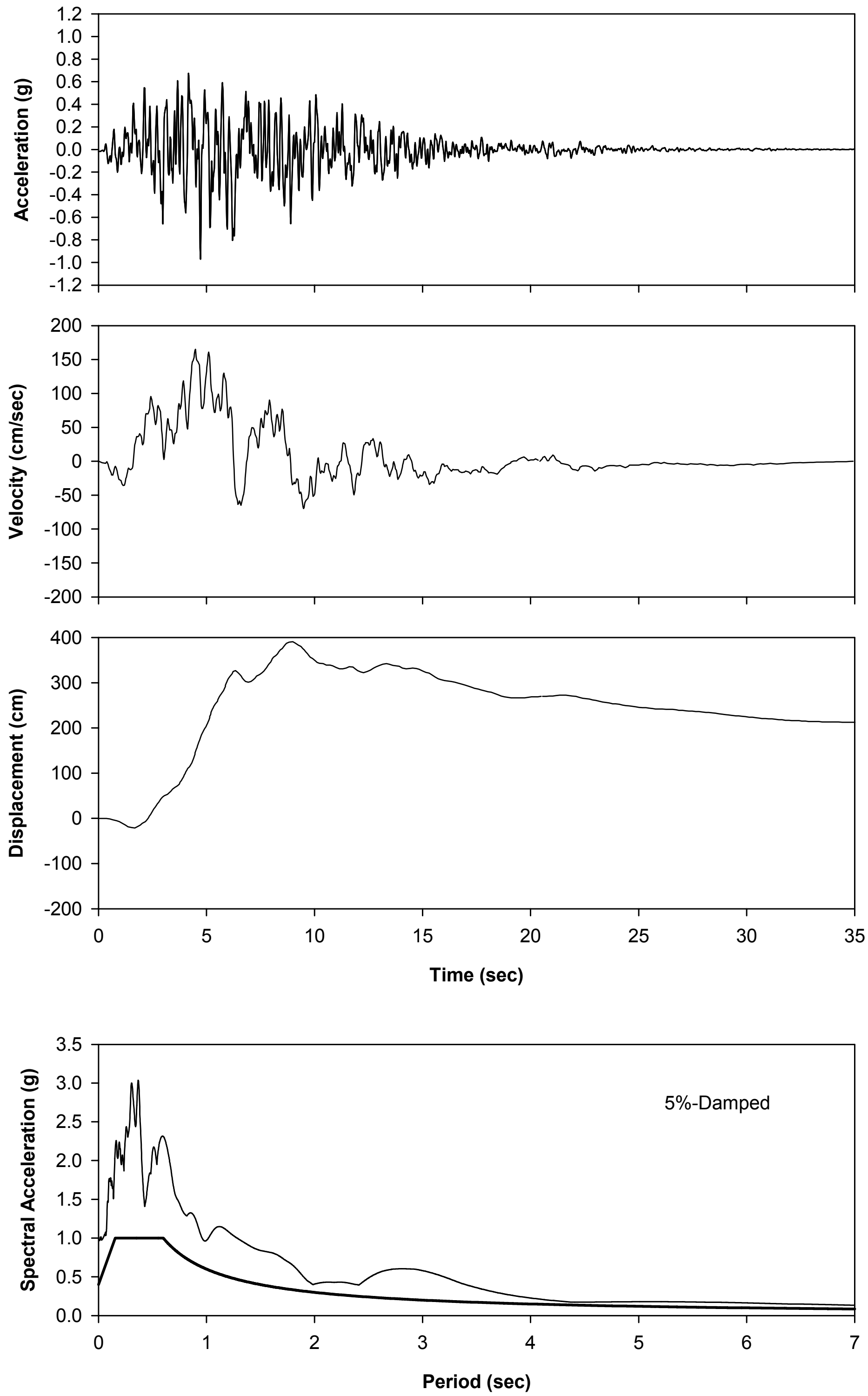

Figure 3-10 Histories of Ground Acceleration, Velocity and Displacement and Response Spectrum of Simulated Motion Parallel to Fault

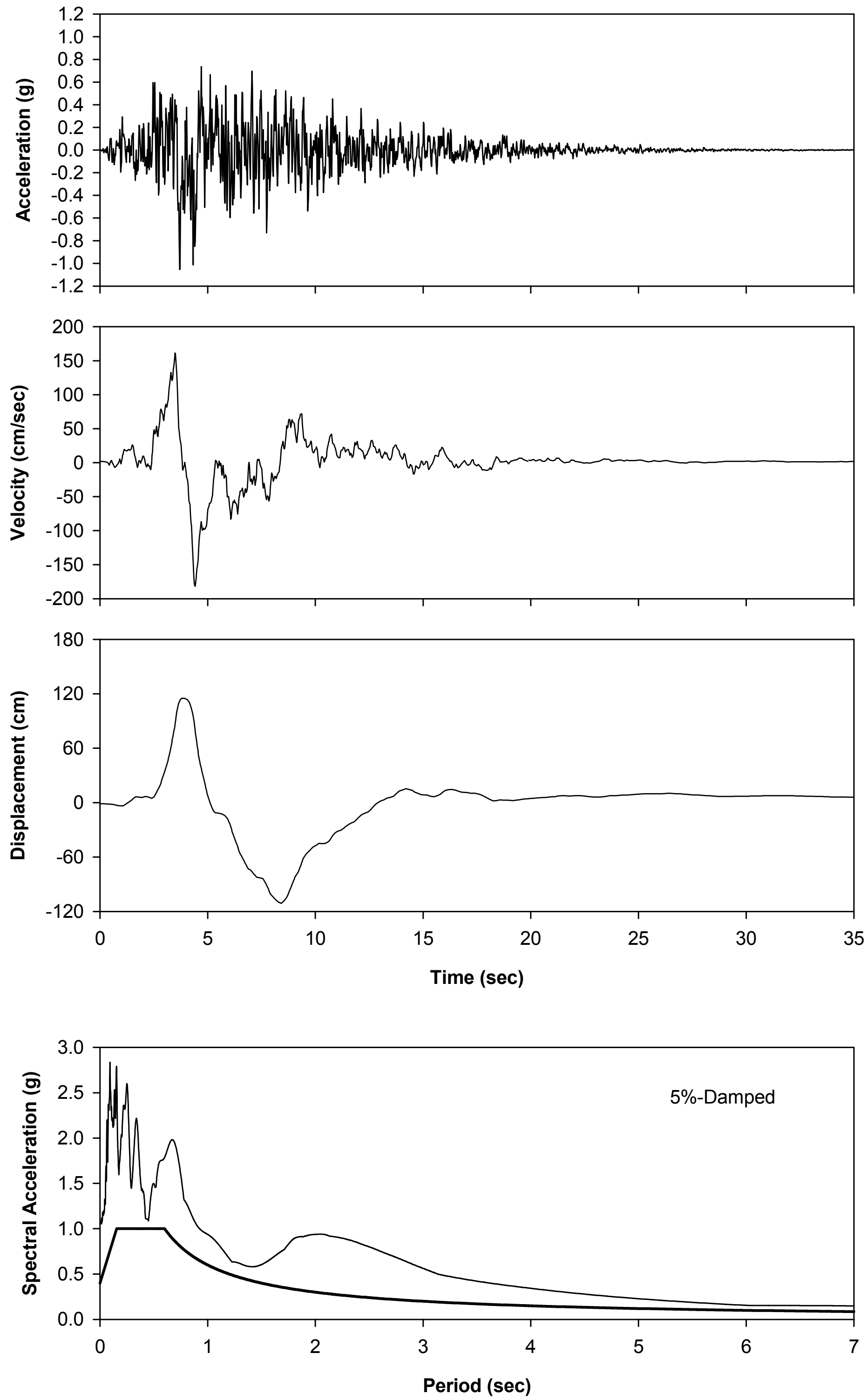

Figure 3-11 Histories of Ground Acceleration, Velocity and Displacement and Response Spectrum of Simulated Motion Normal to Fault

design AASHTO spectrum for the Bolu Viaduct. The simulated motion exhibits clear near-fault characteristics, including forward directivity effects in the fault normal direction and fling effects in the fault parallel direction. The response spectra of the two simulated components are substantially larger than the design spectrum.

3.2.3 Motions Compatible with Design Spectrum in Accordance with AASHTO Guide Specifications

Nonlinear time-history analysis was also performed using three pairs of horizontal ground motion time-history components selected from different recorded events and scaled. The scaling of the time histories was done such that the average of the square root of the sum of the squares (SRSS) of the 5-percent damped spectrum of the scaled components does not fall below 1.3 times the 5-percent damped design spectrum for the period range of 1 to 5 seconds. Table 3.5 presents the three pairs of the selected ground motions along with the scale factors used in the scaling process. This scaling is consistent with the requirements of the 1999 AASHTO Guide Specifications (American Association of State Highway and Transportation Officials, 1999) except that the period range is 1 to 5 sec instead of $0.5T_{eff}$ to $1.5T_{eff}$, where T_{eff} is the effective period. Since the isolation system of the viaduct lacked sufficient restoring force in accordance with the 1999 AASHTO Guide Specifications, the use of the effective period becomes problematic. Accordingly, the period range of 1 to 5 sec was used as described in the 1991 AASHTO Guide Specifications (American Association of State Highway and Transportation Officials, 1991). This allowed for the generation of scaled motions that properly represented the design spectrum without the use of large scale factors.

Table 3-5 Motions Compatible with Design Spectrum in Accordance with AASHTO Guide Specifications for Seismic Isolation Design and Corresponding Scale Factors

Earthquake	Station	Components	Scale Factor
1992 Landers	Yermo	360, 270	1.5
1989 Loma Prieta	Hollister	90, 0	1.5
1971 San Fernando	458	S00W, S90W	1.5

The acceleration response spectra of the scaled ground motions are shown in Figure 3.12. It may be observed that the average of the three SRSS spectra of the scaled motions exceeds or meets the 1.3 times the AASHTO design spectrum in the range of about 0.9 to 7.0 seconds. It should be noted that the scaled motions were developed in the strict sense of the AASHTO Guide Specifications without any frequency scaling of the selected recorded motions.

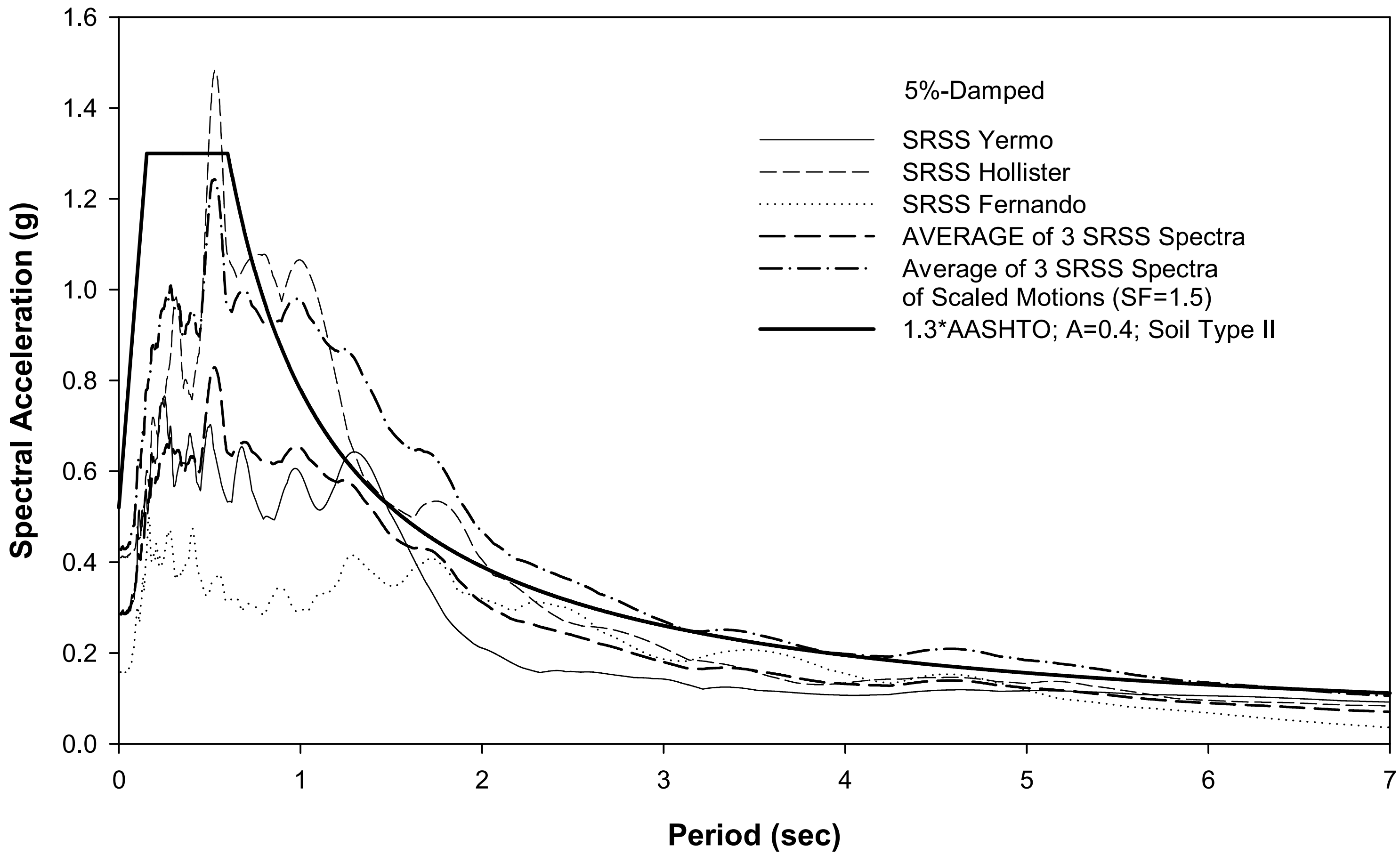

Figure 3-12 SRSS Response Spectra of Scaled Ground Motions Used in Nonlinear Dynamic Analysis

SECTION 4

RESULTS OF ANALYSIS

4.1 Minimum Isolation Displacement Capacity per 1991 AASHTO Guide Specifications

The 1991 AASHTO Guide Specifications for Seismic Isolation Design (American Association of State Highway and Transportation Officials, 1991) encourage a design approach with strong restoring force and penalize designs with weak restoring force. A system with the characteristics depicted in Figure 2.8 and a tributary weight of 14200 kN lacks sufficient restoring force. In accordance with 1991 AASHTO, its displacement capacity should be the greater of $36AS_i$ inches (A=0.4, S_i=1.5) or three times the design displacement. The latter is calculated on the basis of the single mode approach as d_i=263 mm (effective period 2.93 sec, effective damping 0.45, damping coefficient 1.7). Since $36AS_i$ results in 550 mm, the displacement capacity of the isolation system should have been 3×263 or 790 mm.

It is worthy of noting that in accordance with the currently valid AASHTO Guide Specifications (American Association of State Highway and Transportation Officials, 1999), the period of the system on the basis of the tangent stiffness is 7.27 sec (using stiffness of 1080 kN/m, weight of 14200 kN), which exceeds the limit of 6 sec. Accordingly, the use of this system would not be permitted by the 1999 Guide Specifications.

4.2 Isolation System Displacement Demand in the 1999 Duzce Earthquake

Detailed nonlinear dynamic analyses were carried out using the finite element code ANSYS to estimate the response of the seismic-isolated viaduct in the 1999 Duzce earthquake. The analyses were performed using the recorded motions at the Bolu and Duzce stations and the simulated near-fault motion.

Table 4.1 presents the calculated maximum resultant displacement of the isolation system at each pier. Three cases of direction of the seismic excitation were considered in the case of the Bolu and Duzce motions: (a) the recorded East component of the ground motion applied in the longitudinal direction and the recorded North component applied in the transverse direction of the viaduct, (b) the recorded North component applied in the longitudinal direction and the recorded East component applied in the transverse direction of the viaduct, and (c) the recorded East and North components applied at a 25-degree angle with respect to the longitudinal and transverse directions of the viaduct, respectively. The simulated near-fault motion was applied in the fault parallel and fault normal directions assuming that the fault crosses the viaduct at an angle of 25 degrees with respect to the longitudinal direction of the viaduct.

Table 4-1 Calculated Maximum Isolation System Resultant Displacement in Bolu, Duzce and Simulated Near-Fault Motions

Ground Motion	Application Direction		Maximum Isolation System Resultant Displacement (mm)											
	EW Component	**NS Component**	**P10**	**P11**	**P12**	**P13**	**P14**	**P15**	**P16**	**P17**	**P18**	**P19**	**P20**	**Max**
Bolu	Longitudinal Direction	Transverse Direction	325	325	329	337	344	346	342	355	367	380	393	**393**
Bolu	Transverse Direction	Longitudinal Direction	296	311	316	311	317	334	363	358	354	352	353	**363**
Bolu	25° wrt Long. Direction	25° wrt Trans. Direction	321	348	347	344	349	353	349	355	361	368	375	**375**
	EW Component	**NS Component**												
Bolu Truncated	Longitudinal Direction	Transverse Direction	333	335	339	346	352	353	348	361	373	386	399	**399**
Bolu Truncated	Transverse Direction	Longitudinal Direction	293	291	291	290	288	281	266	269	275	282	289	**293**
Bolu Truncated	25° wrt Long. Direction	25° wrt Trans. Direction	330	357	355	351	356	360	355	360	367	374	381	**381**
	EW Component	**NS Component**												
Duzce	Longitudinal Direction	Transverse Direction	441	463	463	463	462	448	401	405	407	404	398	**463**
Duzce	Transverse Direction	Longitudinal Direction	530	525	521	516	515	514	504	511	513	511	509	**530**
Duzce	25° wrt Long. Direction	25° wrt Trans. Direction	439	436	437	438	437	432	412	415	420	424	426	**439**
	Fault Parallel	**Fault Normal**												
Simulated	25° wrt Long. Direction	25° wrt Trans. Direction	1297	1291	1302	1308	1322	1336	1354	1375	1391	1409	1425	**1425**

Table 4.1 also contains results of dynamic analysis in which the ground motion recorded at the Bolu station was used after truncation so that the peak acceleration did not exceed

0.4g. This analysis was performed in order to demonstrate that large ground accelerations are not intrinsically responsible for the response of the isolated viaduct. Furthermore, Figures 4.1 to 4.3 present graphs of the calculated displacement paths of the isolation system (isolation bearings) at selected pier locations during the initial portion of movement for the simulated near-fault, the Bolu station and Duzce station ground motions. Also, Appendix C presents a collection of analysis results that further elucidate the behavior of the isolated viaduct.

The results in Table 4.1, Figures 4.1 to 4.3 and Appendix C reveal the following:

(a) The calculated paths of the isolation system displacement in the Bolu station and the simulated near-fault motions consist of a half cycle of displacement with amplitude of about 100 to 150 mm followed by movement in the opposite direction that exceed the displacement capacity of the bearings. Observations of the scoring on the stainless steel plates of the sliding bearings of the Bolu Viaduct are consistent with the calculated displacement paths (Ghasemi et al., 2000).

(b) The calculated paths of the isolation system displacement in the Duzce station motion show no resemblance to the observed traces on the stainless steel plates of the sliding bearings of the Bolu Viaduct. This observation, together with the longer duration motion and long period energy content seen in the Duzce station record (the Duzce station is located in a basin filled with alluvium up to 100 m deep), suggests that the Duzce record is likely not representative of the conditions at the location of the viaduct.

(c) The peak isolation system resultant displacement in the Bolu station motion does not exceed 400 mm. Analysis using the Bolu station motion truncated to a peak acceleration of 0.4g did not appreciably change the peak response, thus demonstrating that the large accelerations of the Bolu station record are not intrinsically responsible for the response of the viaduct.

(d) The calculated peak displacement response of the isolation system in the simulated near-fault motion is approximately 1400 mm. While this figure may be a conservative estimate, it demonstrates that demand in the Duzce earthquake far exceeded the capacity of the isolation system of the Bolu Viaduct.

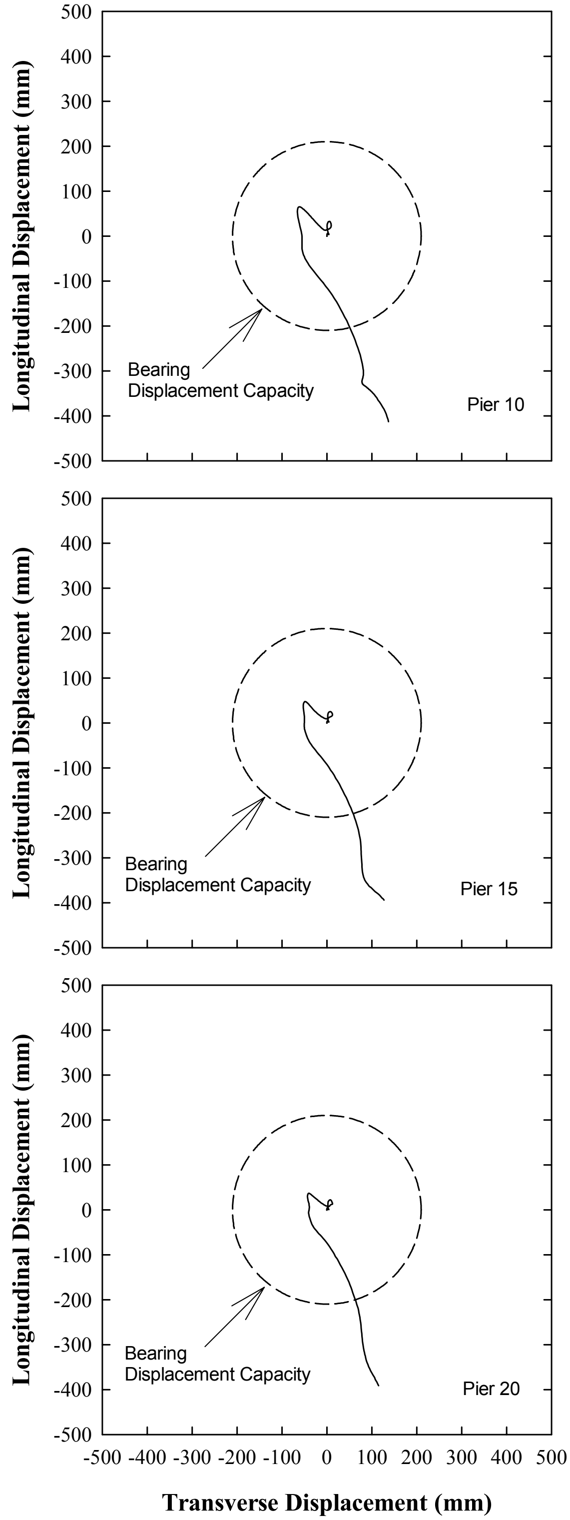

Figure 4-1 Isolation System Displacement Paths at Selected Piers During Initial Portion of Movement for the Simulated Near-Fault Earthquake

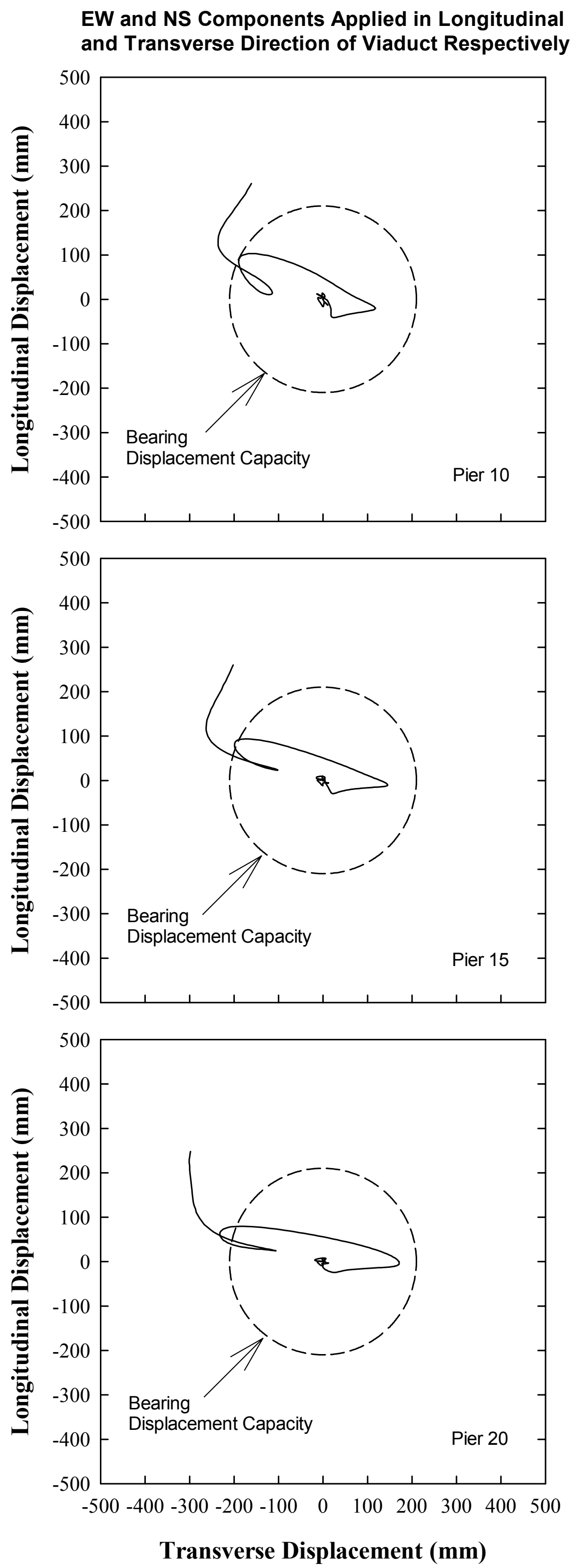

Figure 4-2 Isolation System Displacement Paths at Selected Piers During Initial Portion of Movement for the Ground Motion Recorded at Bolu

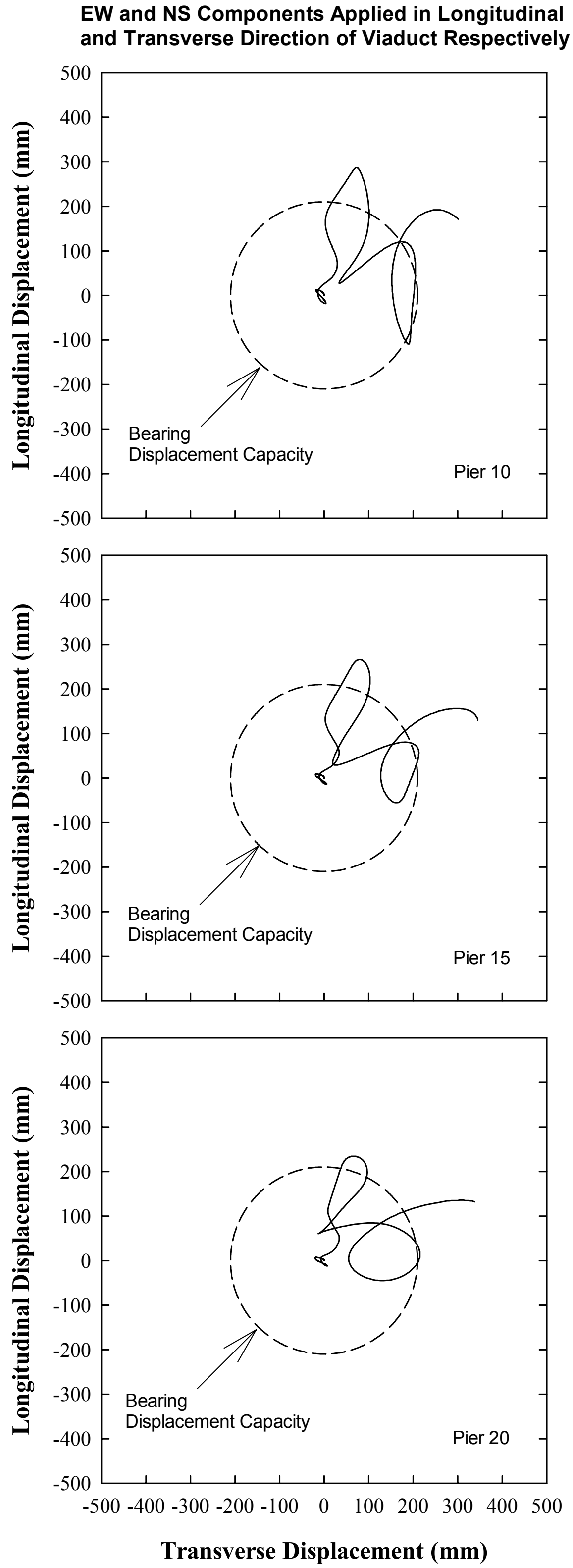

Figure 4-3 Isolation System Displacement Paths at Selected Piers During Initial Portion of Movement for the Ground Motion Recorded at Duzce

(e) The calculated permanent displacement of the isolation system for the Bolu record and for the simulated near-fault motion is small. This is attributed to the existence of a forward velocity pulse followed by backward velocity pulse in these motions, provided of course, that the isolation system displacement capacity exceeded demand.

4.3 Response to Motions Compatible with Design Spectrum

Nonlinear time-history finite element analyses were performed using the three pairs of selected and scaled ground motions compatible with the AASHTO design spectrum.

Each pair of ground motions was applied simultaneously to the model in the longitudinal and transverse directions of the viaduct. Two analyses were performed for each pair of records by switching the directions of application of the two components. The peak resultant displacement at each pier location is presented in Table 4.2. Moreover, a collection of analysis results is presented in Appendix C in graphical form.

Table 4-2 Calculated Maximum Isolation System Resultant Displacement in Ground Motions Scaled to be Representative of Design Spectrum

			Maximum Isolation System Resultant Displacement (mm)											
Scaled Ground Motion	**Component in Longitudinal Direction**	**Component in Transverse Direction**	**P10**	**P11**	**P12**	**P13**	**P14**	**P15**	**P16**	**P17**	**P18**	**P19**	**P20**	**Max**
Landers, Yermo	360	270	487	489	496	506	514	522	531	543	557	569	581	**581**
	270	360	523	519	521	525	527	531	524	521	518	516	515	**531**
Loma Prieta, Hollister	0	90	644	743	742	734	756	790	820	818	815	812	810	**820**
	90	0	587	603	611	615	617	617	612	635	664	687	700	**700**
San Fernando, 458	0	90	363	356	357	361	357	355	355	362	365	367	367	**367**
	90	0	325	341	353	363	372	379	379	385	388	392	397	**397**

The results of analysis of the viaduct for the motions scaled to be representative of the AASHTO design spectrum demonstrate that the displacement capacity of the isolation system should have not been less than 820 mm. This value of the displacement capacity is substantially larger than the 210 mm capacity provided to the isolated viaduct.

SECTION 5

CONCLUSIONS

The results of this study demonstrate the following:

(a) The seismic isolation system for the Bolu Viaduct did not meet the requirements of either the 1991 or the 1999 AASHTO Guide Specifications for Seismic Isolation Design (American Association of State Highway and Transportation Officials, 1991 and 1999).

(b) Analysis of the seismically isolated viaduct with motions scaled in accordance to the AASHTO Guide Specifications resulted in a required displacement capacity of 820 mm. Moreover, a direct application of the minimum requirements of the 1991 AASHTO Guide Specifications resulted in a required displacement capacity of 790 mm. Either value of the displacement capacity is substantially larger than the 210 mm capacity provided.

(c) Analysis of the seismically isolated viaduct for the motions recorded at the nearby Duzce and Bolu stations resulted in isolation system displacements that exceeded capacity by factor of two or more. The Duzce record was deemed not representative of the actual conditions at the viaduct's site primarily due to the lack of resemblance of the calculated displacement paths to those observed. Collaborating evidence was provided by the long duration and long period energy content of the record that indicates basin response rather than near fault characteristics. The Bolu record contained clear near fault characteristics and the calculated displacement paths for this record closely resembled the observed paths. However, the motion was recorded at a distance of approximately 25 km away from the viaduct and, therefore, cannot be deemed representative of the conditions experienced at the viaduct.

(d) Analysis of the seismically isolated viaduct for a simulated near-fault motion with characteristics consistent with the identified fault rupture mechanism and conditions at the viaduct's site resulted in isolation system displacement demands of up to 1400 mm, thus far exceeding capacity.

(e) It appears that had the isolation system been designed in accordance with the 1991 AASHTO Guide Specifications to have a displacement capacity of 820 mm, it would have still suffered damage in the Duzce earthquake given that the displacement demand was likely of the order of 1400 mm.

SECTION 6

REFERENCES

American Association of State Highway and Transportation Officials (1991), "Guide Specifications for Seismic Isolation Design", Washington, D.C.

American Association of State Highway and Transportation Officials (1999), "Guide Specifications for Seismic Isolation Design", Washington, D.C.

American Association of State Highway and Transportation Officials (1992), "Standard Specifications for Highway Bridges", 15th Edition, Washington, D.C.

Anderson, J.and Luco, J. (1983), "Parametric Study of Near-Field Ground Motion for a Strike Slip Dislocation Model", Bulletin of Seismological Society of America, Vol. 73, pp. 23-43.

Astaldi S.p.A. (Contractors) (2000), Miscellaneous documents and diagrams related to the Bolu Viaduct.

Barr, J., Sanders, P., and Davey, S. (2001), " Effect of Kocaeli (M_w 7.4) and Duzce (M_w 7.2) Earthquakes on Seismically Isolated Viaducts on the Istanbul to Ankara Motorway, Turkey", 5th World Congress on Joints and Bearings, 8-11 October 2001, Rome.

Boore, D. (1983), "Stochastic Simulation of High-Frequency Ground Motions Based on Seismological Models of the Radiated Spectra", Bulletin of Seismological Society of America, Vol. 73, No. 6, pp. 1865-1894.

Calvi, G., Priestley, M., and Germani, G. (2001), "Bearing and Isolation Systems for a Long Viaduct Crossing an Active Fault", 7th International Seminar on Seismic Isolation, Passive Energy Dissipation and Active Control of Vibration of Structures, Assisi, Italy, October 2-5, 2001.

Ciampi, V., and Marioni, A. (1991), "New Types of Energy Dissipating Devices for Seismic Protection of Bridges" Proc., Third World Congress on Joint Sealing and

Bearing Systems for Concrete Structures, Vol. 2, National Center for Earthquake Engineering Research, State Univ. of New York at Buffalo, N.Y., pp. 1225-1245.

Erdik, M. (2000), "Report on 1999 Kocaeli and Duzce (Turkey) Earthquakes". http://www.koeri.boun.edu.tr/earthqk/Kocaelireport.pdf

Ghasemi, H., Cooper, J., Imbsen, R., Piskin, H., Inal, F., and Tiras, A. (2000), "The November 1999 Duzce Earthquake: Post-Earthquake Investigation of the Structures on the TEM", Publication No, FHWA-RD-00-146. http://www.tfhrc.gov/structur/00-146.pdf

Luco, J. and Anderson, J. (1983), "Steady State Response of an elastic half-space to a Moving Dislocation of Finite Width", Bulletin of Seismological Society of America, Vol. 73, pp. 1-22.

Marioni, A. (1997), "Development of a New Type of Hysteretic Damper for the Seismic Protection of Bridges", Proc. Fourth World Congress on Joint Sealants and Bearing Systems for Concrete Structtures, SP-164, Vol. 2, American Concrete Institute, pp. 955-976.

Marioni, A. (2000), "Behaviour of Large Base Isolated Prestressed Concrete Bridges During the Recent Exceptional Earthquakes in Turkey". http://192.107.65.2/GLIS/HTML/gn/turchi/g5turchi.htm

Priestley, M., and Calvi, G. (1996), "Seismic Design and Retrofit of Bridges", John Wiley & Sons, Inc.

Silva, W. and Green, R. (1989), "Magnitude and Distance Scaling of Response Spectral Shapes for Rock Sites with Applications to North American Tectonic Environment", Earthquake Spectra, 5, 591-623.

Swanson Analysis Systems IP, Inc. (1996), "ANSYS Finite Element Program and User's Manual", Version 5.3, Houston, PA.

Tsopelas, P., and Constantinou, M. (1997), "Study of Elastoplastic Bridge Seismic Isolation System", Journal of Structural Engineering, ASCE, 123, (4), pp.489-498.

Xiao, Y., Yaprak, T., Tokgozoglu, F. (2000), “Observations of the November 12, 1999, Duzce Earthquake”.
http://www.usc.edu/dept/civil_eng/structural_lab/eq-rp/Turkey-99-11-12.html

Purdue Univ. (2000), “Damage to Bolu Viaduct from Recent Earthquakes in Turkey”.
http://bridge.ecn.purdue.edu/~anatolia/viaduct/research/report.html

Universita di Pavia “Certificato di Prova N.23414/184” Dipartimento di Meccanica Strutturale, June, 1993.

APPENDIX A

FINITE ELEMENT MODEL IN ANSYS

Finite Element Model in ANSYS

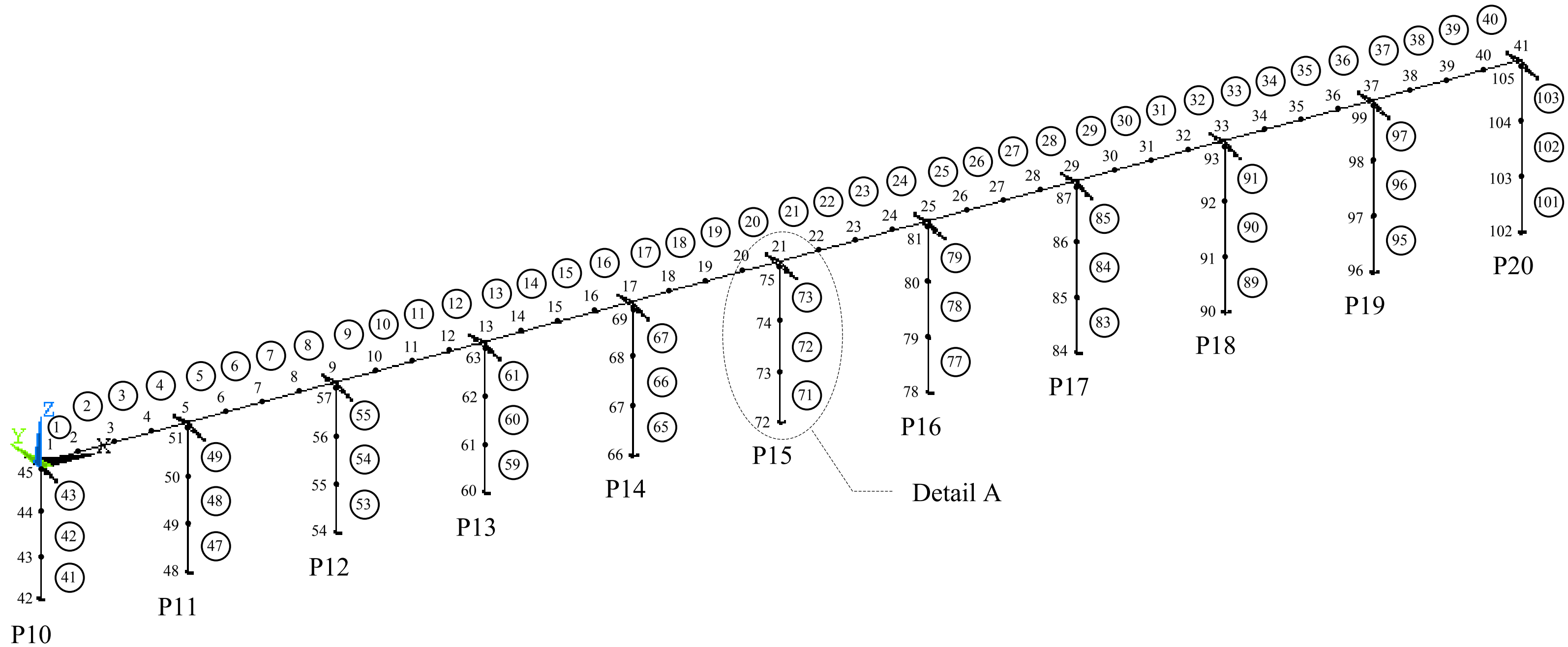

Detail A

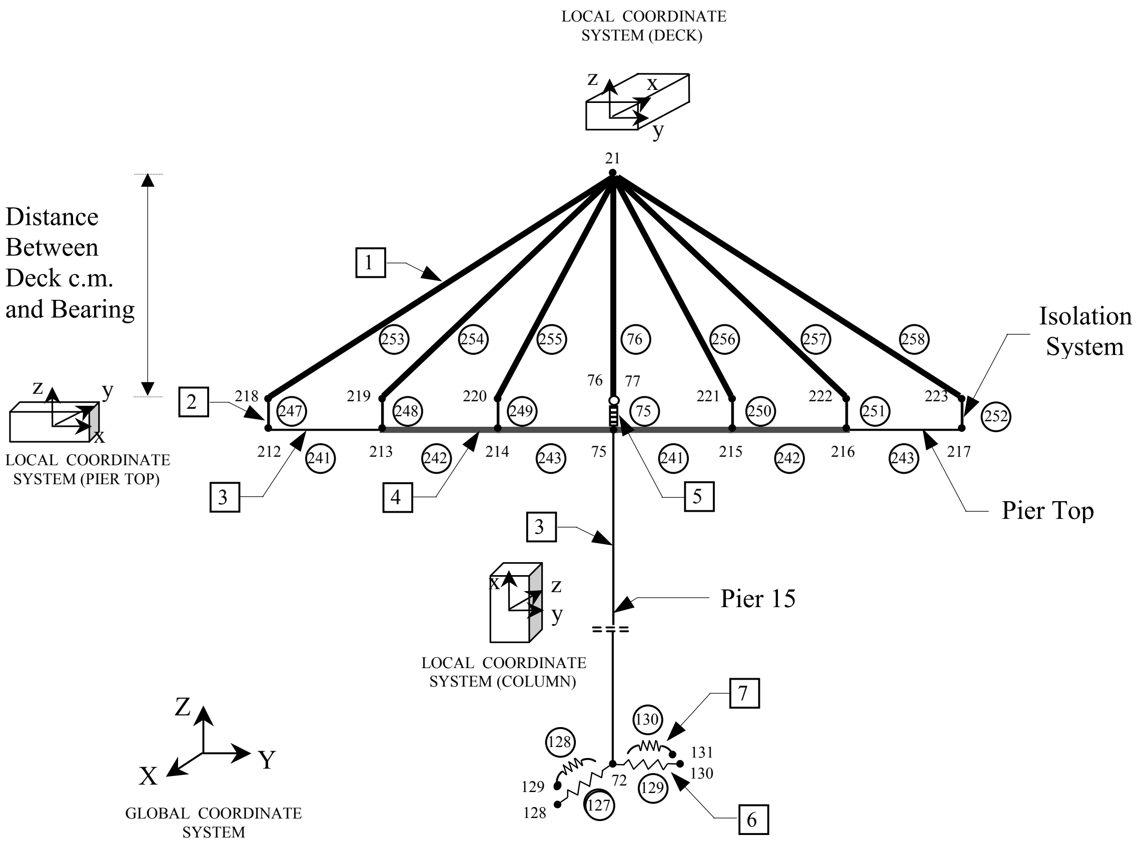

1 Very Stiff Elastic Beam Elements without Density (BEAM4)

2 Very Stiff Truss Elements (LINK8)

3 Elastic Beam Elements (BEAM4)

4 Very Stiff Elastic Beam Elements with Density (BEAM4)

5 Bilinear Hysteretic Pipe Element (PIPE20)

6 Translational Springs (COMBIN14)

7 Rotational Springs (COMBIN14)

APPENDIX B

RESULTS OF MODAL ANALYSIS

Mode 1: Frequency = 0.284 Hz

Modal Participation Mass Fractions:

X	Y	Z	RotX	RotY	RotZ
0.706	0.000	0.000	0.000	0.000	0.000

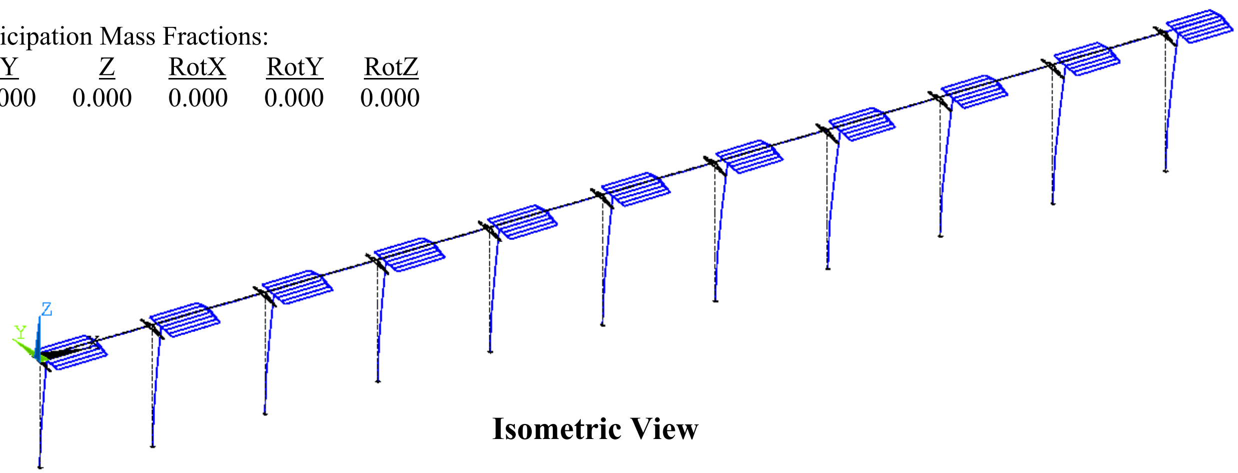

Isometric View

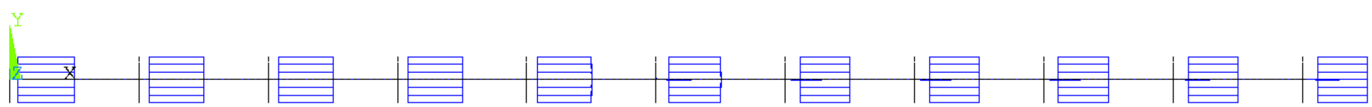

Plan View

Mode 2: Frequency = 0.298 Hz

Modal Participation Mass Fractions:

X	Y	Z	RotX	RotY	RotZ
0.000	0.842	0.000	0.725	0.000	0.988

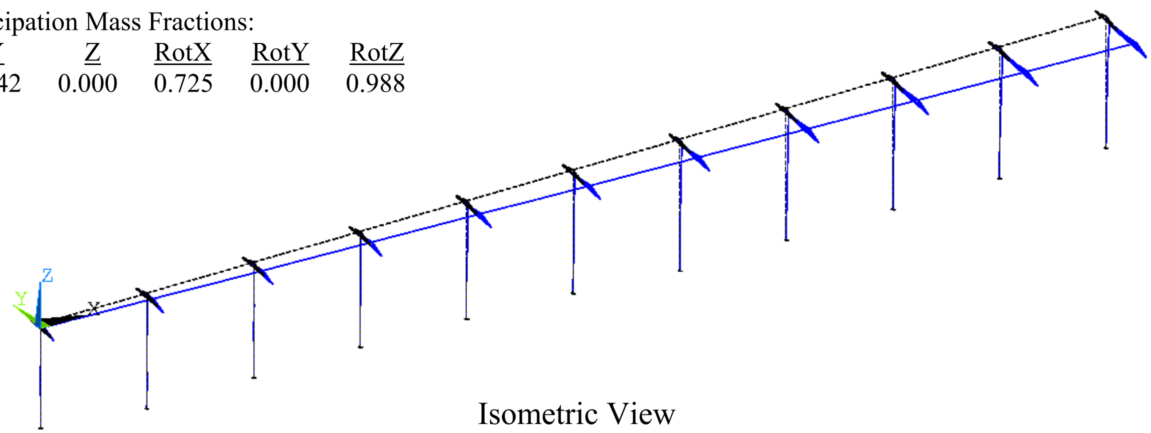

Isometric View

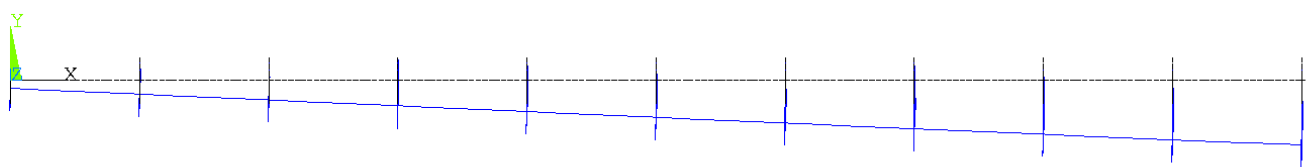

Plan View

Mode 3: Frequency = 0.305 Hz

Modal Participation Mass Fractions:

X	Y	Z	RotX	RotY	RotZ
0.000	0.158	0.000	0.272	0.000	0.011

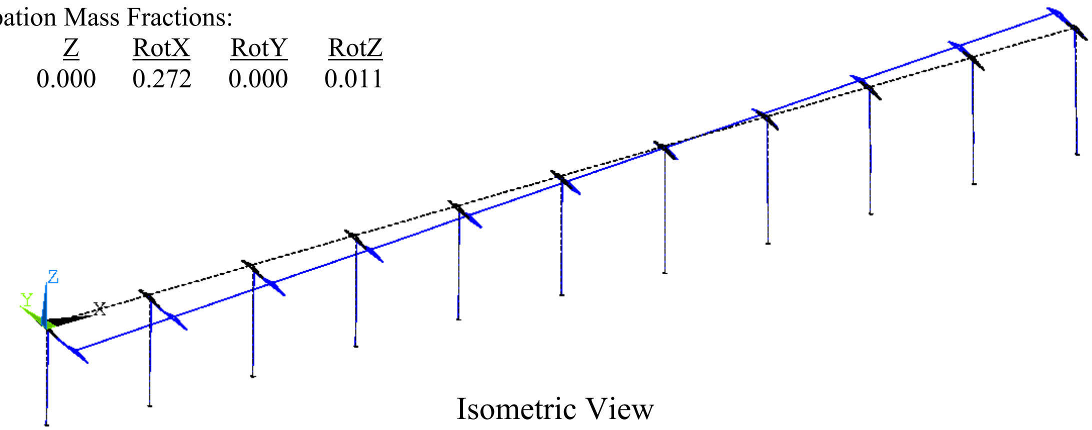

Isometric View

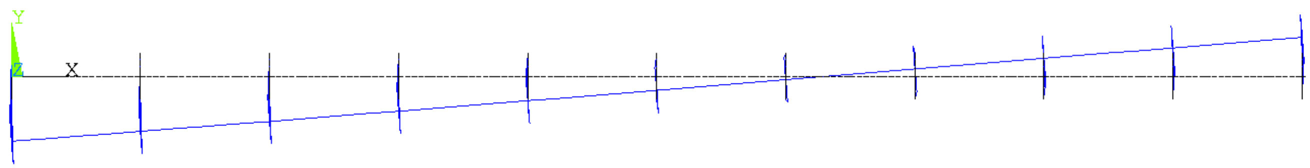

Plan View

Mode 4: Frequency = 0.495 Hz

Modal Participation Mass Fractions:

X	Y	Z	RotX	RotY	RotZ
0.000	0.000	0.000	0.000	0.072	0.000

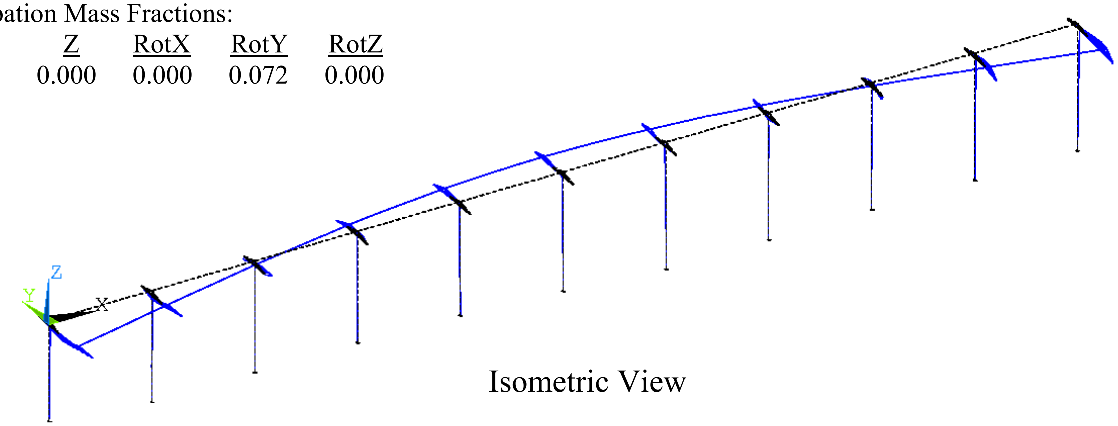

Isometric View

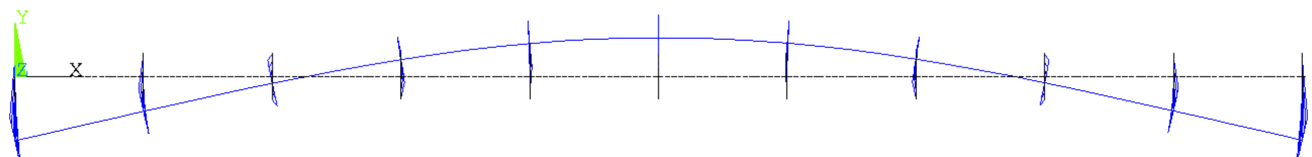

Plan View

Mode 5: Frequency = 0.717 Hz

Modal Participation Mass Fractions:

X	Y	Z	RotX	RotY	RotZ
0.000	0.000	0.000	0.000	0.140	0.000

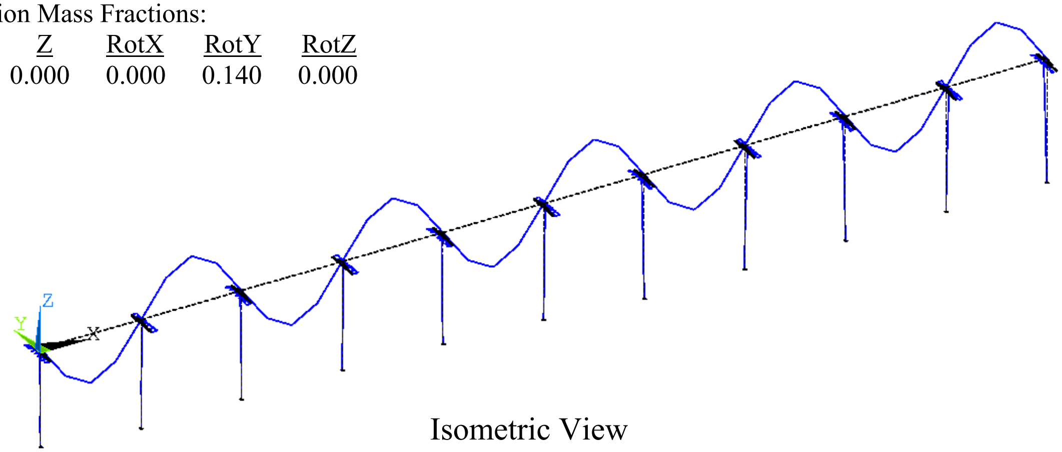

Isometric View

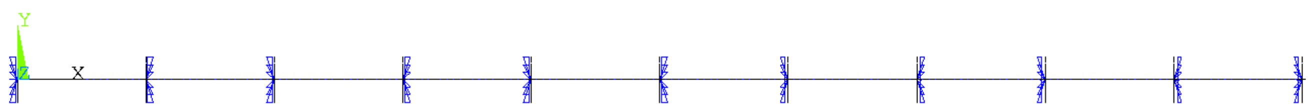

Plan View

Mode 6: Frequency = 0.738 Hz

Modal Participation Mass Fractions:

X	Y	Z	RotX	RotY	RotZ
0.000	0.000	0.250	0.000	0.150	0.000

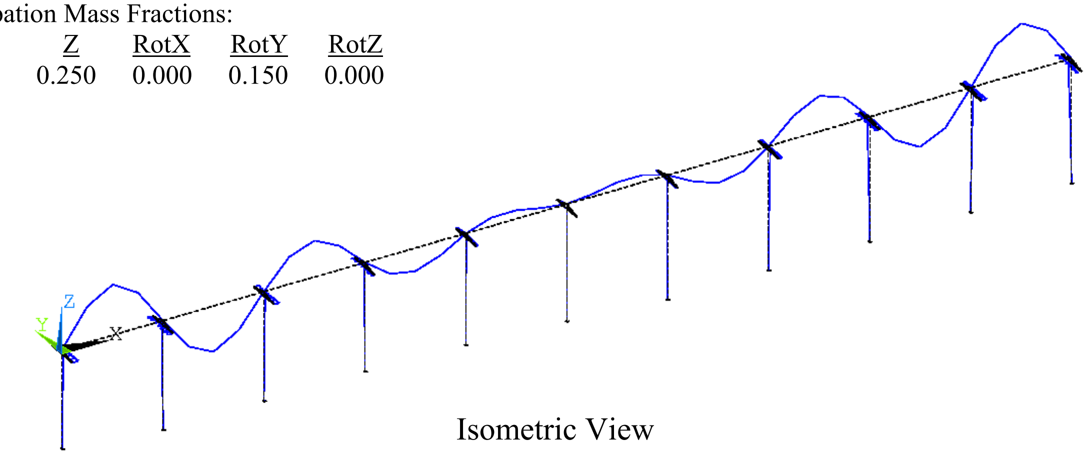

Isometric View

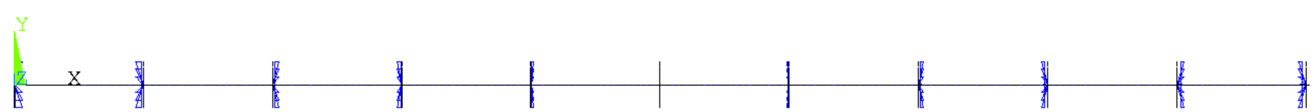

Plan View

Mode 7: Frequency = 0.795 Hz

Modal Participation Mass Fractions:

X	Y	Z	RotX	RotY	RotZ
0.000	0.000	0.000	0.000	0.166	0.000

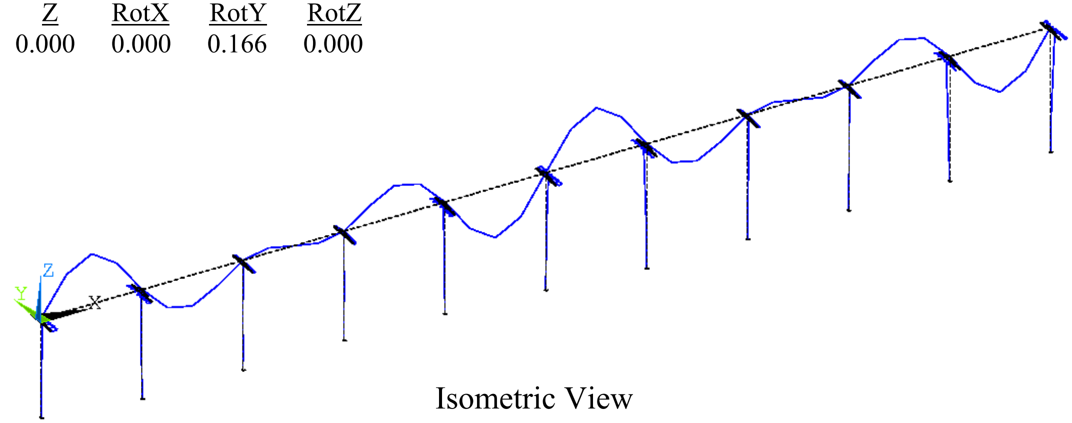

Isometric View

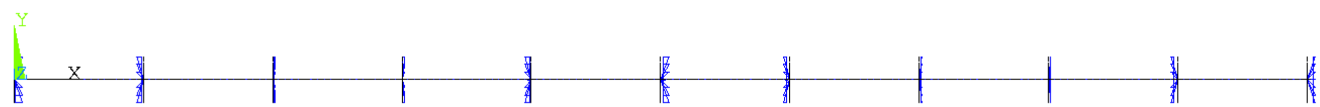

Plan View

Mode 8: Frequency = 0.882 Hz

Modal Participation Mass Fractions:

X	Y	Z	RotX	RotY	RotZ
0.000	0.000	0.294	0.000	0.000	0.000

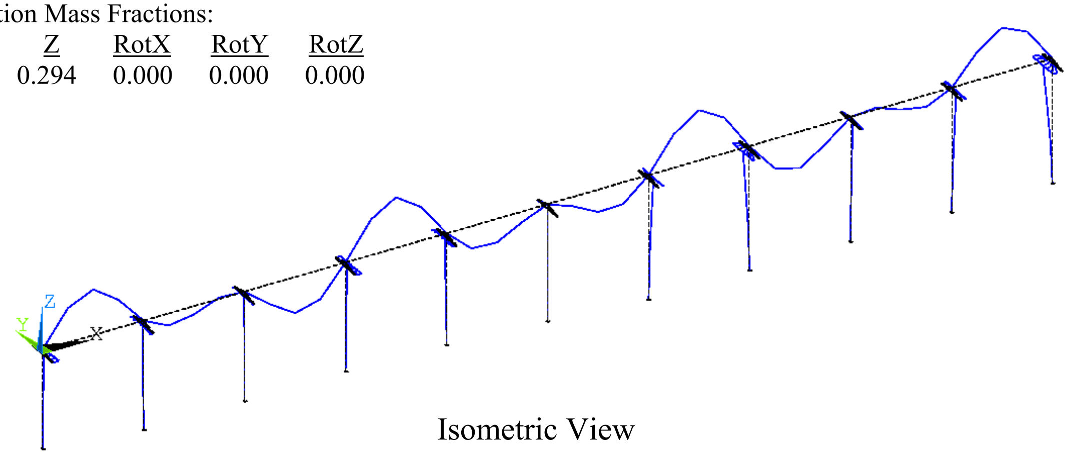

Isometric View

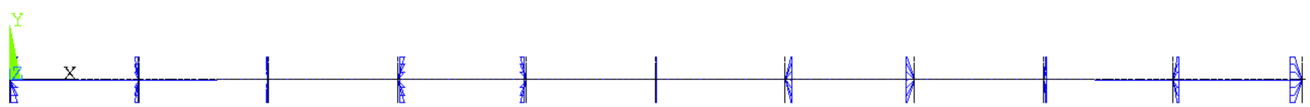

Plan View

Mode 9: Frequency = 0.949 Hz

Modal Participation Mass Fractions:

X	Y	Z	RotX	RotY	RotZ
0.011	0.000	0.000	0.000	0.000	0.000

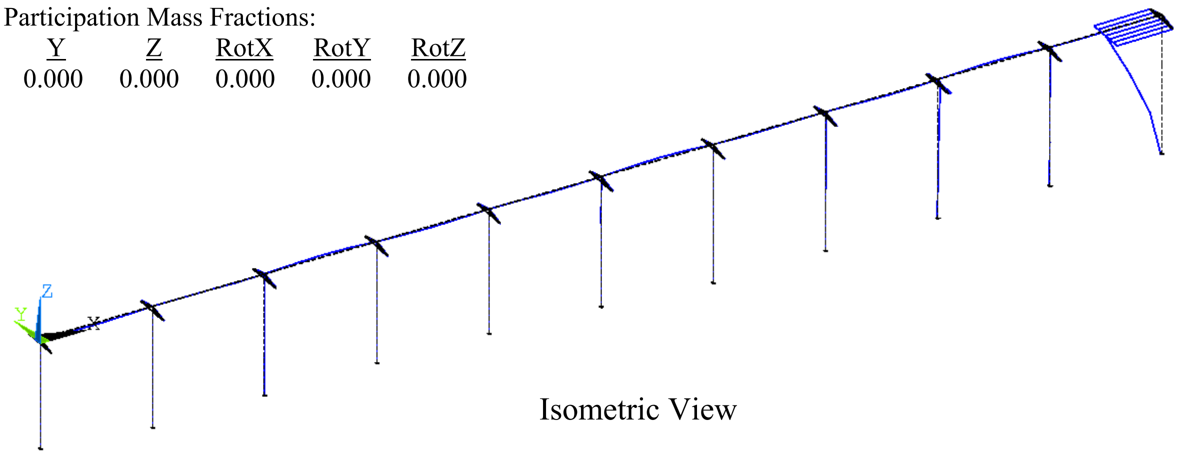

Isometric View

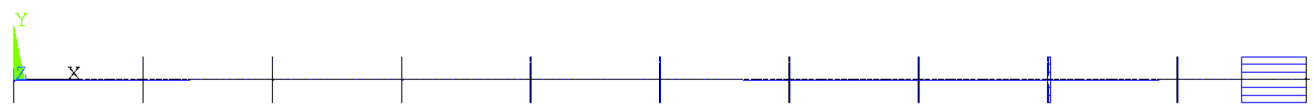

Plan View

Mode 10: Frequency = 0.959 Hz

Modal Participation Mass Fractions:

X	Y	Z	RotX	RotY	RotZ
0.022	0.000	0.002	0.000	0.017	0.000

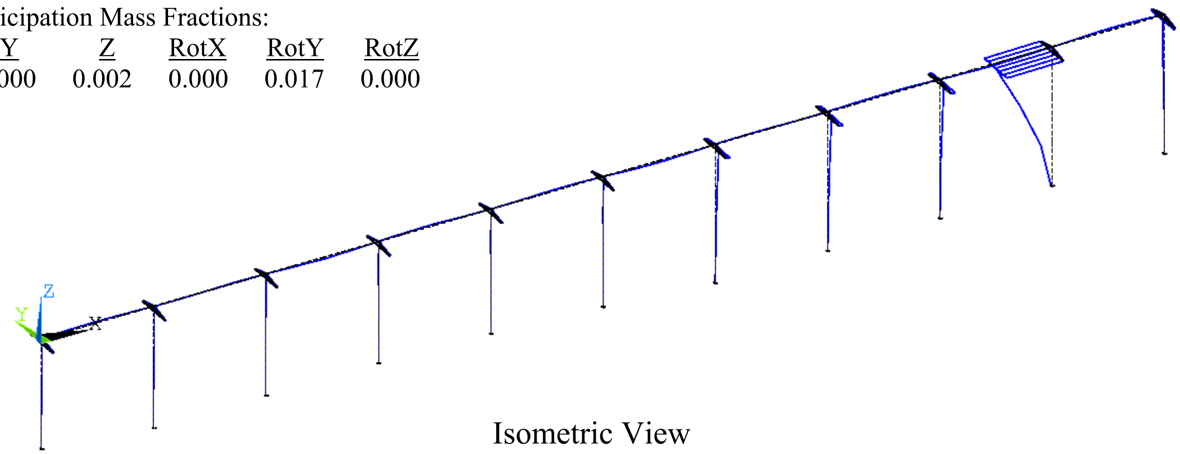

Isometric View

Plan View

Mode 11: Frequency = 0.966 Hz

Modal Participation Mass Fractions:

X	Y	Z	RotX	RotY	RotZ
0.019	0.000	0.000	0.000	0.000	0.000

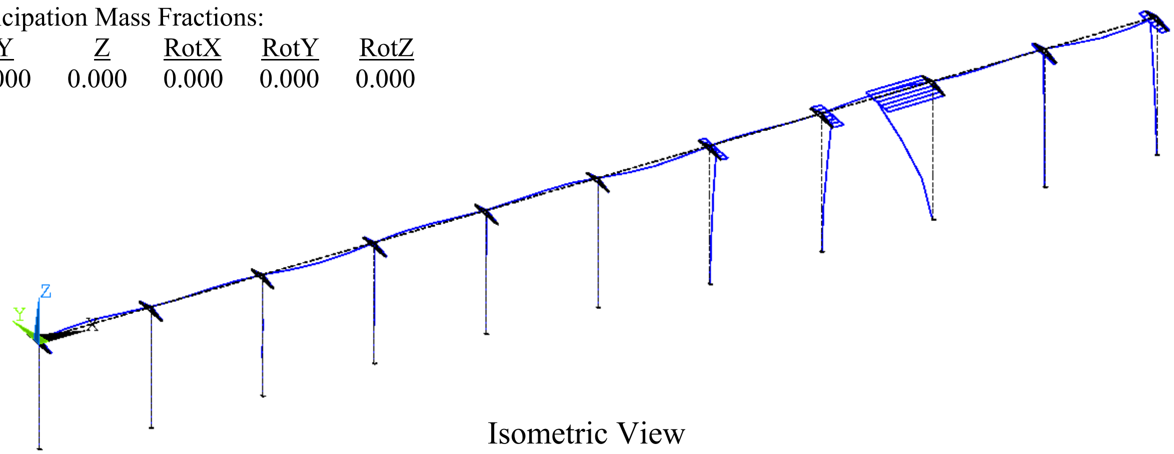

Isometric View

Plan View

Mode 12: Frequency = 0.974 Hz

Modal Participation Mass Fractions:

X	Y	Z	RotX	RotY	RotZ
0.042	0.000	0.001	0.000	0.000	0.000

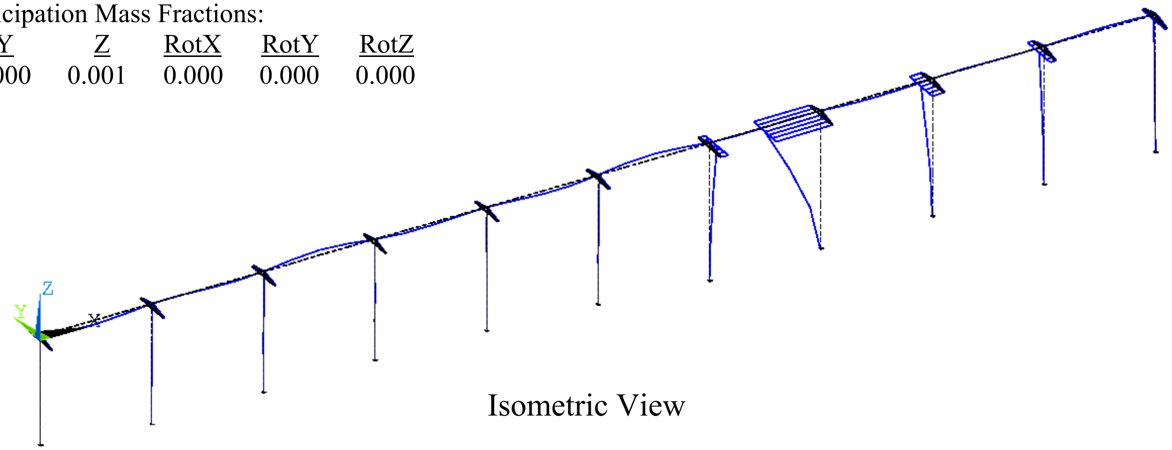

Isometric View

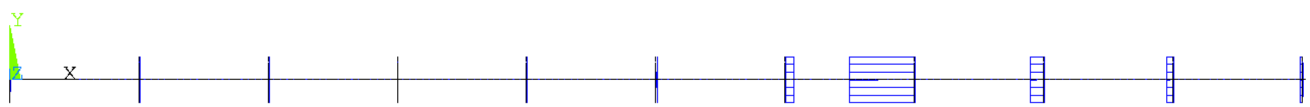

Plan View

Mode 13: Frequency = 0.980 Hz

Modal Participation Mass Fractions:

X	Y	Z	RotX	RotY	RotZ
0.055	0.000	0.001	0.000	0.193	0.000

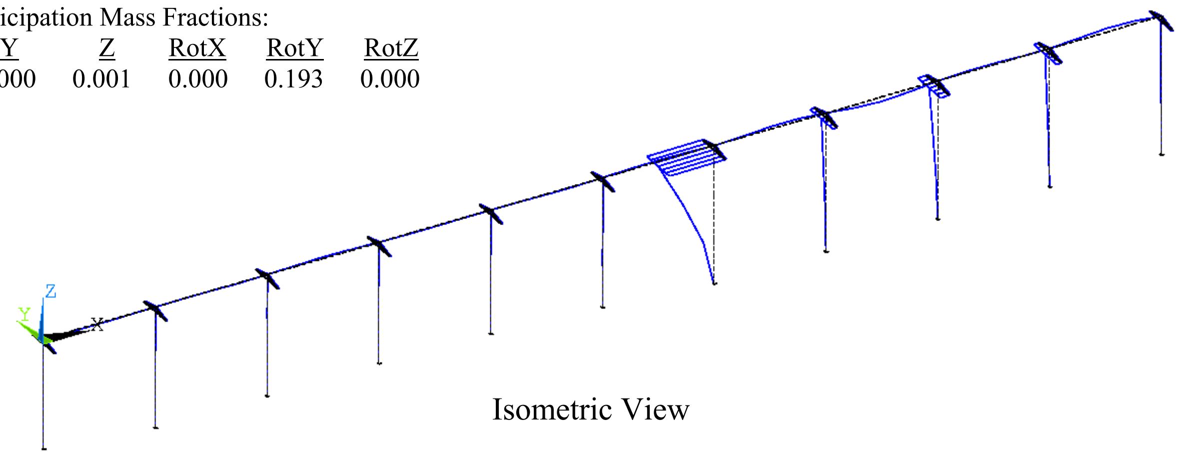

Isometric View

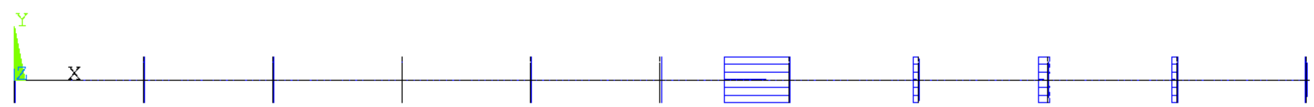

Plan View

Mode 14: Frequency = 0.995 Hz

Modal Participation Mass Fractions:

X	Y	Z	RotX	RotY	RotZ
0.002	0.000	0.000	0.000	0.000	0.000

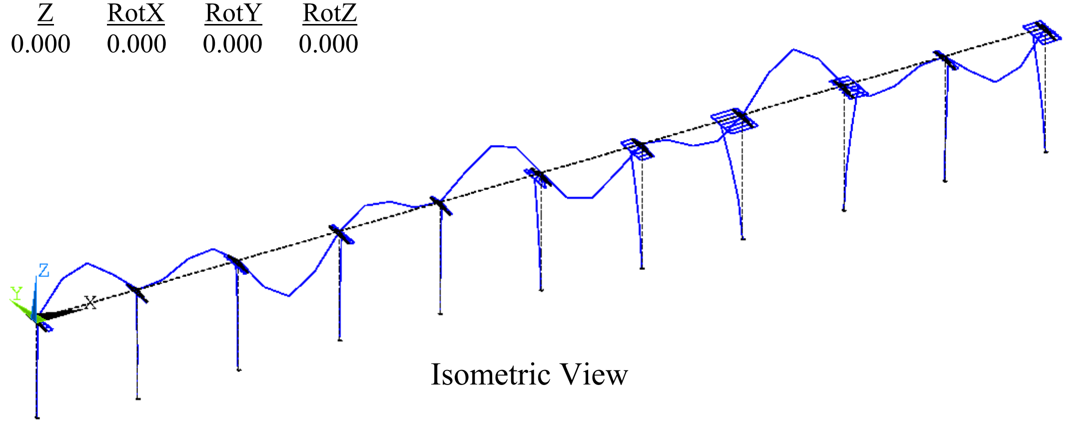

Isometric View

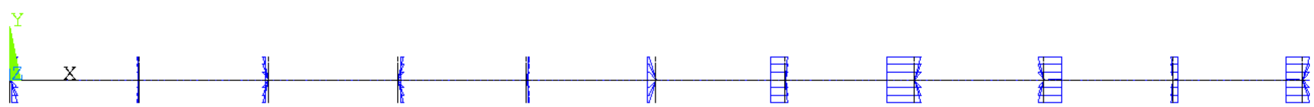

Plan View

<u>Mode 15</u>: Frequency = 1.075 Hz

Modal Participation Mass Fractions:

X	Y	Z	RotX	RotY	RotZ
0.036	0.000	0.000	0.000	0.000	0.000

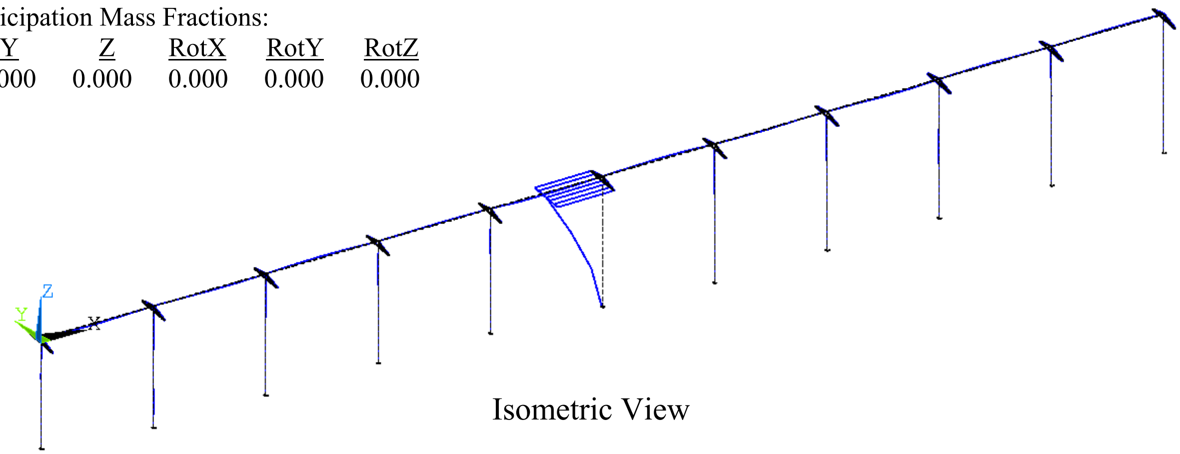

Isometric View

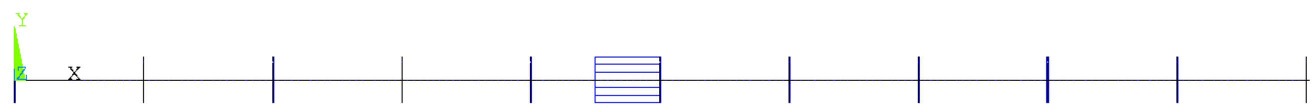

Plan View

Mode 16: Frequency = 1.100 Hz

Modal Participation Mass Fractions:

X	Y	Z	RotX	RotY	RotZ
0.000	0.000	0.000	0.003	0.252	0.011

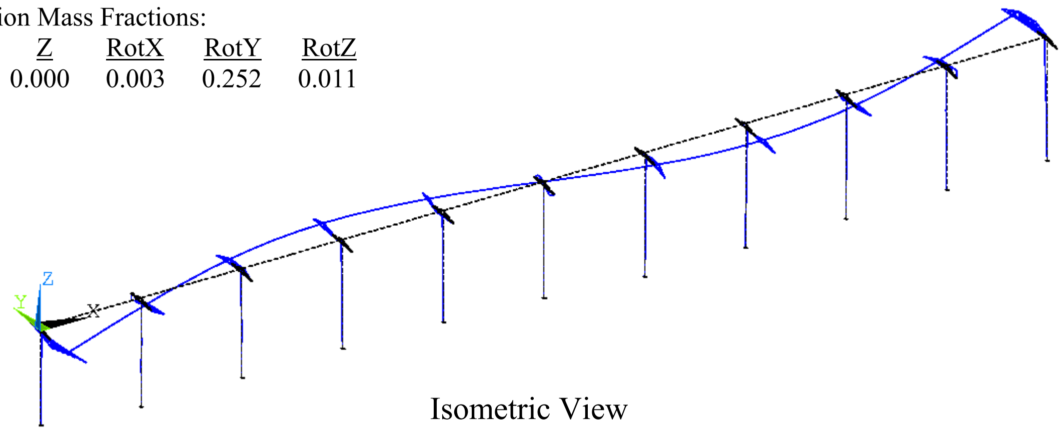

Isometric View

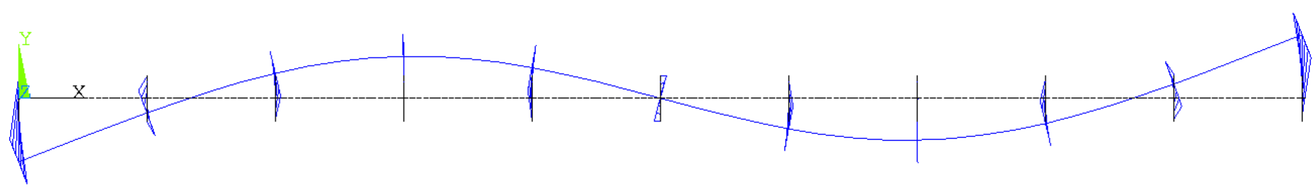

Plan View

Mode 17: Frequency = 1.117 Hz

Modal Participation Mass Fractions:

X	Y	Z	RotX	RotY	RotZ
0.000	0.000	0.439	0.000	0.000	0.000

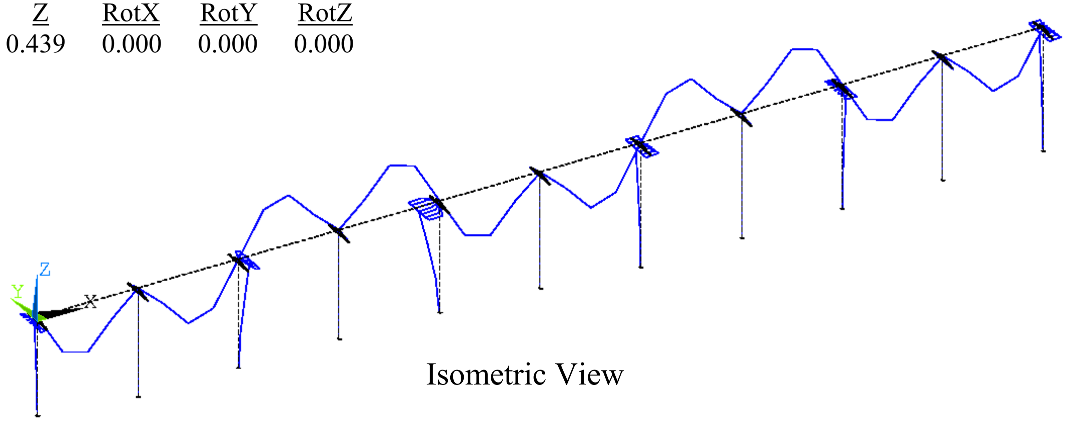

Isometric View

Plan View

Mode 18: Frequency = 1.150 Hz

Modal Participation Mass Fractions:

X	Y	Z	RotX	RotY	RotZ
0.034	0.000	0.009	0.000	0.001	0.000

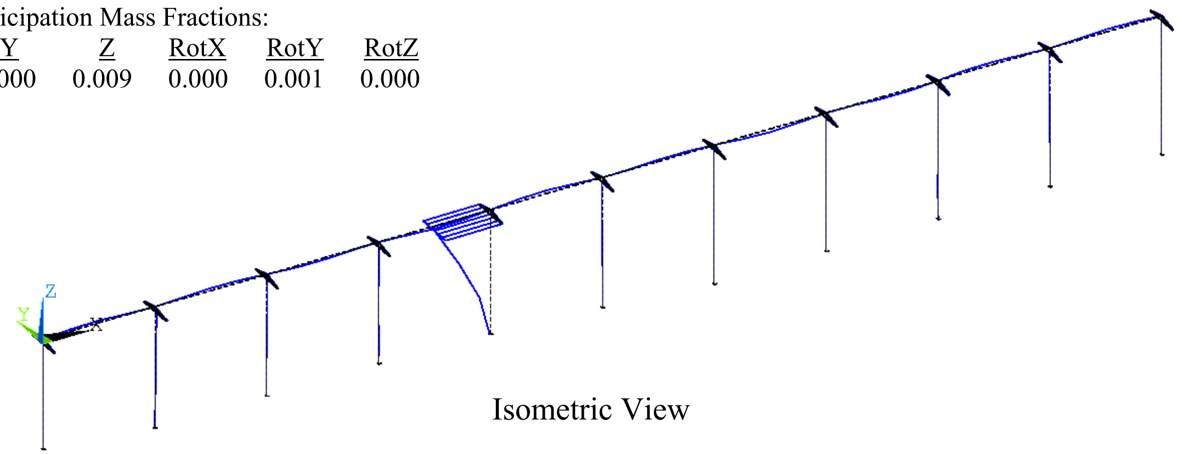

Isometric View

Plan View

<u>Mode 19</u>: Frequency = 1.176 Hz

Modal Participation Mass Fractions:

X	Y	Z	RotX	RotY	RotZ
0.001	0.000	0.000	0.000	0.001	0.000

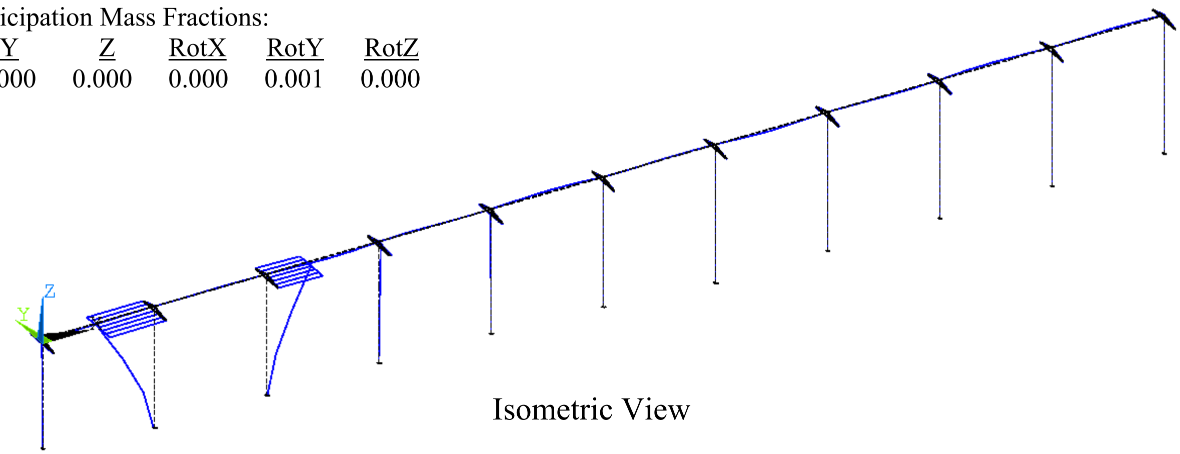

Isometric View

Plan View

<u>Mode 20</u>: Frequency = 1.177 Hz

Modal Participation Mass Fractions:

X	Y	Z	RotX	RotY	RotZ
0.072	0.000	0.003	0.000	0.007	0.000

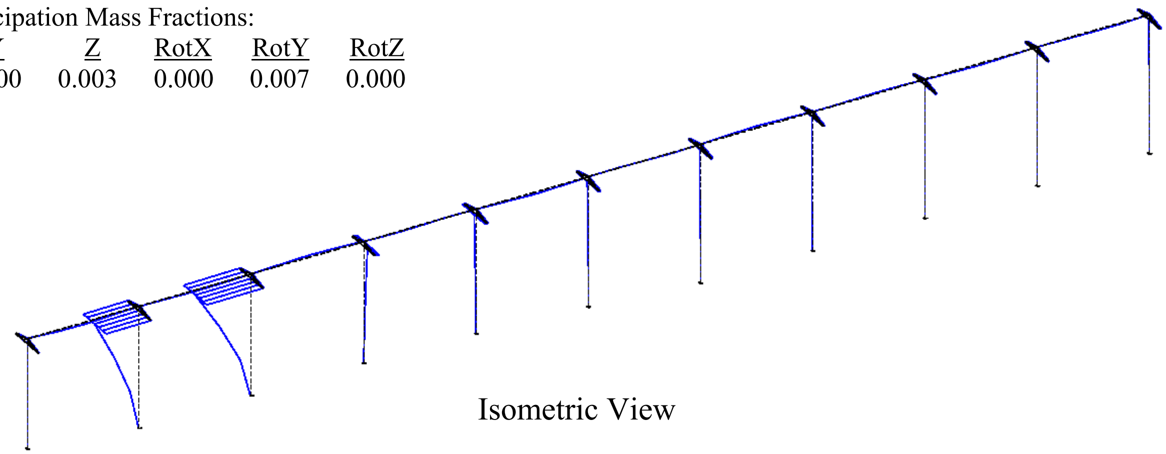

Isometric View

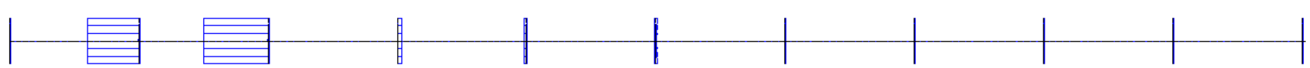

Plan View

APPENDIX C

SAMPLE RESULTS OF NONLINEAR DYNAMIC ANALYSIS

RESPONSE IN LONGITUDINAL DIRECTION FOR SIMULATED NEAR-FAULT GROUND MOTION

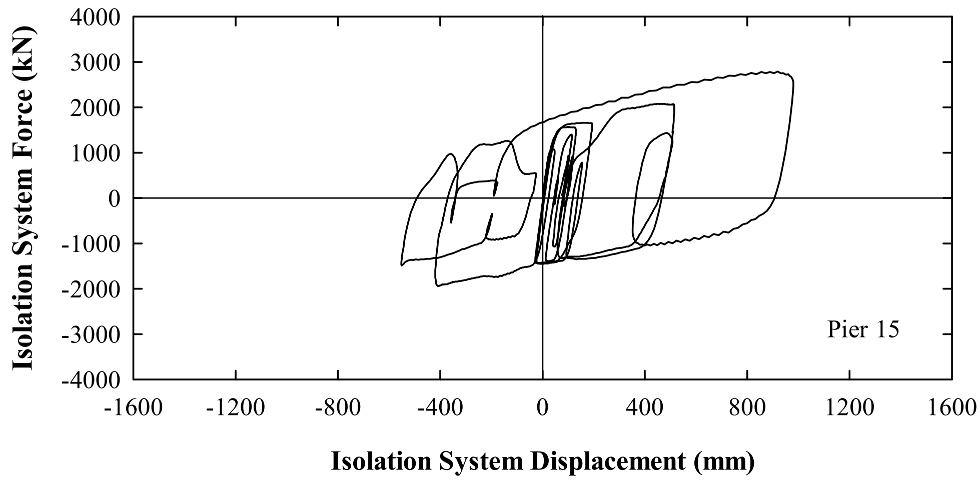

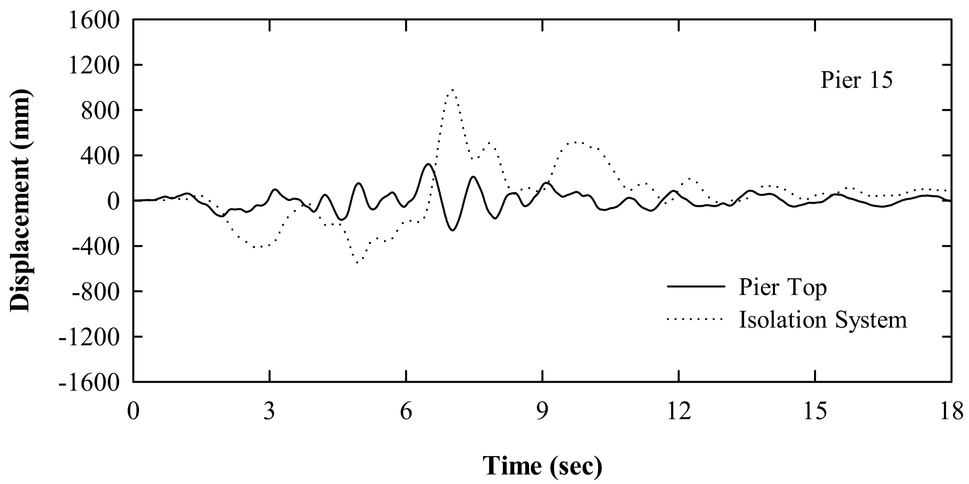

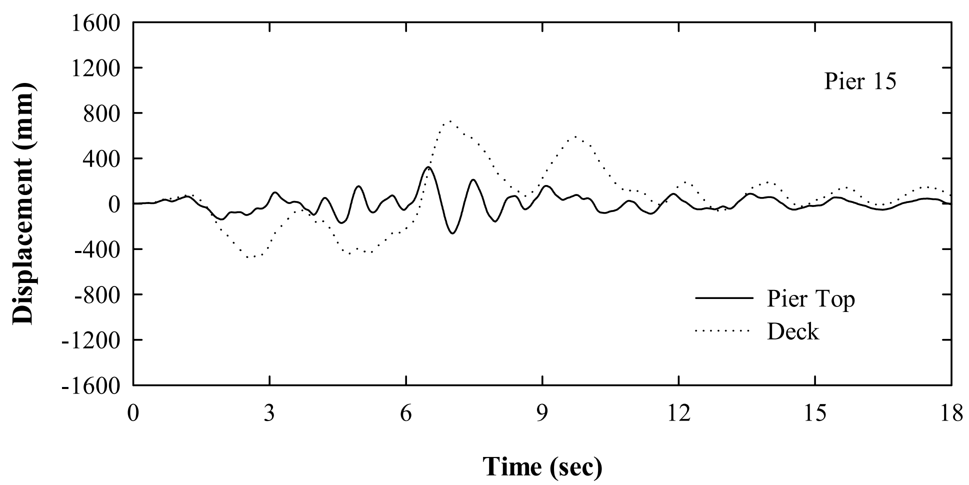

RESPONSE IN TRANSVERSE DIRECTION FOR SIMULATED NEAR-FAULT GROUND MOTION

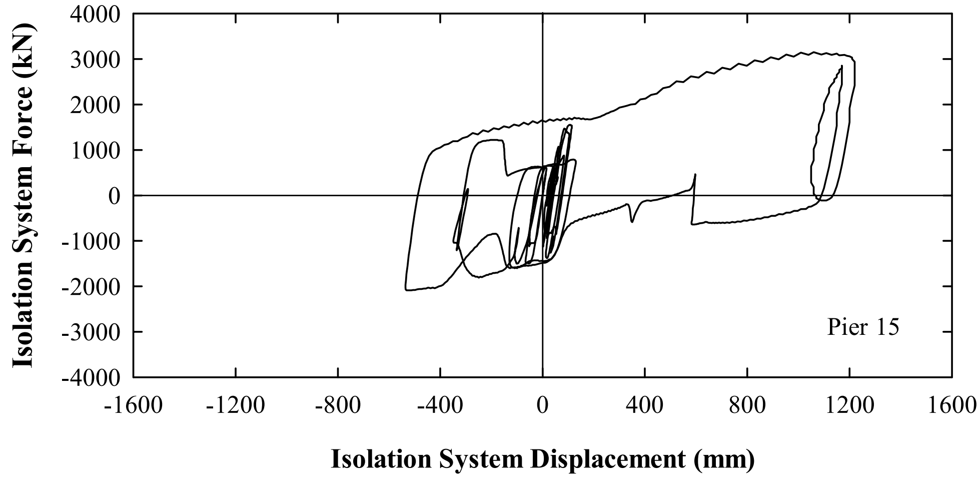

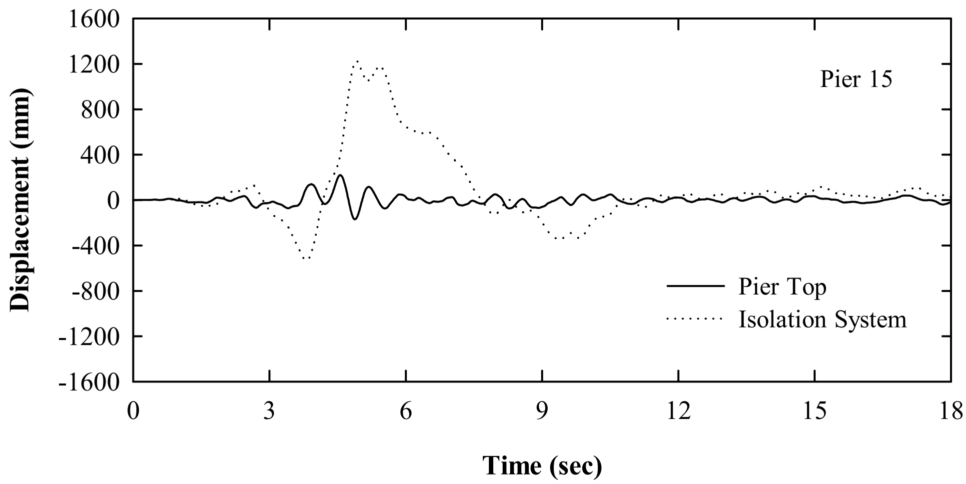

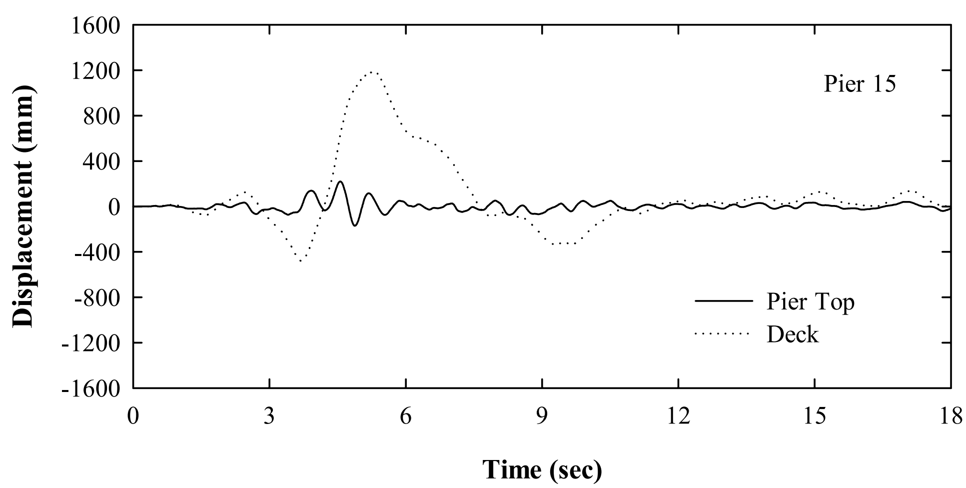

RESPONSE IN LONGITUDINAL DIRECTION FOR SIMULATED NEAR-FAULT GROUND MOTION

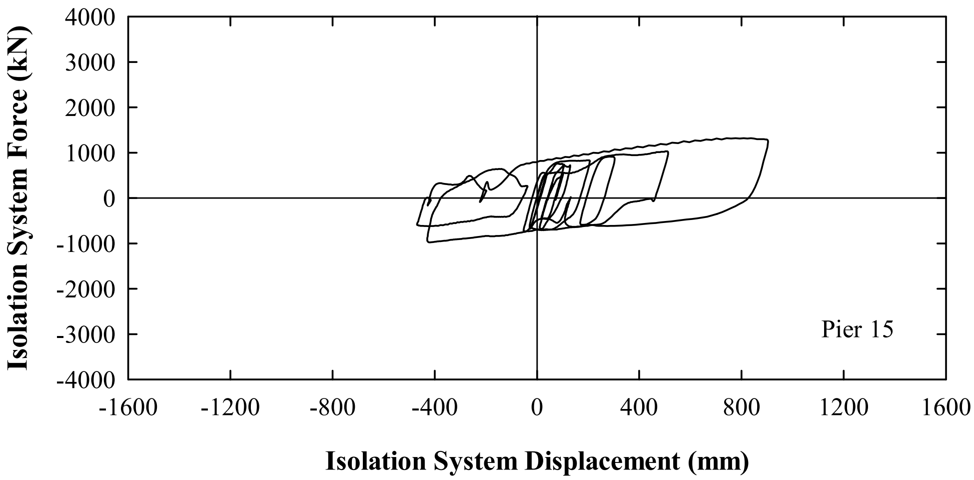

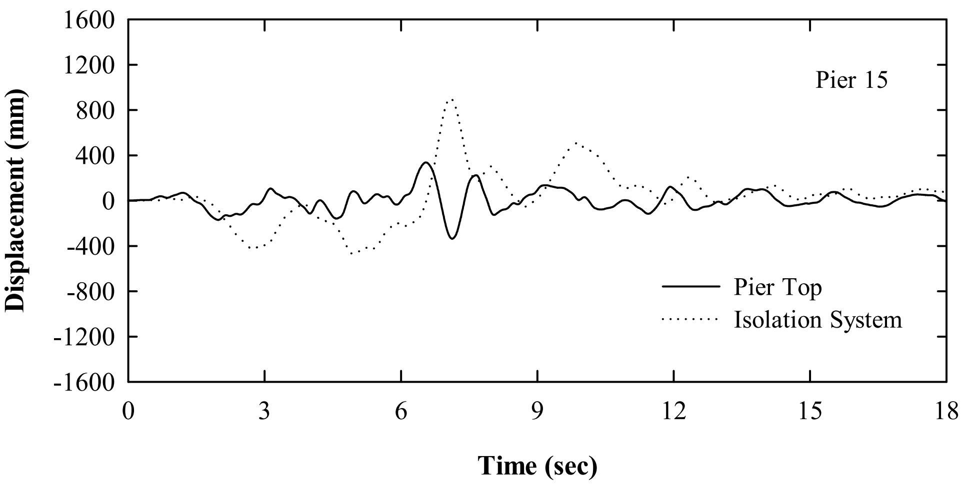

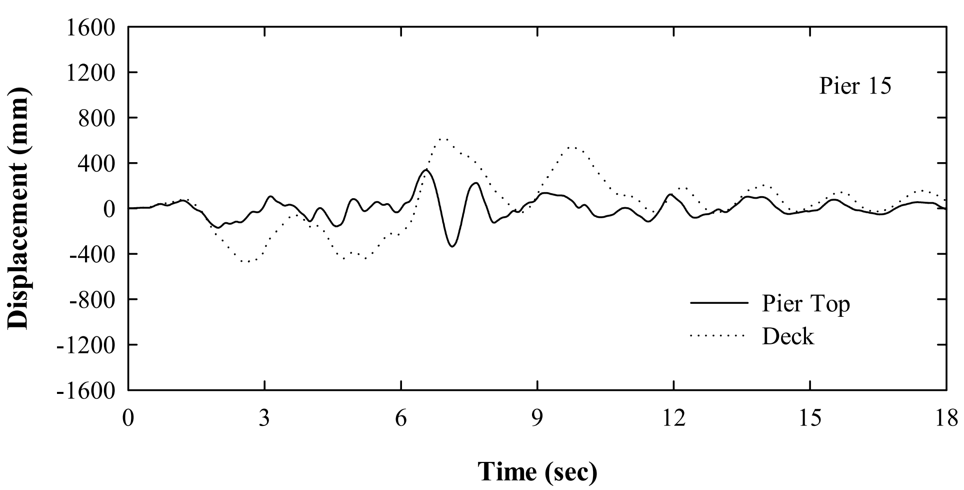

RESPONSE IN TRANSVERSE DIRECTION FOR SIMULATED NEAR-FAULT GROUND MOTION

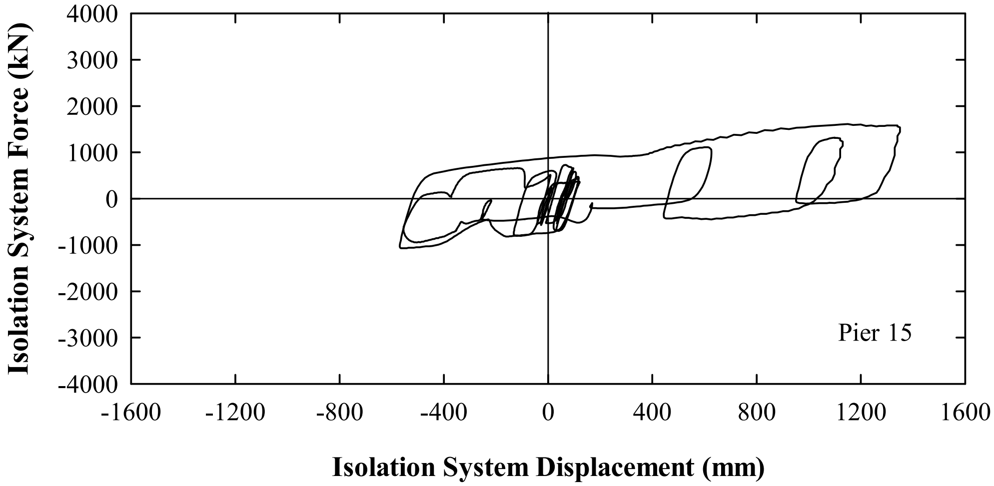

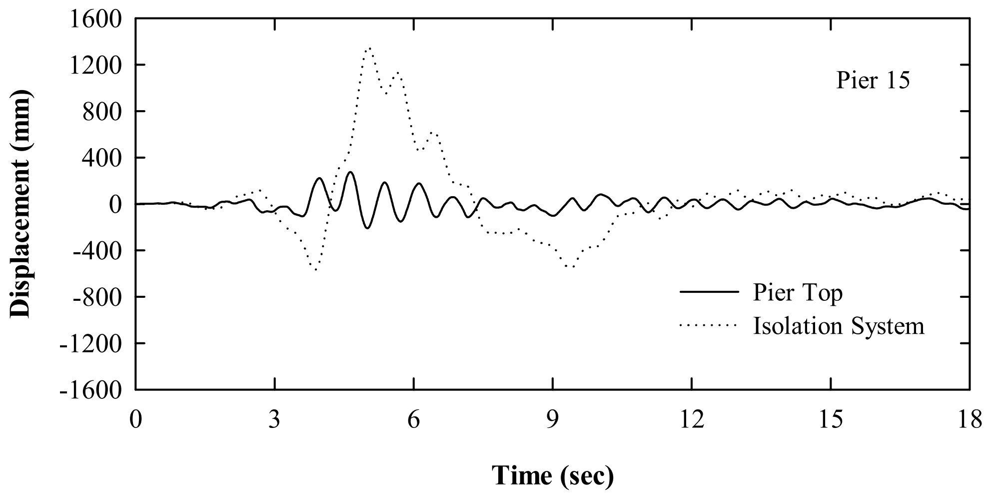

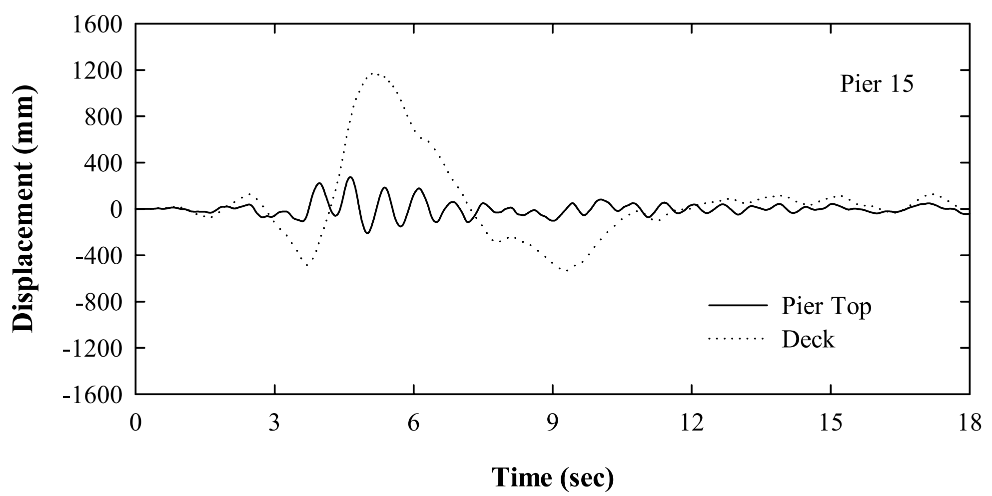

LONGITUDINAL DIRECTION RESPONSE IN 1999 DUZCE, BOLU

EAST COMPONENT APPLIED IN LONGITUDINAL DIRECTION

NORTH COMPONENT APPLIED IN TRANSVERSE DIRECTION

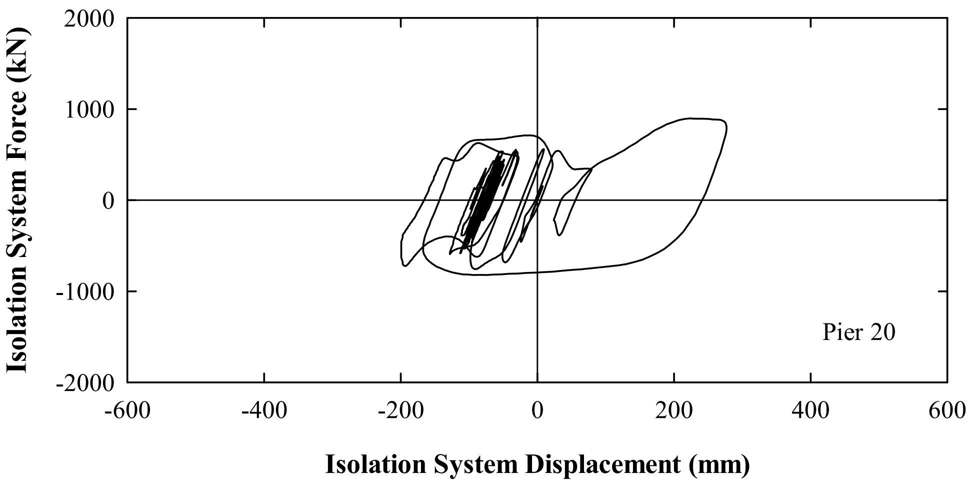

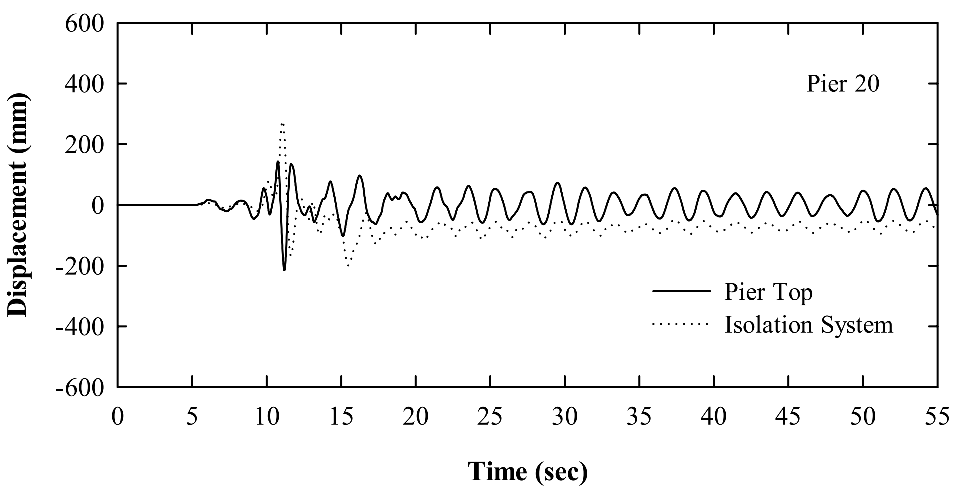

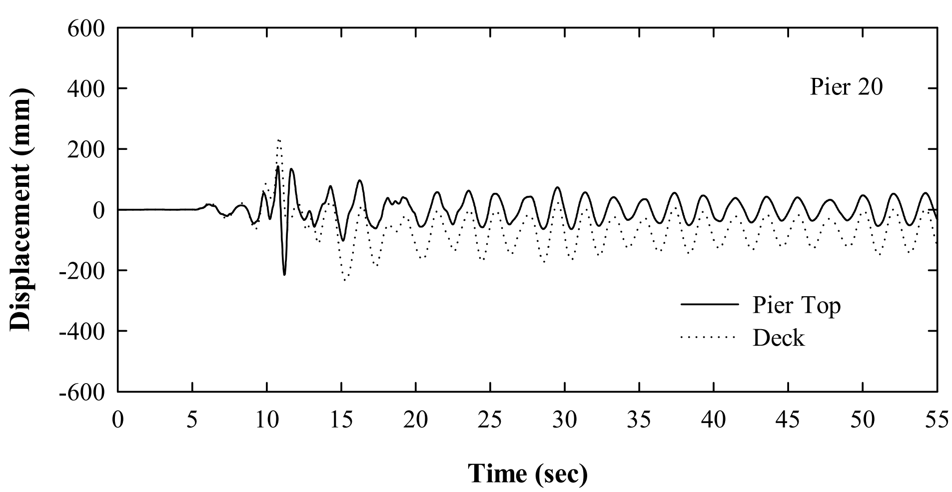

TRANSVERSE DIRECTION RESPONSE IN 1999 DUZCE, BOLU

EAST COMPONENT APPLIED IN LONGITUDINAL DIRECTION

NORTH COMPONENT APPLIED IN TRANSVERSE DIRECTION

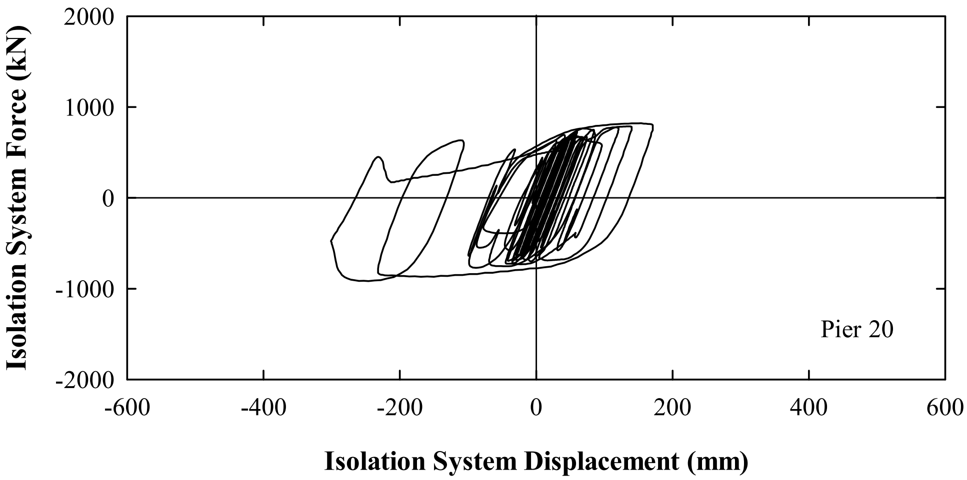

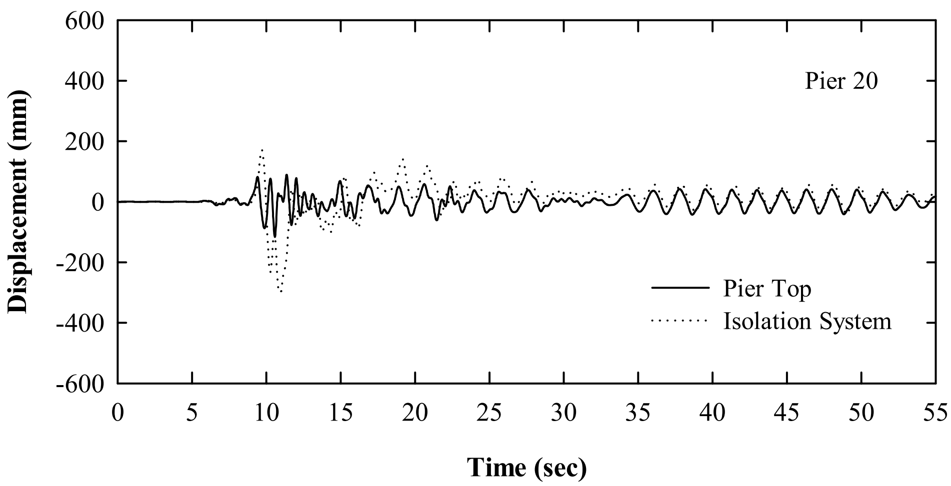

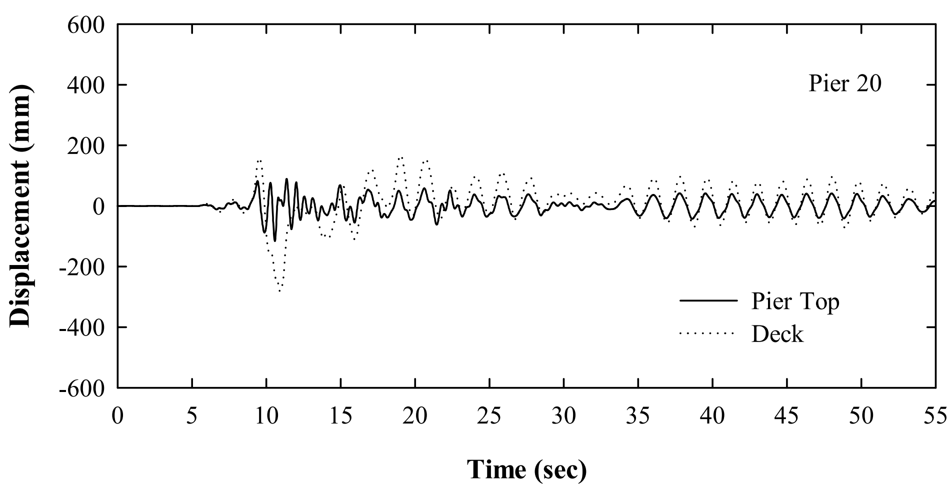

LONGITUDINAL DIRECTION RESPONSE IN 1999 DUZCE, BOLU

NORTH COMPONENT APPLIED IN LONGITUDINAL DIRECTION

EAST COMPONENT APPLIED IN TRANSVERSE DIRECTION

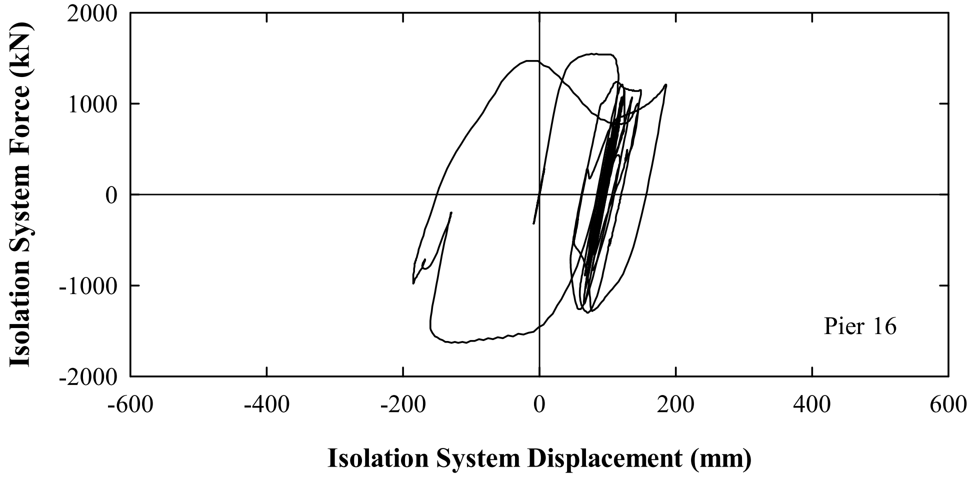

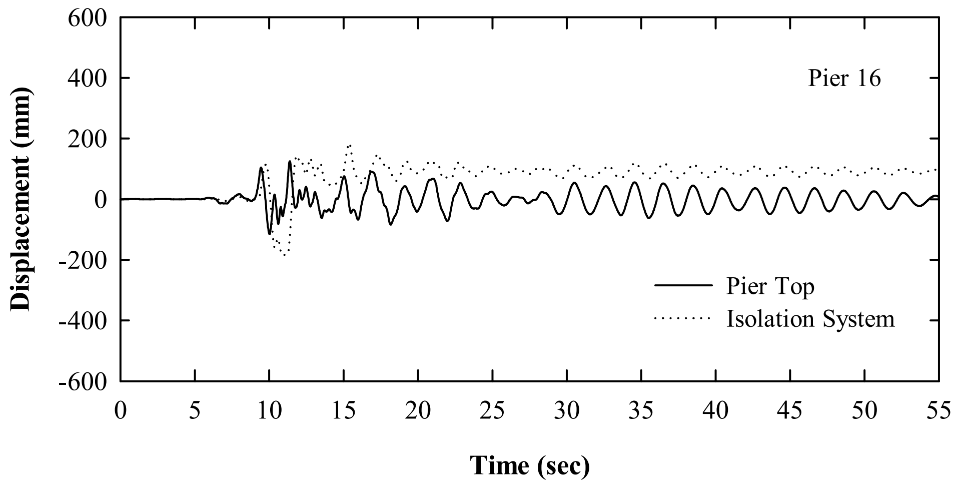

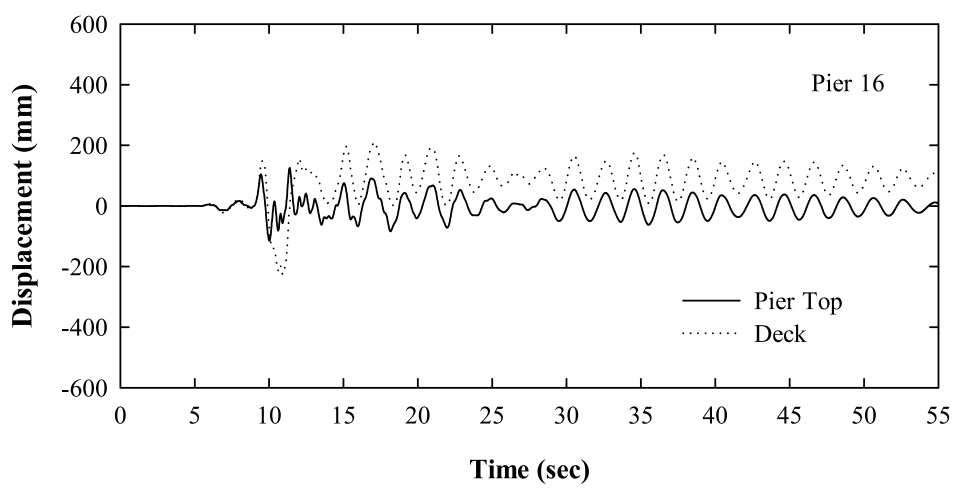

TRANSVERSE DIRECTION RESPONSE IN 1999 DUZCE, BOLU

NORTH COMPONENT APPLIED IN LONGITUDINAL DIRECTION

EAST COMPONENT APPLIED IN TRANSVERSE DIRECTION

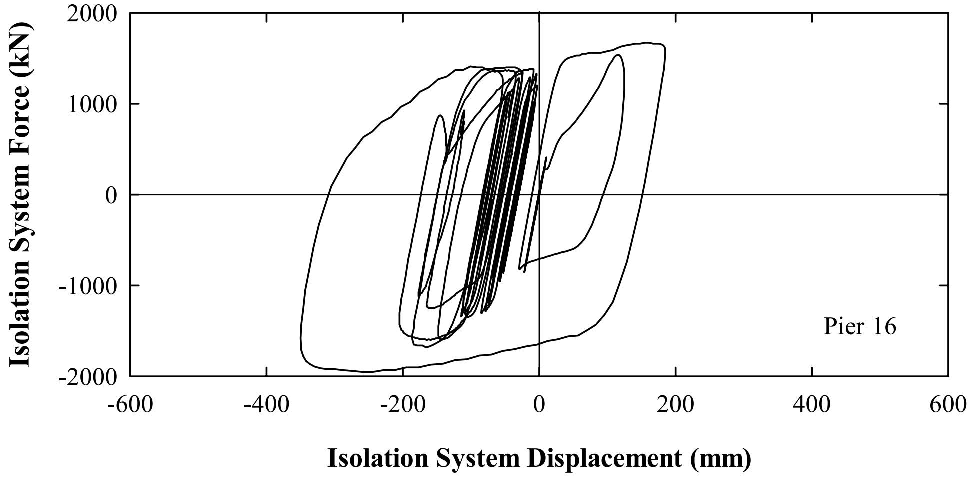

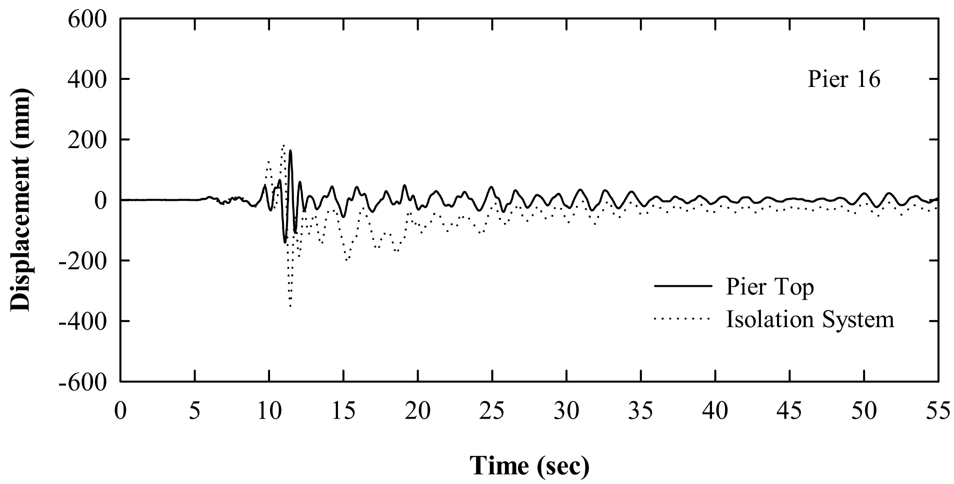

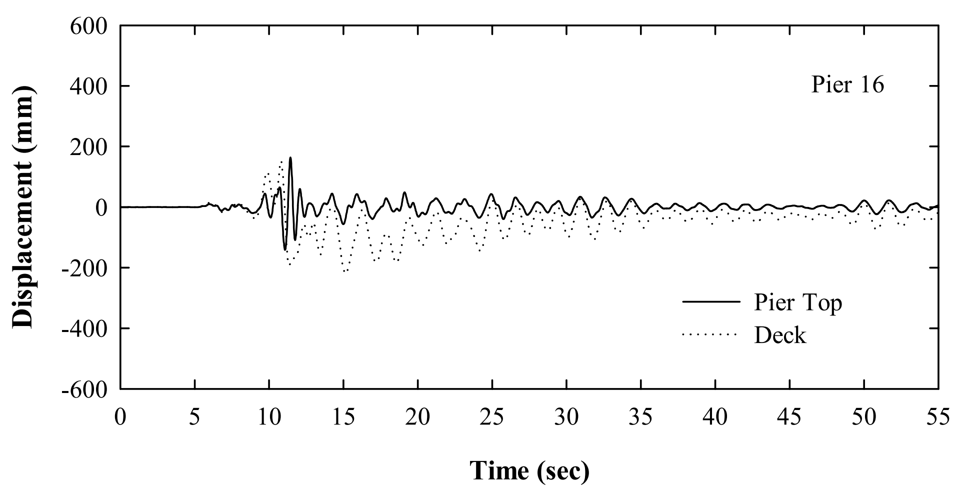

LONGITUDINAL DIRECTION RESPONSE IN 1999 DUZCE, DUZCE

WEST COMPONENT APPLIED IN LONGITUDINAL DIRECTION

SOUTH COMPONENT APPLIED IN TRANSVERSE DIRECTION

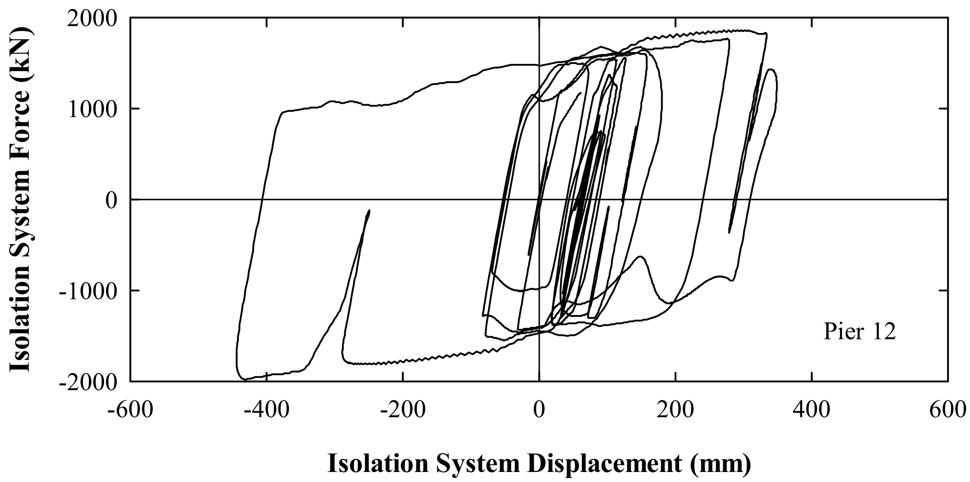

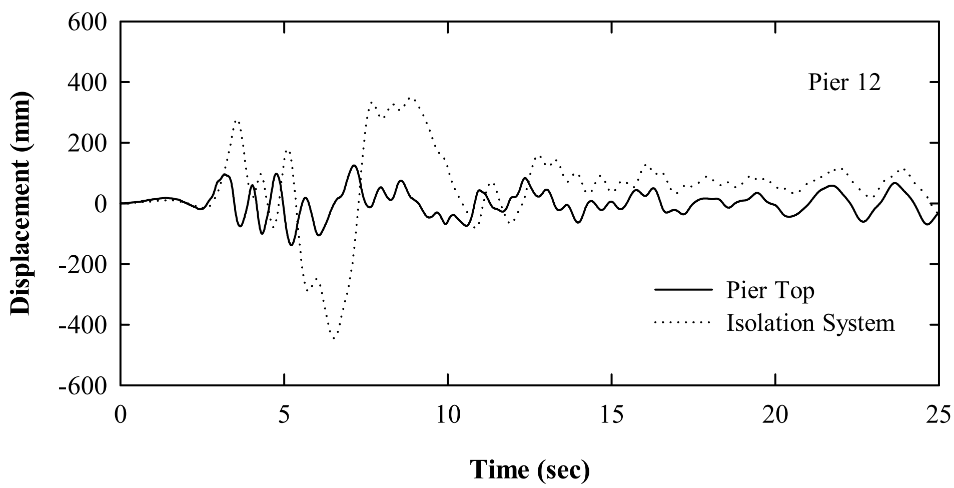

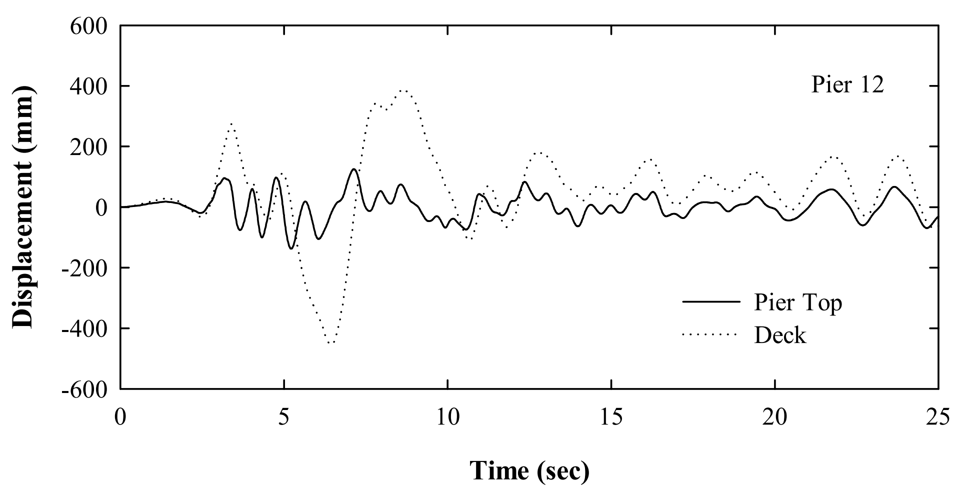

TRANSVERSE DIRECTION RESPONSE IN 1999 DUZCE, DUZCE

WEST COMPONENT APPLIED IN LONGITUDINAL DIRECTION

SOUTH COMPONENT APPLIED IN TRANSVERSE DIRECTION

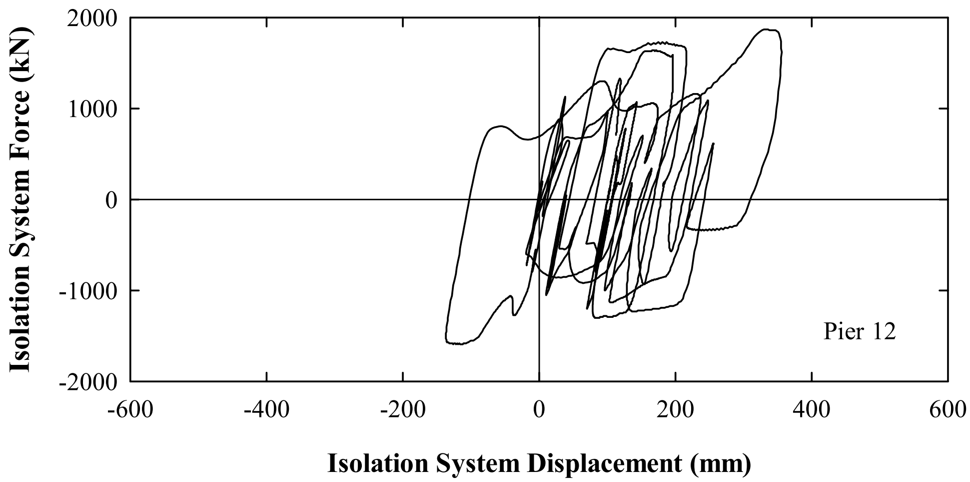

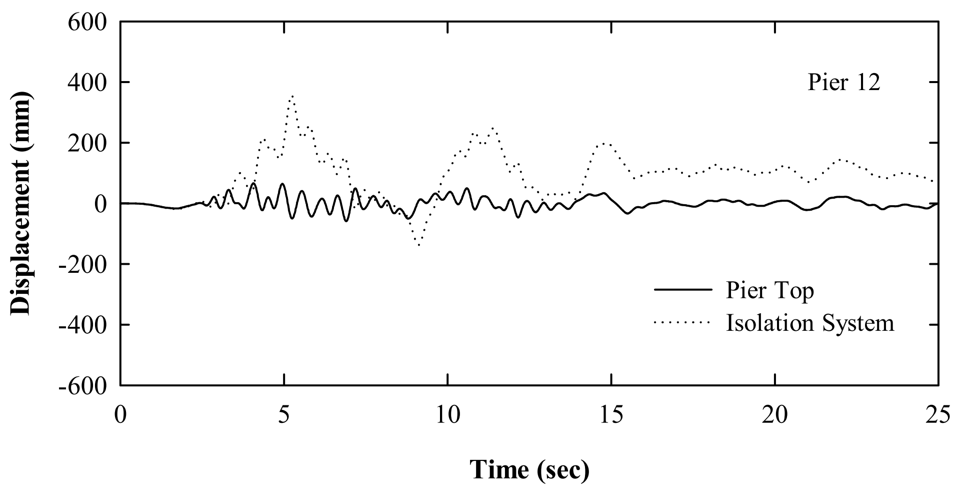

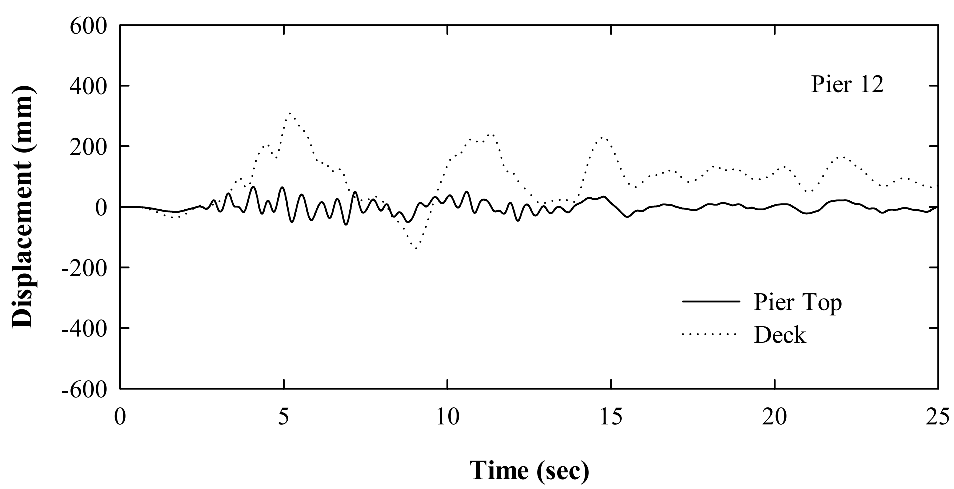

LONGITUDINAL DIRECTION RESPONSE IN 1999 DUZCE, DUZCE

SOUTH COMPONENT APPLIED IN LONGITUDINAL DIRECTION

WEST COMPONENT APPLIED IN TRANSVERSE DIRECTION

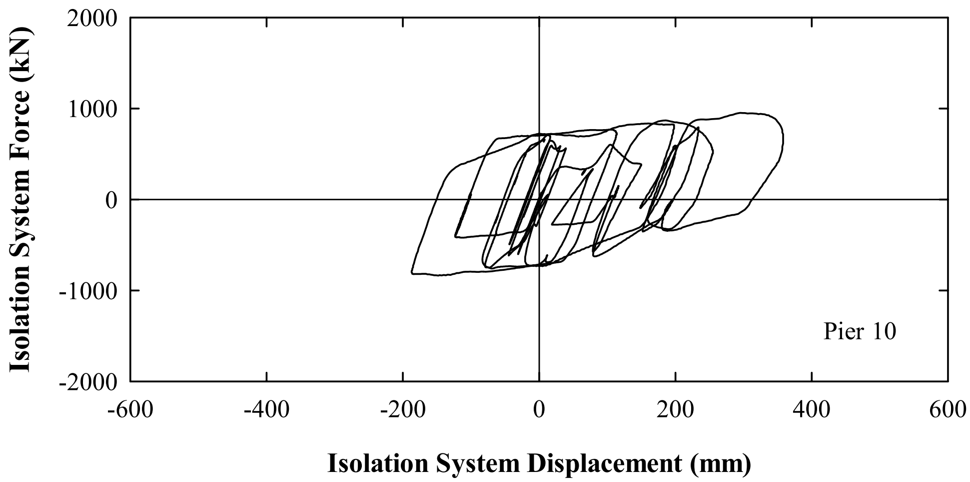

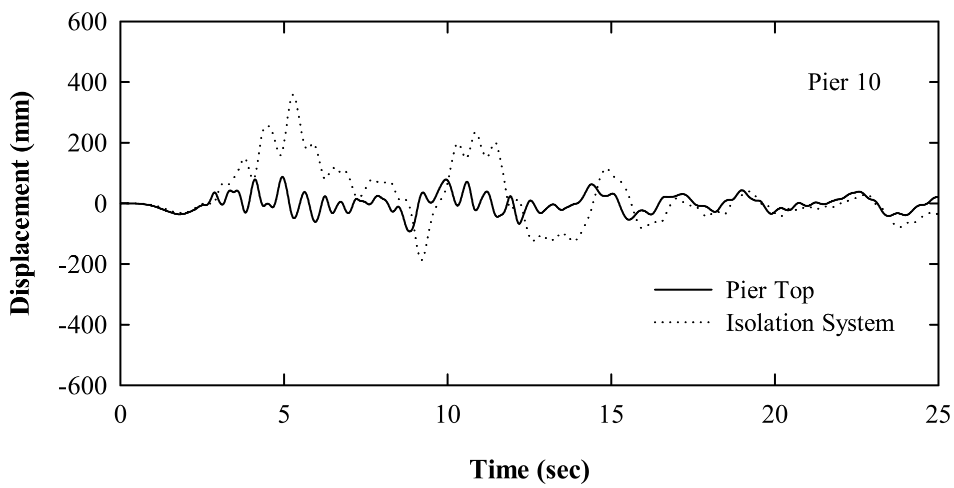

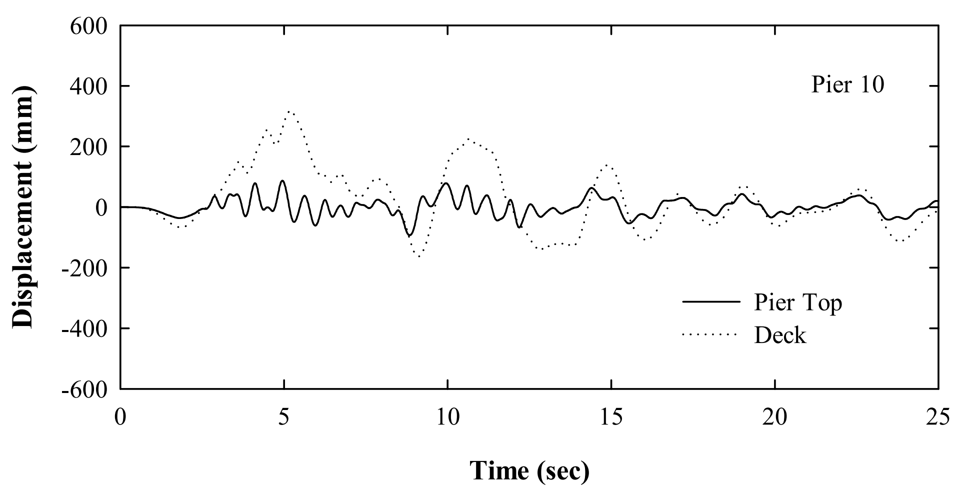

TRANSVERSE DIRECTION RESPONSE IN 1999 DUZCE, DUZCE

SOUTH COMPONENT APPLIED IN LONGITUDINAL DIRECTION

WEST COMPONENT APPLIED IN TRANSVERSE DIRECTION

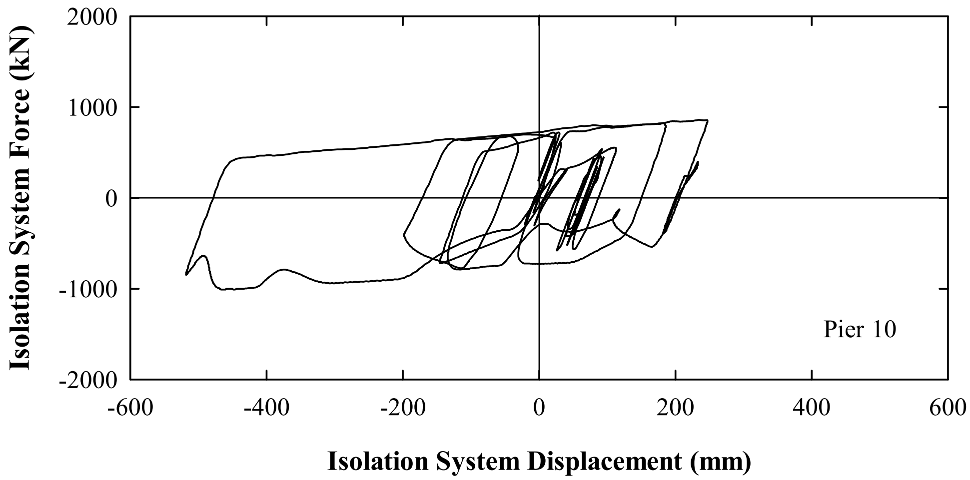

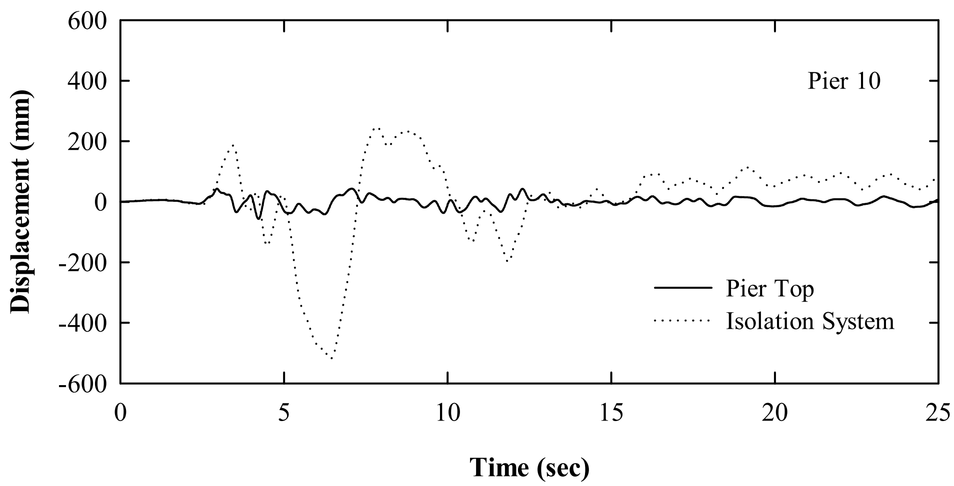

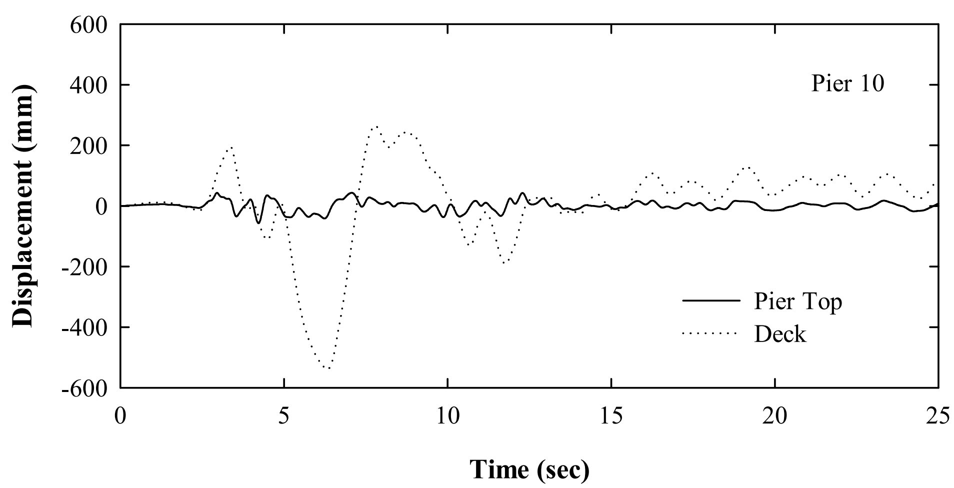

LONGITUDINAL DIRECTION RESPONSE IN 1992 LANDERS, YERMO

360° COMPONENT APPLIED IN LONGITUDINAL DIRECTION

270° COMPONENT APPLIED IN TRANSVERSE DIRECTION

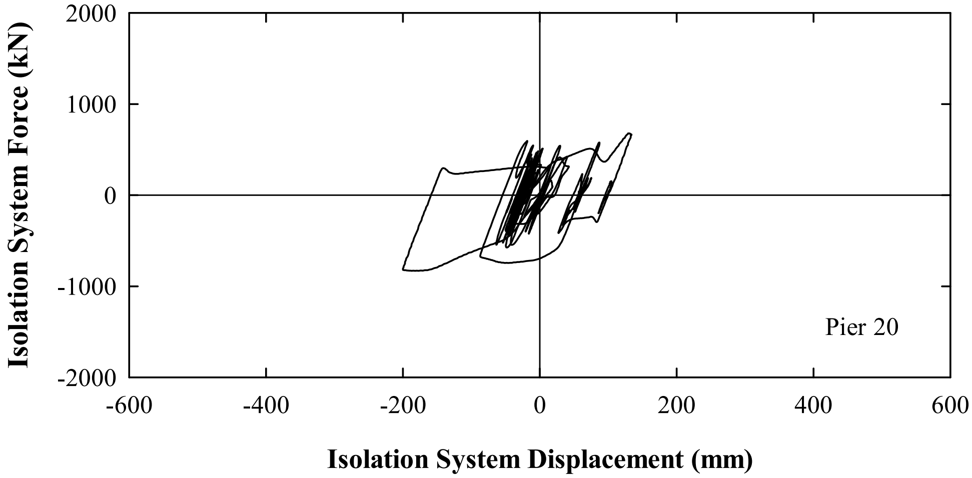

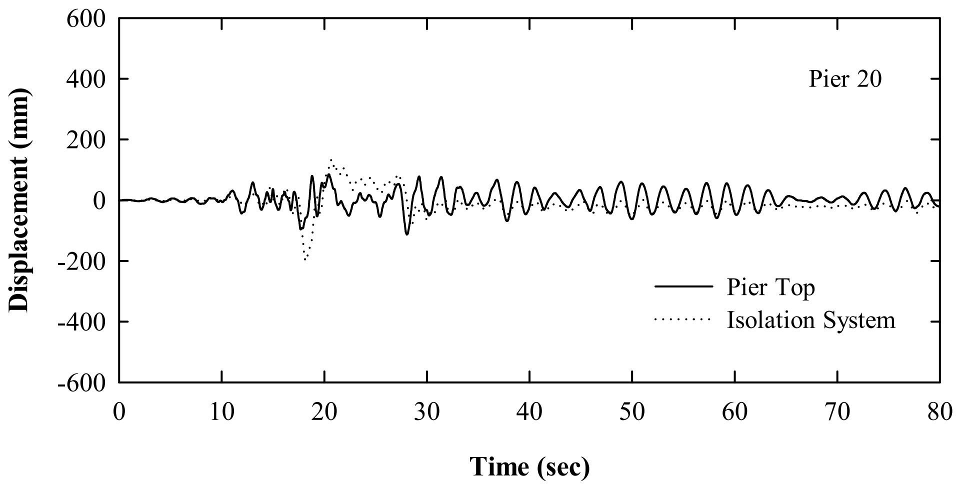

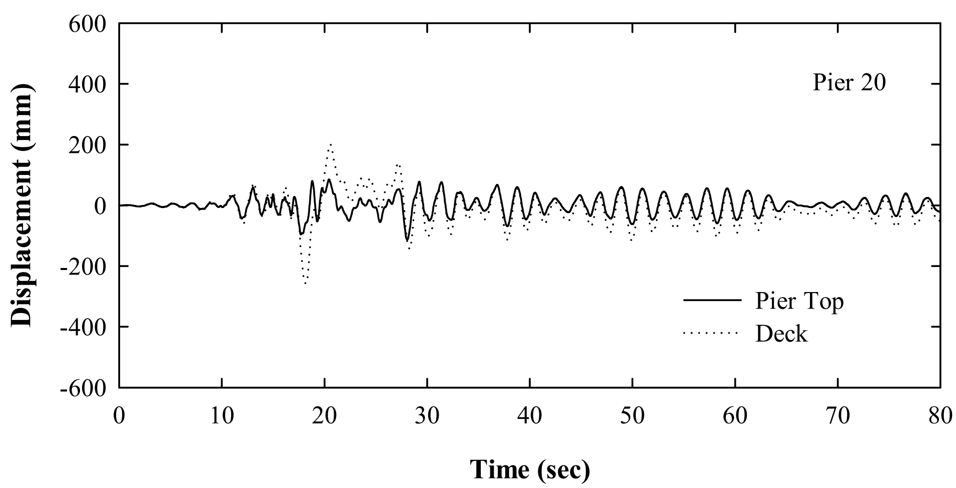

TRANSVERSE DIRECTION RESPONSE IN 1992 LANDERS, YERMO

360° COMPONENT APPLIED IN LONGITUDINAL DIRECTION

270° COMPONENT APPLIED IN TRANSVERSE DIRECTION

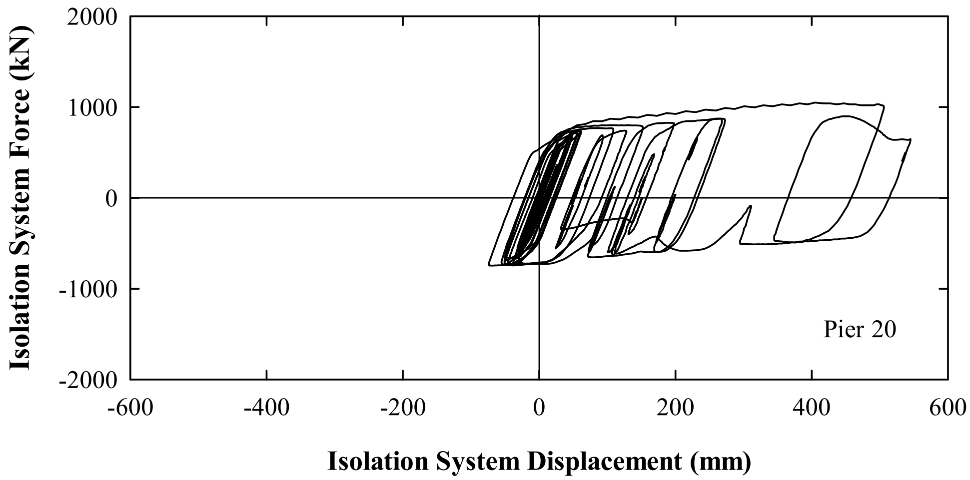

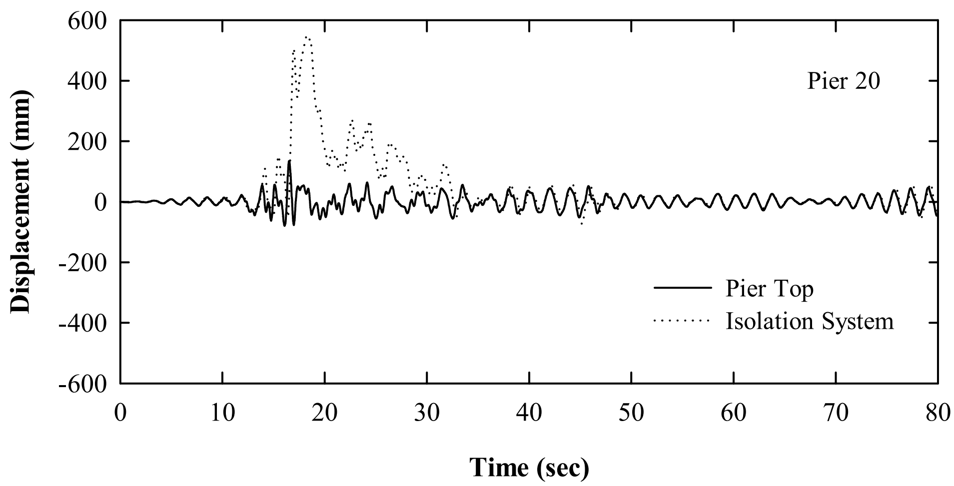

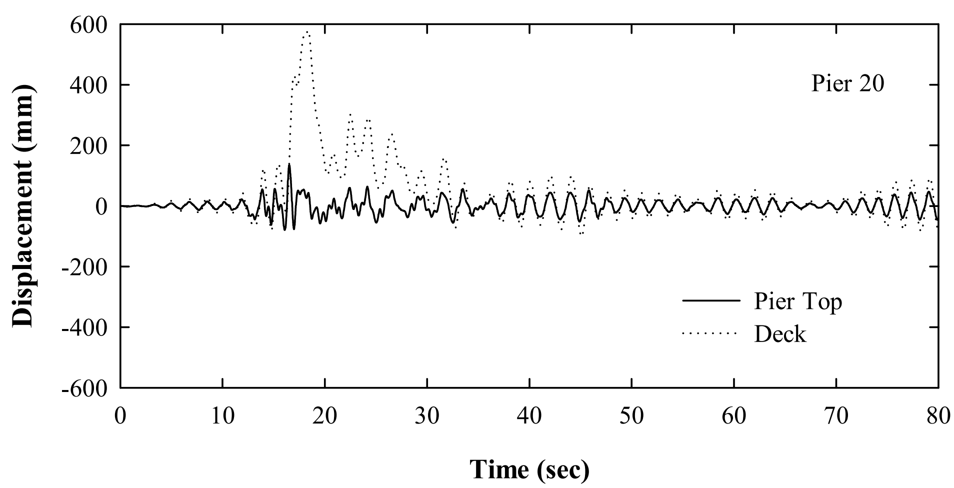

LONGITUDINAL DIRECTION RESPONSE IN 1992 LANDERS, YERMO

270° COMPONENT APPLIED IN LONGITUDINAL DIRECTION

360° COMPONENT APPLIED IN TRANSVERSE DIRECTION

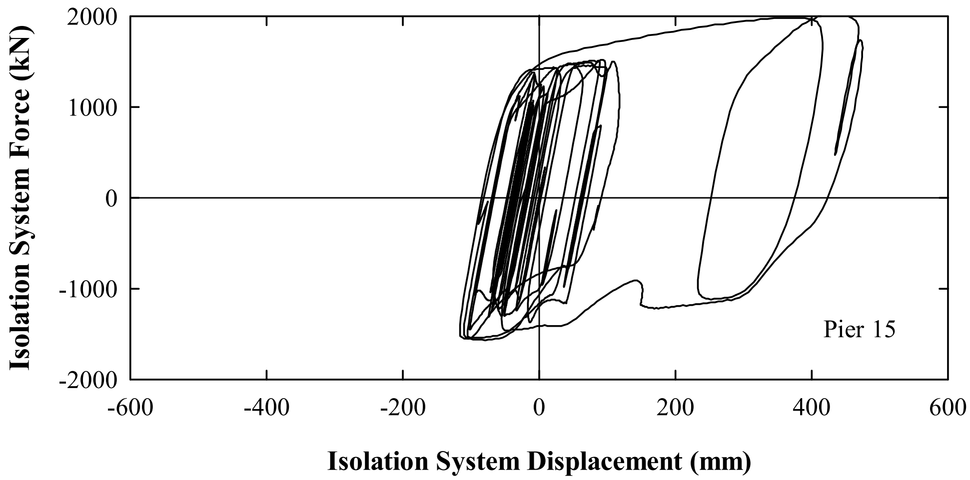

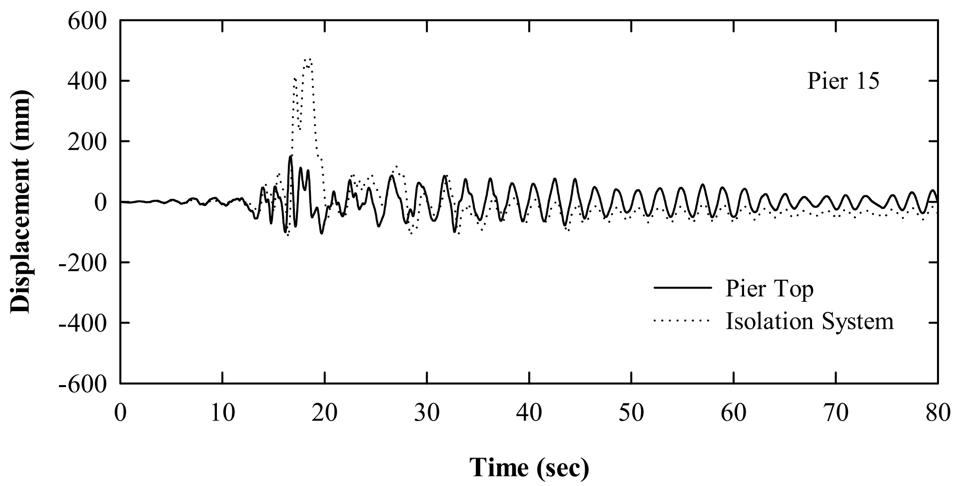

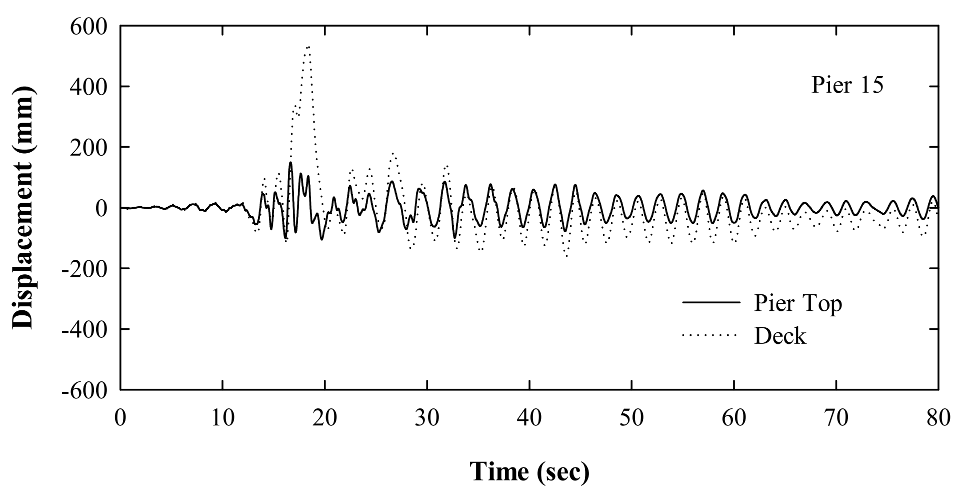

TRANSVERSE DIRECTION RESPONSE IN 1992 LANDERS, YERMO

270° COMPONENT APPLIED IN LONGITUDINAL DIRECTION

360° COMPONENT APPLIED IN TRANSVERSE DIRECTION

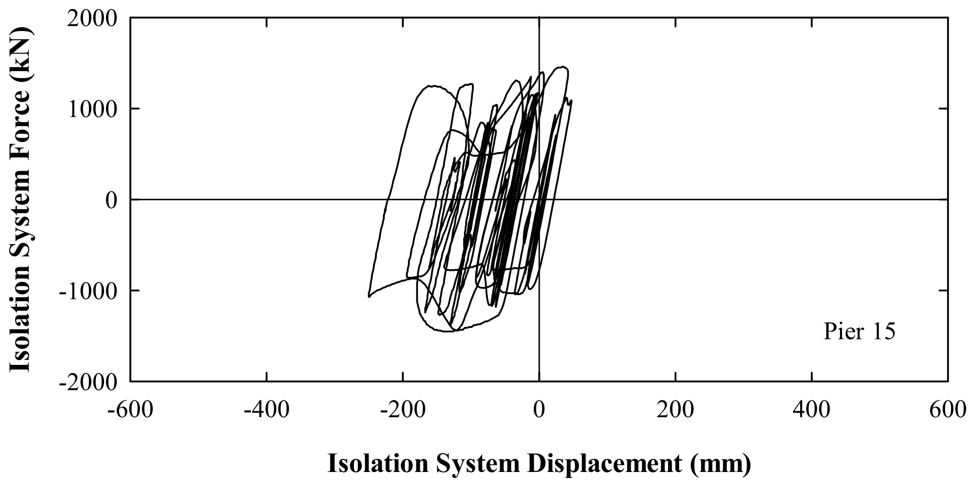

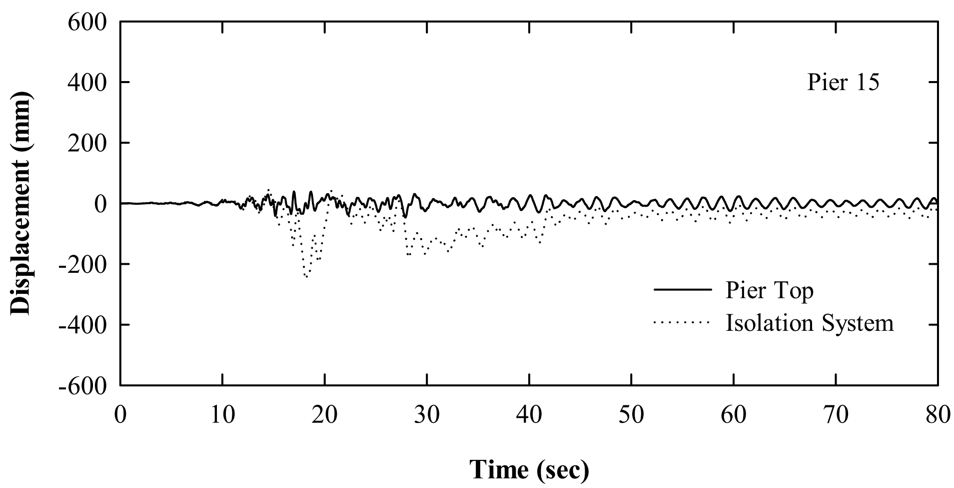

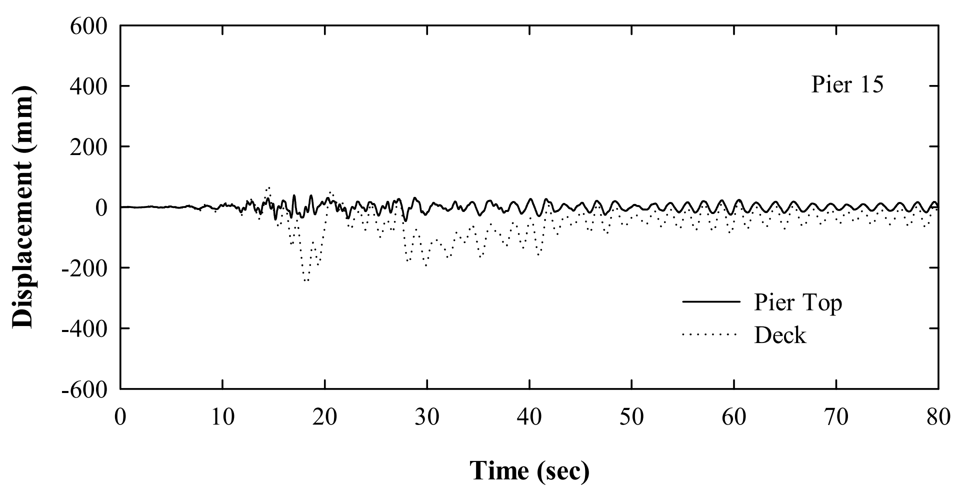

LONGITUDINAL DIRECTION RESPONSE IN 1989 LOMA PRIETA, HOLLISTER

0° COMPONENT APPLIED IN LONGITUDINAL DIRECTION

90° COMPONENT APPLIED IN TRANSVERSE DIRECTION

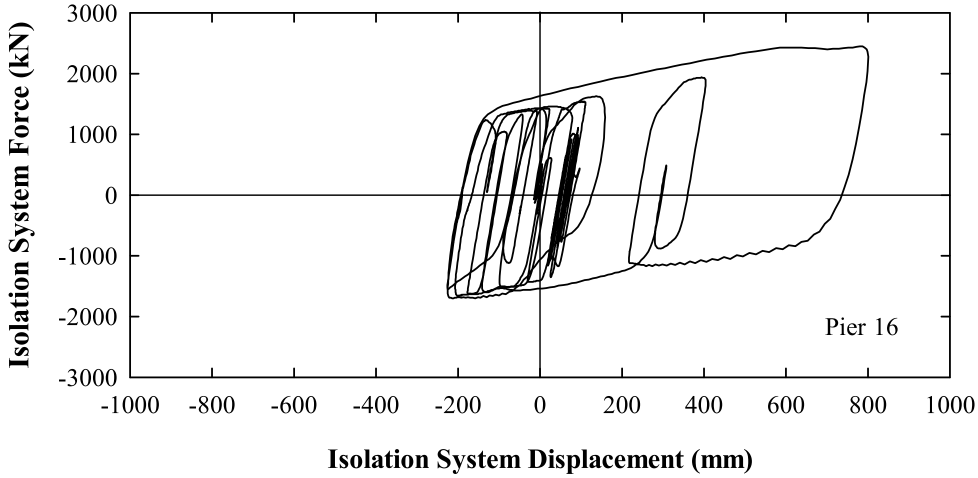

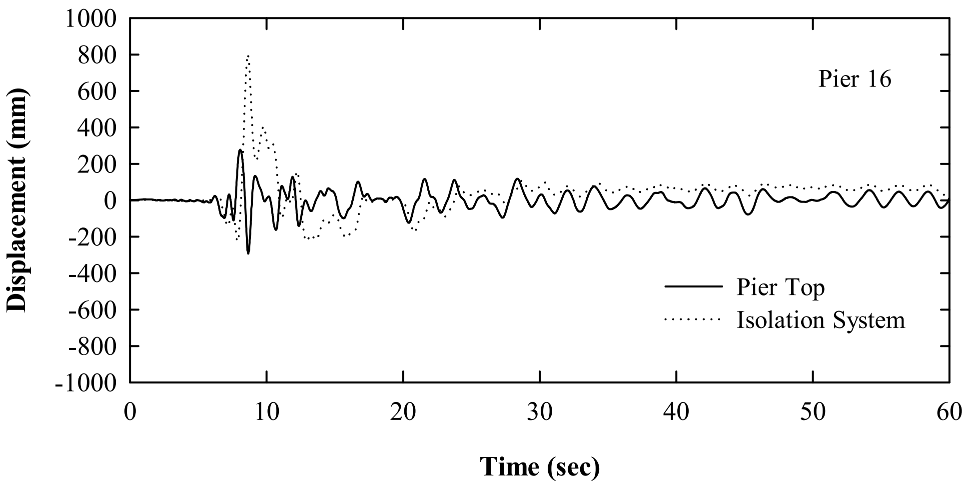

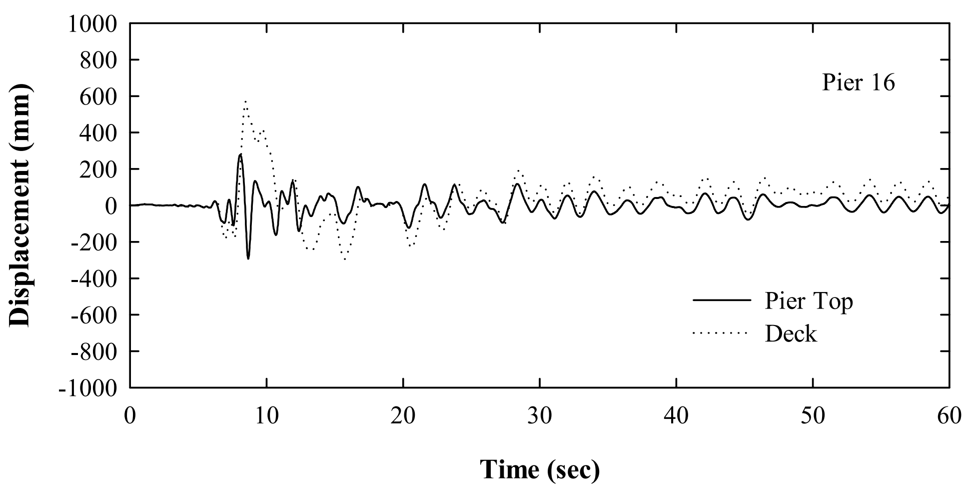

TRANSVERSE DIRECTION RESPONSE IN 1989 LOMA PRIETA, HOLLISTER

0° COMPONENT APPLIED IN LONGITUDINAL DIRECTION

90° COMPONENT APPLIED IN TRANSVERSE DIRECTION

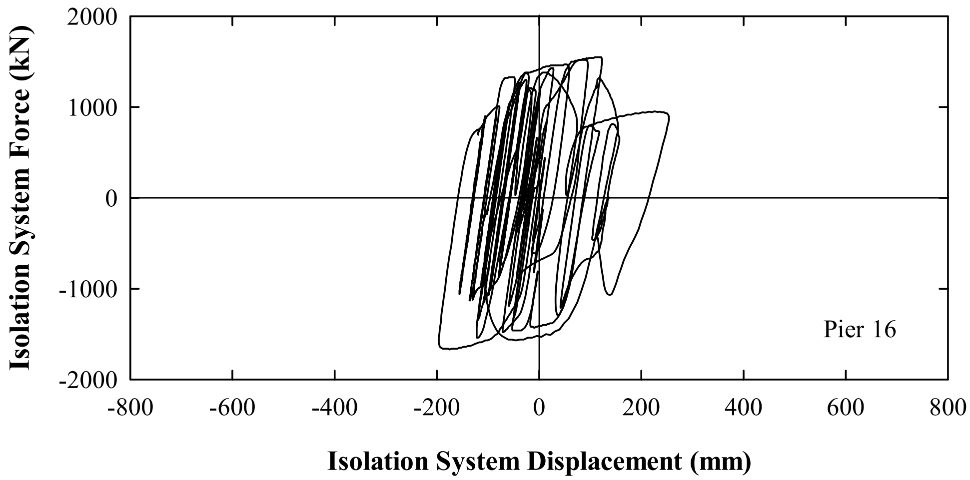

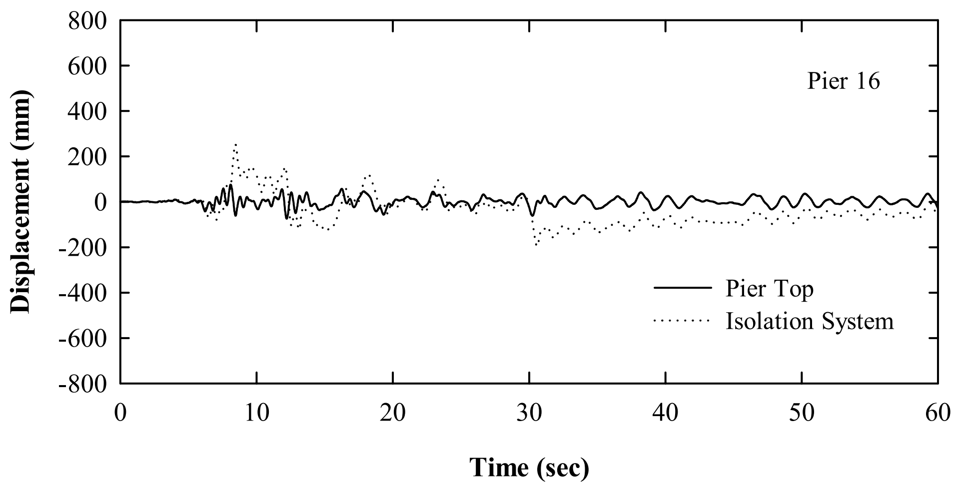

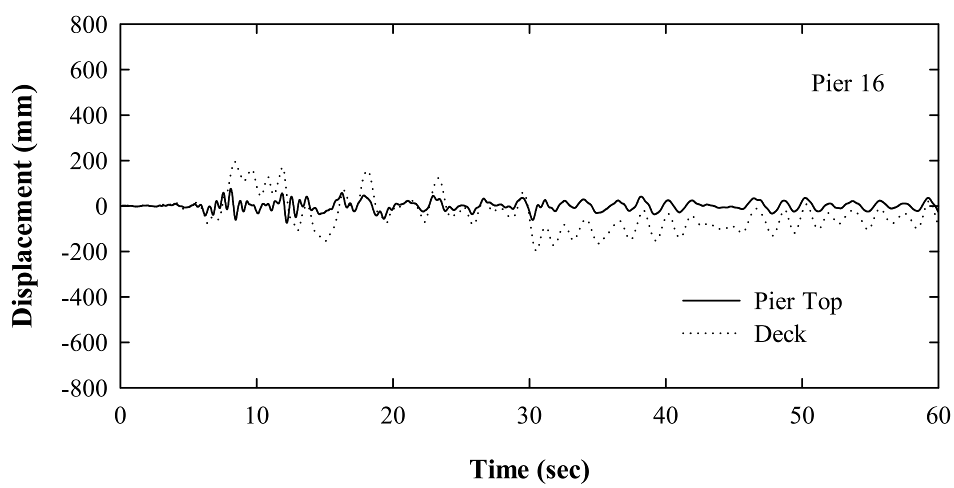

LONGITUDINAL DIRECTION RESPONSE IN 1989 LOMA PRIETA, HOLLISTER

90° COMPONENT APPLIED IN LONGITUDINAL DIRECTION

0° COMPONENT APPLIED IN TRANSVERSE DIRECTION

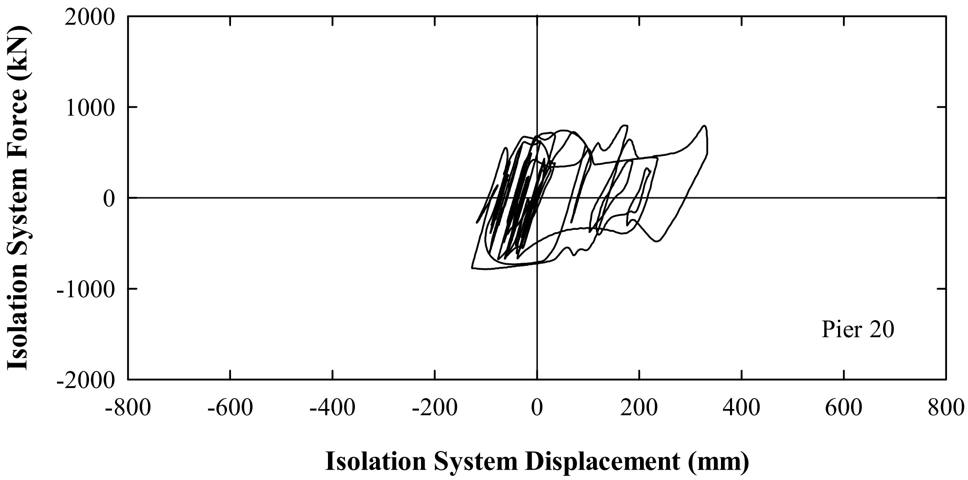

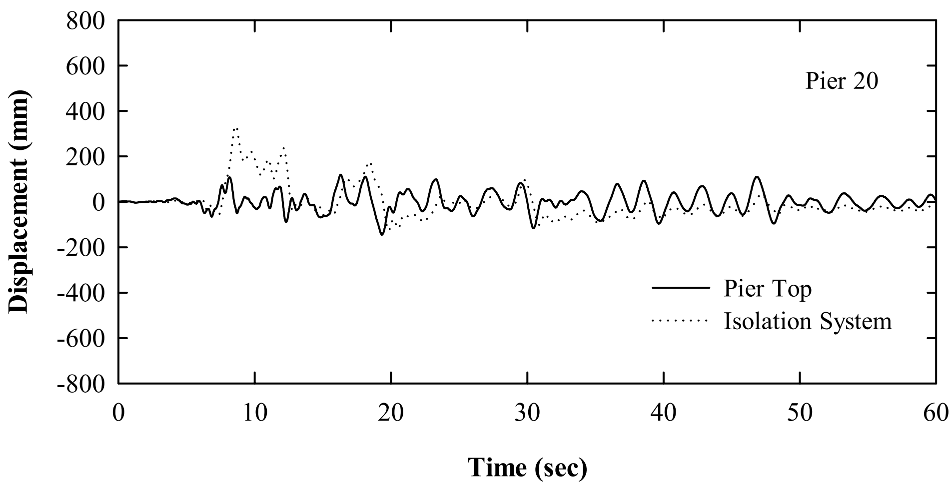

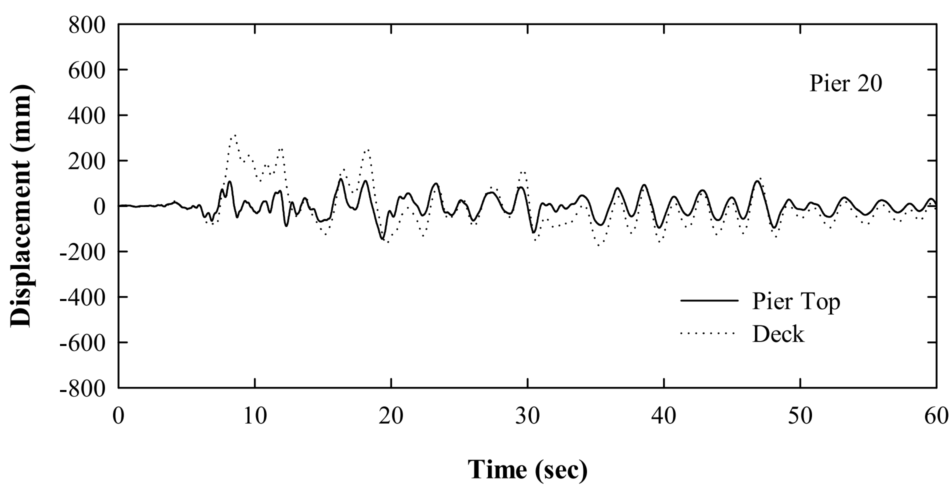

TRANSVERSE DIRECTION RESPONSE IN 1989 LOMA PRIETA, HOLLISTER

90° COMPONENT APPLIED IN LONGITUDINAL DIRECTION

0° COMPONENT APPLIED IN TRANSVERSE DIRECTION

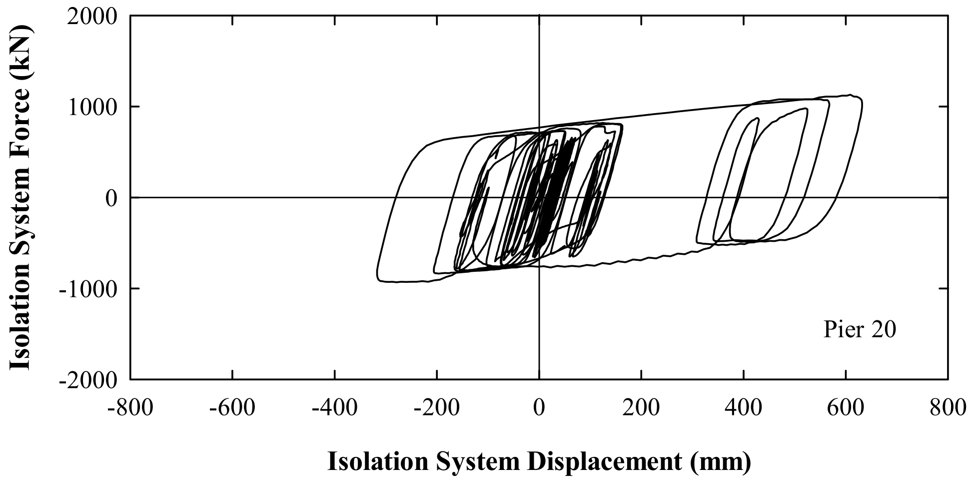

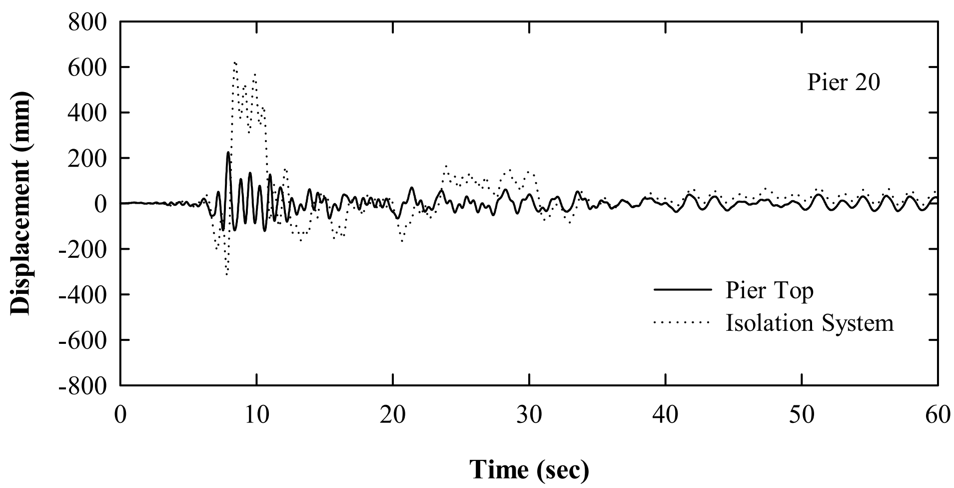

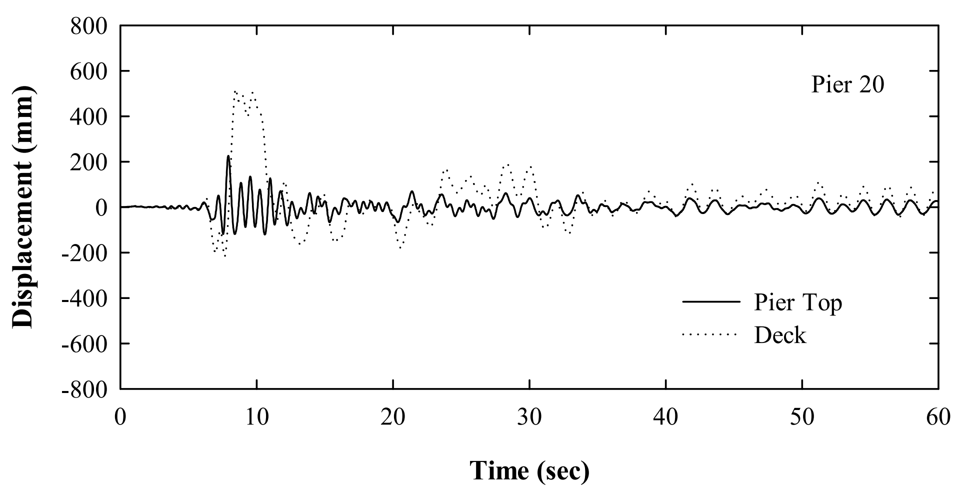

LONGITUDINAL DIRECTION RESPONSE IN 1971 SAN FERNANDO, 458

0° COMPONENT APPLIED IN LONGITUDINAL DIRECTION

90° COMPONENT APPLIED IN TRANSVERSE DIRECTION

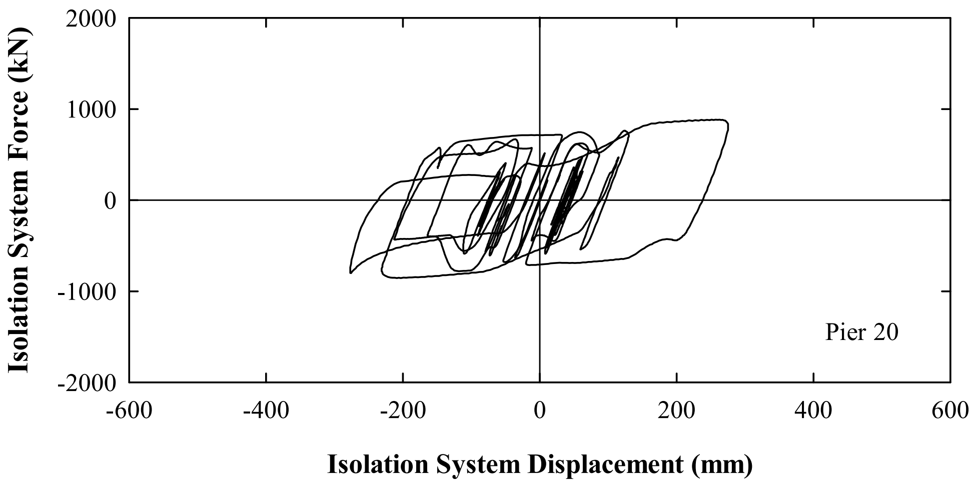

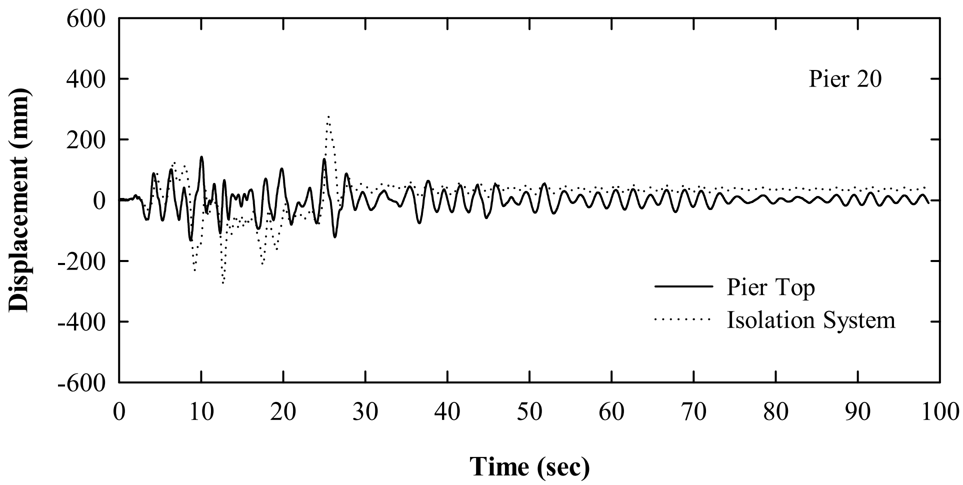

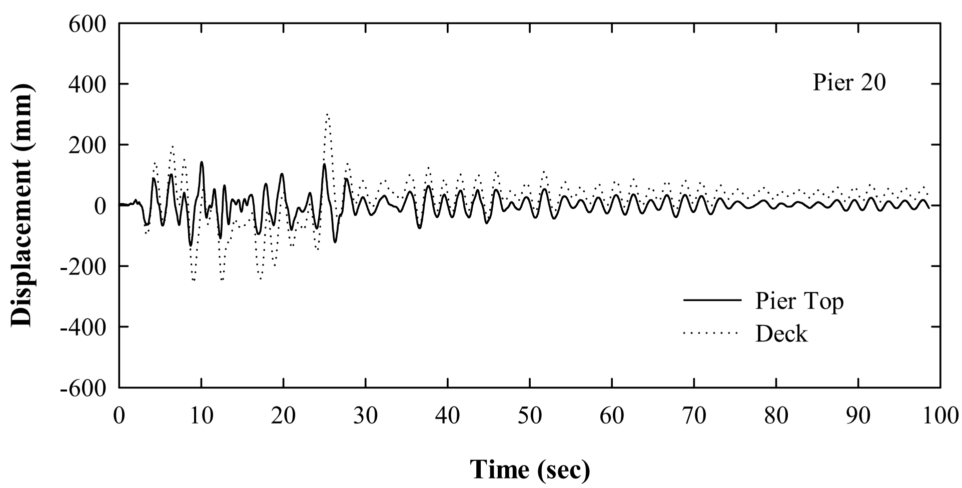

TRANSVERSE DIRECTION RESPONSE IN 1971 SAN FERNANDO, 458

0° COMPONENT APPLIED IN LONGITUDINAL DIRECTION

90° COMPONENT APPLIED IN TRANSVERSE DIRECTION

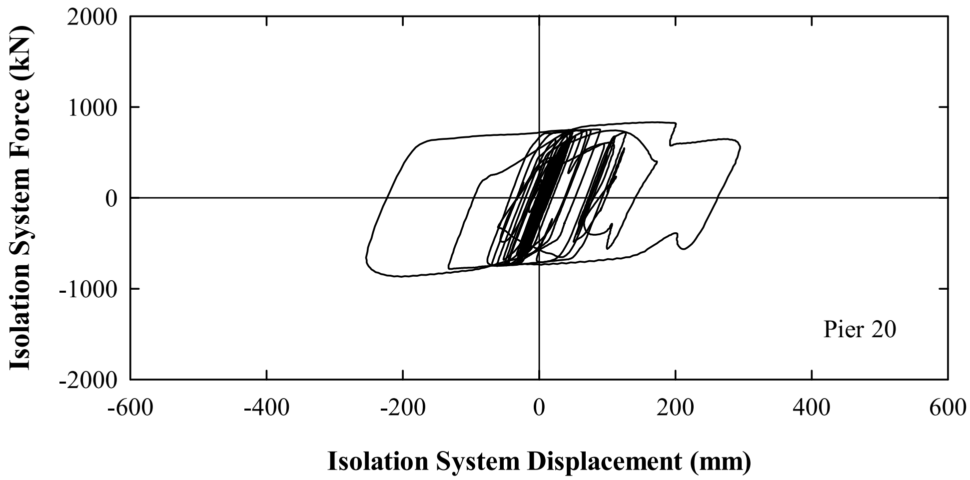

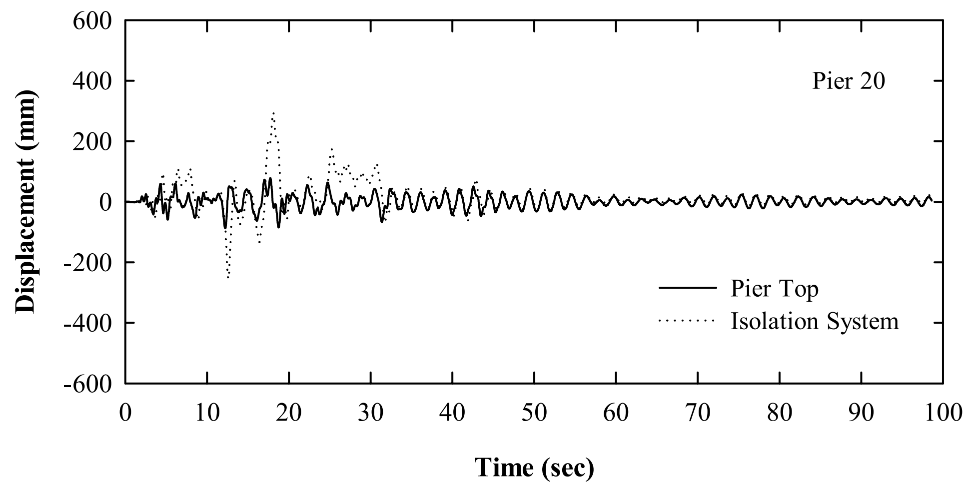

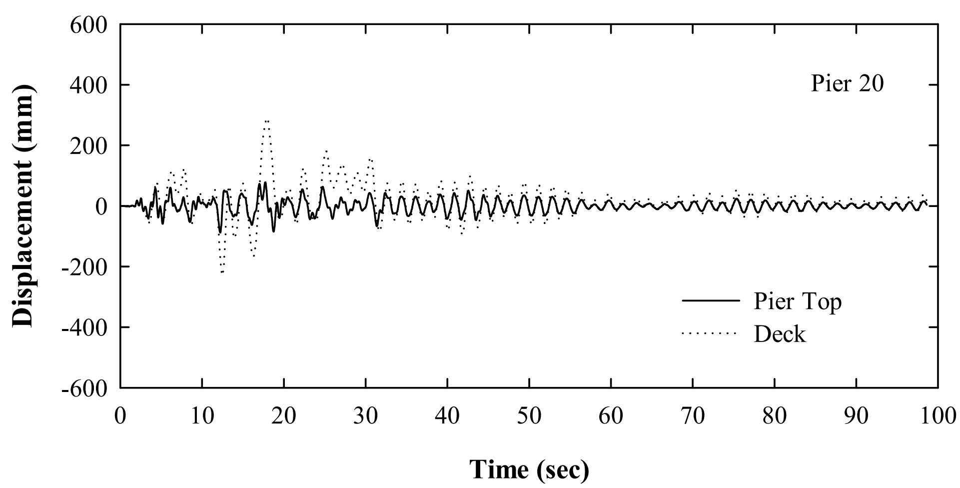

LONGITUDINAL DIRECTION RESPONSE IN 1971 SAN FERNANDO, 458

90° COMPONENT APPLIED IN LONGITUDINAL DIRECTION

0° COMPONENT APPLIED IN TRANSVERSE DIRECTION

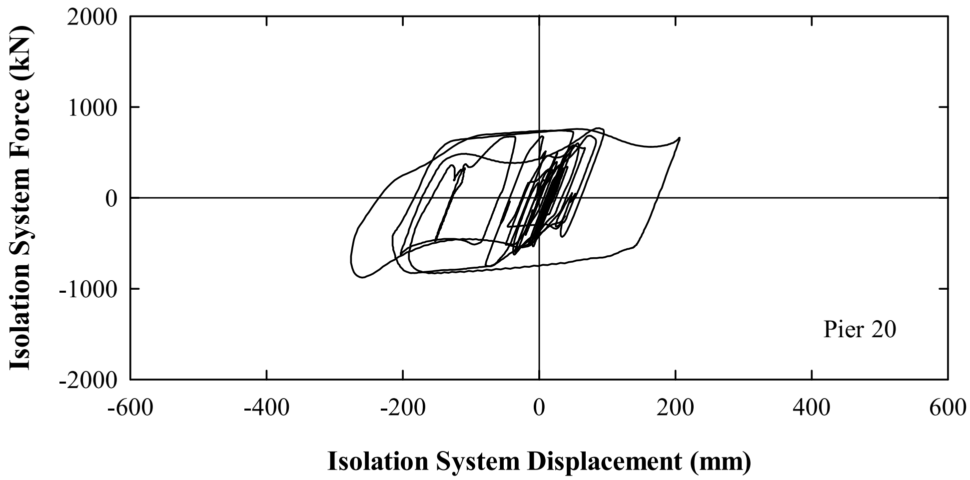

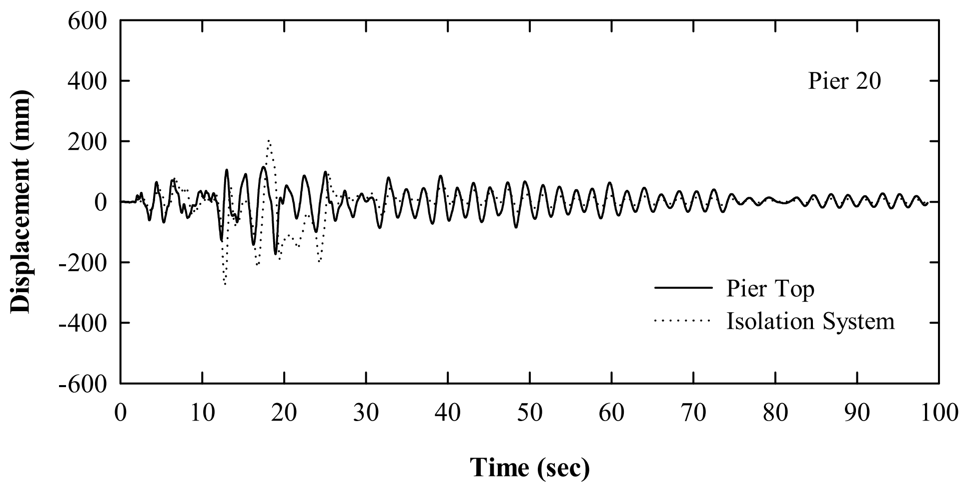

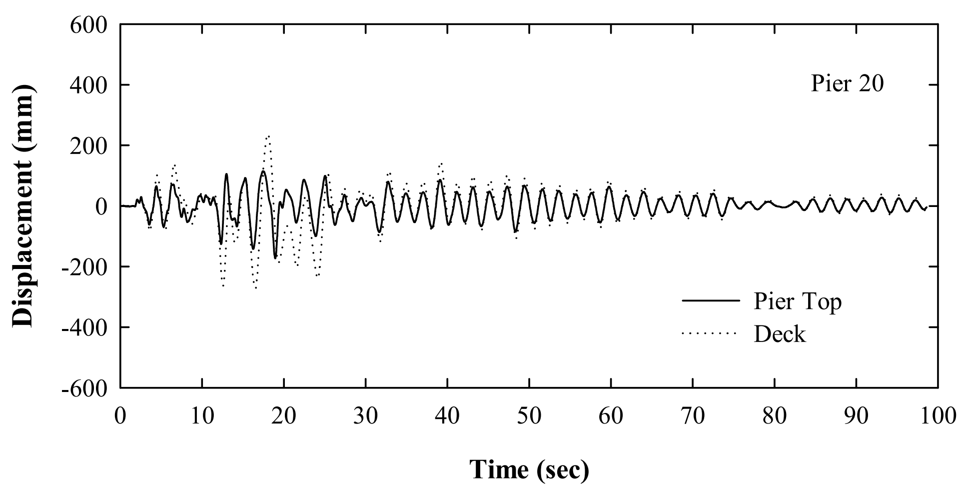

TRANSVERSE DIRECTION RESPONSE IN 1971 SAN FERNANDO, 458

90° COMPONENT APPLIED IN LONGITUDINAL DIRECTION

0° COMPONENT APPLIED IN TRANSVERSE DIRECTION

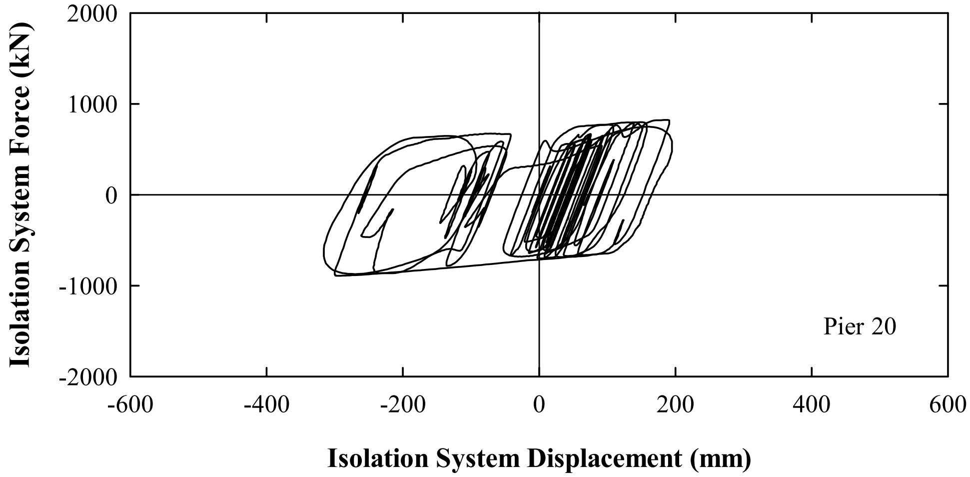

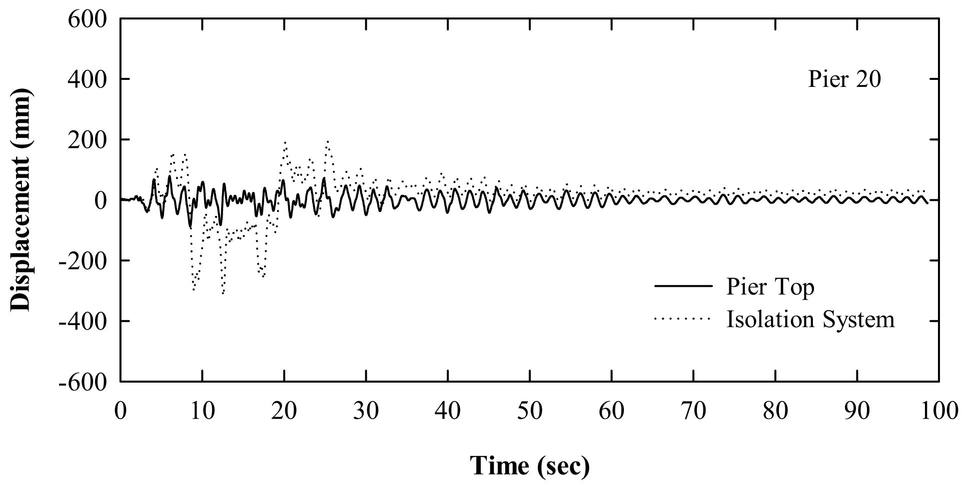

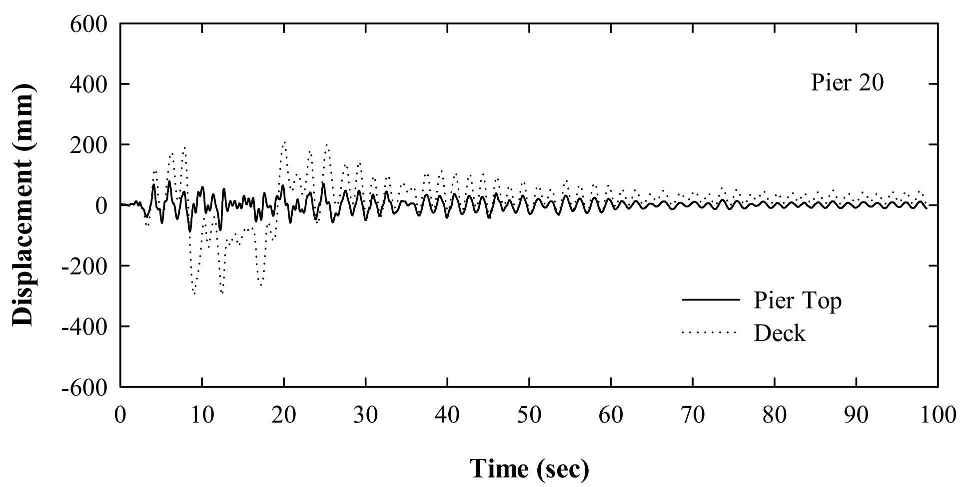

MCEER
MULTIDISCIPLINARY CENTER FOR EARTHQUAKE ENGINEERING RESEARCH
A National Center of Excellence in Advanced Technology Applications

University at Buffalo, State University of New York
Red Jacket Quadrangle ■ Buffalo, New York 14261-0025
Phone: 716/645-3391 ■ Fax: 716/645-3399
E-mail: mceer@acsu.buffalo.edu ■ WWW Site: http://mceer.buffalo.edu

University at Buffalo *The State University of New York*

ISSN 1520-295X